

**ULTRAVIOLET LIGHT APPLICATIONS FOR THE  
DEGRADATION OF NATURAL ORGANIC  
MATTER IN WATER MATRICES**

By

Sean Alexander MacIsaac

Submitted in partial fulfilment of the requirements  
For the degree of Doctor of Philosophy

at

Dalhousie University  
Halifax, Nova Scotia  
March 2021

© Copyright by Sean Alexander MacIsaac, 2021

# TABLE OF CONTENTS

<b>LIST OF TABLES .....</b>	<b>vi</b>
<b>LIST OF FIGURES .....</b>	<b>vii</b>
<b>ABSTRACT .....</b>	<b>x</b>
<b>ACKNOWLEDGEMENTS .....</b>	<b>xii</b>
<b>1 Introduction.....</b>	<b>1</b>
1.1 Research rationale.....	1
1.2 Research Objectives.....	3
1.3 Organization of Thesis.....	4
<b>2 Review of Advanced Oxidation Processes, Reactors, and Applications for Natural Organic Matter.....</b>	<b>6</b>
2.1 Current UV Technologies .....	6
2.1.1 Mercury Halogen Ballasted UV Emitters .....	7
2.1.2 Vacuum UV Emitters .....	9
2.1.3 UV Light Emitting Diode Emitters.....	10
2.1.4 Xenon-Flash Excimers for UV Emittance.....	11
2.1.5 UV Side Emitting Optical Fibers.....	12
2.1.6 Future Prospects for UV Technologies .....	12
2.2 Advanced oxidation processes and pathways .....	13
2.2.1 Hydrogen Peroxide Based Advanced Oxidation Technologies.....	13
2.2.2 Ozone Based Advanced Oxidation Technologies.....	14
2.2.3 Chlorine-Based Advanced Oxidation Technologies .....	14
2.2.4 Titanium dioxide-based UV AOP .....	15
2.3 Scavenging properties of advanced oxidation processes.....	17
2.4 Radical Probing for Advanced Oxidation Processes .....	18
2.5 Disinfection Byproduct Formation.....	19

### **3 Characterization of Geosmin Removal Using Advanced Oxidation Processes on a Natural Water Matrix..... 20**

3.1	Abstract.....	20
3.2	Introduction.....	20
3.3	Methods.....	24
3.3.1	Pockwock Lake Water Quality.....	24
3.3.2	Advanced Oxidation Experimental Design.....	24
3.3.3	Hydroxyl Radical Kinetics.....	25
3.3.4	Fractionation of Pockwock Lake Water.....	26
3.3.5	Resin Cleaning Protocols.....	27
3.3.6	Geosmin Preparation and Addition to Natural Water Matrices.....	29
3.3.7	Water Quality Parameter Sample Preparation.....	29
3.3.8	Fluorescence Excitation Emission Matrix (FEEM) Preparation.....	30
3.3.9	Parallel Factor Analysis (PARAFAC).....	31
3.4	Results.....	33
3.4.1	pCBA Kinetics for AOP Conditions.....	33
3.4.2	Geosmin Removal via Advanced Oxidation Processes.....	36
3.4.3	Changes in SUVA After Advanced Oxidation Exposure.....	38
3.4.4	Comparison of 2010 and 2012 NOM Fractional Distribution.....	39
3.4.5	Parallel Factor Analysis (PARAFAC) of AOP Exposed Pockwock Lake Water	43
3.5	Conclusion.....	48

### **4 Assessment of disinfection by-product formation potential in a natural water matrix after exposure to advanced oxidation processes..... 50**

4.1	Abstract.....	50
4.2	Introduction.....	50
4.2.1	Pottle Lake Water Treatment Plant.....	51
4.2.2	Disinfection Byproduct Formation Potential.....	52
4.2.3	DBP Precursor Material.....	53
4.3	Methods.....	54

4.3.1	THM and HAA quantification .....	54
4.3.2	Size Exclusion Chromatography Analysis.....	54
4.4	Results and Discussion.....	55
4.4.1	Pottle Lake DBP Formation Potential .....	55
4.4.2	Parallel Factor Analysis (PARAFAC) of AOP Exposed Pottle Lake Water 57	
4.5	Conclusion.....	62
<b>5 Modelling of fluorescent excitation emission matrices to assess the changes in natural organic matter after advanced oxidation treatment.....</b>		<b>64</b>
5.1	Abstract.....	64
5.2	Introduction.....	65
5.3	Principal Component Analysis.....	68
5.4	Principal Component Analysis Code Workflow .....	69
5.5	Methods.....	70
5.5.1	Synthetic Water Matrix.....	70
5.5.2	Natural Water Matrix.....	71
5.5.3	Fluorescence Excitation Emission Matrices (FEEM) .....	71
5.6	Data Management.....	72
5.7	Results and discussion .....	73
5.7.1	Contour Loading Plots .....	76
5.7.2	K-means clustering of PCA scores.....	78
5.8	Conclusion.....	84
<b>6 Development of a wavelength tunable, high throughput UV exposure tool.....</b>		<b>86</b>
6.1	Abstract.....	86
6.2	Introduction.....	87
6.3	Materials and Methods.....	90
6.3.1	Light Source Actinometry.....	91
6.3.2	Calculation of Light Intensity .....	93
6.3.3	Microplate oxidation .....	94

6.3.4	LC-MS analysis.....	96
6.4	Results and Discussion.....	97
6.4.1	Actinometry Lamp Characterization.....	97
6.4.2	Amino Acid Degradation.....	98
6.4.3	Environmental Applications.....	101
6.5	Conclusions.....	103
<b>7</b>	<b>Conclusions and Recommendations .....</b>	<b>105</b>
7.1	Summary and Conclusions.....	105
7.2	Recommendations for Future Work.....	106
	<b>References .....</b>	<b>109</b>
	<b>APPENDIX A: Pockwock Lake Water Quality Data and R Code for Plots.....</b>	<b>145</b>
	<b>APPENDIX B: R Code for Kinetics Data.....</b>	<b>150</b>
	<b>APPENDIX C: Additional Data for Pottle Lake .....</b>	<b>155</b>
	<b>APPENDIX D: R Code for Contour plots.....</b>	<b>158</b>
	<b>APPENDIX E: Matlab Code for PCA Analysis of FEEM Data</b>	<b>169</b>
	<b>APPENDIX F: High Throughput UV Exposure Supplemental Material .....</b>	<b>186</b>

## LIST OF TABLES

<b>Table 3-1</b> Typical water quality values for post-filter Pockwock Lake during the experimental timeframe. $\pm$ values represent a 95% confidence interval about the mean.....	24
<b>Table 3-2</b> Typical NOM fractions and Chemical Groups. Adapted from Edzwald (1993).....	27
<b>Table 3-3</b> Typical NOM fractions with corresponding excitation and emission fluorescent regions. Adapted from Marhaba (2000).....	31
<b>Table 3-4</b> Observed pseudo-first order fluence based rate constant for pCBA oxidation ( $L\ mg^{-1}$ ).....	35
<b>Table 3-5</b> Fluorescent NOM regions described by modelled PARAFAC components for AO treatments .....	47
<b>Table 4-1</b> Typical values for Pottle Lake during the experimentation period. $\pm$ values represent a 95% confidence interval about the mean.....	52
<b>Table 4-2</b> Summary of fluorescent NOM PARAFAC models for Pottle Lake .....	59
<b>Table 5-1</b> Variance explained and emission/excitation wavelength peaks for the first 4 principal components .....	75
<b>Table 5-2</b> K-means clustering distribution of PC2 vs PC3 for each of the AOP treatments for the natural water matrix dataset. ....	82
<b>Table A-1</b> Summary statistics for Pockwock Lake SUVA.....	147
<b>Table F-2</b> UV fluence regression equations for 255nm to 280nm where t is in seconds of UV exposure.....	187

## LIST OF FIGURES

<b>Figure 2-1</b> Visible light and UV spectrum. UV-C is the primary range of the UV wavelength spectrum that is used in disinfection and oxidation applications and is noted by the asterisk.....	7
<b>Figure 2-2</b> Cross-section of a typical mercury halogen UV lamp .....	8
<b>Figure 2-3:</b> Collimated beam arrangement for a typical bench-scale UV exposure experiment.....	9
<b>Figure 2-4</b> Photoelectrical mechanism for reactions between TiO <sub>2</sub> and UV light. Adapted from Hoffmann (1995).....	16
<b>Figure 3-1</b> Reaction kinetics of UV and UV/H <sub>2</sub> O <sub>2</sub> based AOPs where the slope of the line represents the fluences based first order reaction constant for •OH radical production.....	33
<b>Figure 3-2</b> R <sub>OH UV</sub> values for each of the observed AO conditions in the degradation of pCBA.....	36
<b>Figure 3-3</b> Average geosmin removal for untreated Pockwock Lake water and AOP treated Pockwock Lake water with a 95% confidence interval about the mean.....	38
<b>Figure 3-4</b> Box and whisker plot of Pockwock Lake SUVA data for each AOP treatment.....	39
<b>Figure 3-5</b> Comparison of NOM fractions for Pockwock Lake from 2010 (left) and 2012 (right). The units are reported as mg L <sup>-1</sup> . 2010 data was gathered from Montreuil (2011) .....	41
<b>Figure 3-6</b> PARAFAC model for untreated post-filter Pockwock Lake water samples. (n=44).....	44
<b>Figure 3-7</b> PARAFAC model for UV and 10 mg L <sup>-1</sup> H <sub>2</sub> O <sub>2</sub> treated Pockwock Lake Water. (n=46) .....	45
<b>Figure 3-8</b> PARAFAC model for UV and 10 mg L <sup>-1</sup> O <sub>3</sub> treated Pockwock Lake Water. (n=46).....	46
<b>Figure 4-1</b> Pottle Lake THM concentration before and after AOP exposure .....	56
<b>Figure 4-2</b> Pottle Lake HAA concentration before and after AOP exposure.....	57

<b>Figure 4-3</b> PARAFAC model for untreated post-filter Pottle Lake water samples. (n=24).....	58
<b>Figure 4-4</b> PARAFAC model for UV and 10 mg L <sup>-1</sup> H <sub>2</sub> O <sub>2</sub> post-filter Pottle Lake water samples. (n=45).....	59
<b>Figure 4-5</b> Average SEC chromatogram comparing untreated samples to AOP processes that changed NOM the most. The grey area illustrates the range of SEC response across the dataset and the black line indicated the average. ....	61
<b>Figure 5-1</b> Principal component analysis outcomes. Adapted from (Wold, et al., 1987).....	69
<b>Figure 5-2</b> Contour plots for the first four principal component loadings for the synthetic water matrix.....	76
<b>Figure 5-3</b> Contour plots for the first four principal component loadings for the natural water matrix.....	77
<b>Figure 5-4</b> Principal component scores after k-means classification for 2 clusters for the synthetic water matrix dataset. ....	79
<b>Figure 5-5</b> Principal component scores after K-means classification for 2 clusters for the natural water matrix dataset. ....	81
<b>Figure 6-1</b> Actinometry handling protocol when exposing microplate wells to UV light.....	92
<b>Figure 6-2</b> Factorial design of amino acid exposure conditions on multi-well plates. ....	95
<b>Figure 6-3</b> Actinometry-based UV-C fluence curves for wavelengths between 255 and 280nm. Actinometry was conducted using the potassium ferrioxalate method described by Bolton (Bolton et al., 2011).....	98
<b>Figure 6-4</b> Percentage of residual amino acid after UV exposure for the eight experimental conditions that were tested in this study. Samples with >100% recovery experienced evaporation during the UV exposure process leading to an increased concentration of the analyte.....	100
<b>Figure A-1</b> Pockwock Lake post plant filtered TOC data. Error Bars indicate standard deviation. ....	145

**Figure A-2** Pockwock Lake post plant filtered DOC data. Error Bars indicate standard deviation. ....146

## ABSTRACT

Ultraviolet light, in combination with chemical oxidants has been hypothesized as a universal treatment technology for the degradation of harmful organic compounds in water matrices. Advanced oxidation processes (AOPs) non-selectively degrades organic contaminants from water matrices via the production of hydroxyl radicals. A thorough understanding of the nature of the specific natural organic matter (NOM) profile for a surface water is necessary to mitigate negative side effects of AOP use, such as the formation of disinfection byproducts (DBPs). The goal of this research was to examine the changes in natural organic matter that is partially oxidized during AOP exposure. This goal was achieved via the following objectives:

1. Assess the AOP removal efficiency for a seasonal taste and odor compound found in surface waters in Atlantic Canada (geosmin) using a natural water matrix (Pockwock Lake, Halifax, Nova Scotia).
2. Examine the impact that AOPs have on DBPs using a source water that historically has elevated disinfection byproduct concentrations in their finished water (Pottle Lake, Sydney, Nova Scotia).
3. Model the primary changes in oxidized NOM from a fluorescent excitation/emission perspective.
4. Development of a high throughput approach for more efficient UV exposure experimentation using common NOM constituents as challenge compounds.

Geosmin was effectively removed below human detection levels in 1000 mJ cm<sup>-2</sup> fluence, 10 mg L<sup>-1</sup> hydrogen peroxide samples, suggesting that peroxide-based AOPs are better suited for taste and odor compound removal when compared UV and UV/ozone-based AOPs. Peroxide-based AOPs caused increases in DBP formation potential for both THM and HAAs, which exceeded the respective Health Canada guidelines of 100 µg L<sup>-1</sup> and 80 µg L<sup>-1</sup>. Parallel factor (PARAFAC) fluorescent excitation emission matrix (FEEM) models revealed that hydrophobic acidic and basic fractions are susceptible to ozone AOPs whereas peroxide-based UV-AOPs initially oxidize hydrophilic acidic, hydrophobic basic and hydrophobic basic fractions. A high throughput approach for rapid UV exposure of samples was also developed and validated through proof-of-concept testing using tryptophan and tyrosine as model NOM compounds. The high throughput approach allows for faster, and more efficient bench scale AO experiment design while also allowing for tunable UV emittance via a microplate reader.

## LIST OF ABBREVIATIONS USED

NOM	Natural Organic Matter
AO	Advanced Oxidation
AOP	Advanced Oxidation Processes
UV	Ultraviolet
T&O	Taste and Odor
SUVA	Specific UV Absorbance
TOC	Total Organic Carbon
DOC	Dissolved Organic Carbon
DBP	Disinfection Byproduct
I-DBP	Iodinated Disinfection Byproduct
DBP <sub>fp</sub>	Disinfection Byproduct Formation Potential
FP	Formation Potential
LP	Low Pressure
MP	Medium Pressure
LED	Light Emitting Diode
SEOF	Side Emitting Optical Fibers
HPLC	High Pressure Liquid Chromatography
SPE	Solid-Phase Extraction
PLWTP	Pottle Lake Water Treatment Plant
JDKWTP	JD Kline Water Treatment Plant
SEC	Size Exclusion Chromatography

## **ACKNOWLEDGEMENTS**

I would like to thank my supervisor Dr. Graham Gagnon for the opportunity and encouragement to pursue research which began when I was a Co-op student in the Centre for Water Resources during my undergraduate degree. I would also like to thank my supervisory committee, consisting of Dr. Jennie Rand and Dr. Adam Donaldson, for providing valuable feedback throughout the process of grad school.

Thanks to all of my colleagues at the Centre for Water Resources. Undertaking the challenge of a graduate program can be a very isolating experience, but it is a much easier ride through the ups and downs when there is a supportive, dynamic, and not to mention fun group of peers that have been populating the CWRS for the last number of years. Specific thanks Kyle Rauch, Jessica Bennett, Isobel Demont, David Scholts, Lindsay Anderson, Dewey Dunnington, and Yuri Park for reading drafts of thesis chapters throughout the writing process and provide lots of feedback and discussion during that time. I would also like to thank all of staff at CWRS, including Heather Daurie and Tarra Chartrand for all of the technical and administrative help over the years.

I would also like to thank all of those who I have been able to work and interact with at the T Room. Working and managing the Sexton Campus student bar has been an excellent outlet during grad school and several patrons and coworkers are now close friends.

Thank you to National Sciences and Engineering Research Council and Dalhousie University for financial support during my period of study.

Finally, I would like to thank my family for being so supportive during this process. Thank you to Aliya, for the loving support throughout all of my decisions and work during my PhD. Thank you to my parents, for always encouraging me to work towards my goals and encouraging my interest in science.

# 1 Introduction

## 1.1 Research rationale

Removal of natural organic matter (NOM) within source waters is a primary concern for drinking water treatment facilities. Traditional technologies, such as coagulation and filtration have historically provided sufficient treatment for providing safe water to communities (Sharp et al., 2006). Although achieving water with zero risk to public health is not possible, drinking water regulations do change over time as more is learned about chemicals that are present or formed during treatment processes (Khan & Cwiertny, 2020). NOM profiles are further segmented into fractions of compounds of similar characteristics. These compounds are typically bisected into hydrophilic and hydrophobic groups and sub classified into acidic, basic, and neutral compounds.

The onset of climate change is causing an increase of algal activity and changes in organic matter within source waters, meaning that the treatment processes for providing safe drinking water are becoming more complex and more expensive (Díaz, 2016; Díaz et al., 2017). The changing nature of source water quality requires novel treatment technologies to effectively remove emerging contaminants. Taste and odor (T&O) compounds, algal toxins, and disinfection byproduct (DBP) precursor material are some of the main constituents of concern for water utilities as they contend with a changing water matrix. Advanced oxidation processes (AOPs) produce radical oxidative species within a water matrix that are capable of degrading any organic compound provided the correct conditions.

AOPs have several advantages over traditional treatment technologies such as coagulation, sedimentation, and dissolved air floatation because they are able to remove all fractions of the NOM profile for a water matrix. The production of oxidative

radicals within a water matrix means that AOPs are able to remove portions of the NOM that traditional technologies are chemically and physically incapable in removing from a water matrix. Furthermore, the fractions of NOM that are most difficult to remove via traditional technologies have demonstrated to be correlated with disinfection byproduct (DBP) formation (Kent et al., 2014; Lamsal et al., 2012). Another benefit of using AOPs is the ability to retrofit already existing treatment facilities with UV reactors and oxidation reservoirs. Retrofitting of existing facilities allows for the extension of facilities life cycles and provides water utilities with a tool to react to changing water matrices as a result of climate change (Chong et al., 2012; Gude, 2017). AOPs are a relatively new technology that requires rigorous research in order to fully understand the implications of use it has when applied to real water matrices at full scale.

The outcomes and side-effects AOPs have on NOM is an important consideration to make when working with natural water matrices. Proper monitoring of NOM after AOP exposure is necessary to ensure that the resultant NOM profile is not more susceptible to DBP formation when compared to non-AOP treated water. Fluorescent excitation emission matrices (FEEM) are a powerful tool in monitoring how NOM changes due to treatment technologies (Baghoth et al., 2011b; Baker, 2001; Henderson et al., 2009; Peleato & Andrews, 2015; Valencia et al., 2014). Fluorometers measure the excitation and emission of light for fluorophores where electrons of excitable organic material absorb light and are raised to a higher energy level before returning to their ground state and emitting light at a lower energy level (fluorescence). Fluorescent material is associated with some of the main constituents of natural waters including humic material and protein-like material (Markechová et al., 2013). Humic and protein-like portions of the FEEM profile are able to be used to describe the nature of the NOM of the water matrix. Studies state that fluorescence is an undervalued tool in water treatment because it is cheap, sensitive, and selective in detecting contamination events (Henderson et al., 2009). There are several statistical approaches that are used to model the state of fluorescent NOM within a water matrix and they leverage the volume of data that FEEM provide when collected. Using a data-

driven model for understanding how treatment processes impact fluorescent NOM of a water matrix a powerful tool for utilities. FEEM samples are relatively cheap to collect, are non-destructive, and do not require additional chemical addition to measure. Furthermore, coupling AOP with FEEM monitoring allows for a robust toolbox for understand the performance of AOP at both the bench and full-scale.

## 1.2 Research Objectives

The main objectives of the work presented in this thesis document are as follows:

- Test the application of AOPs to small molecular weight/T&O/emerging contaminant as a response to changing surface water quality (e.g., taste and odor compounds or disinfection byproducts)
- Characterize the changes in NOM, with a focus on the fluorescent profile that is present in natural water matrices as a result of exposure to advanced oxidation processes (AOP) at the scale required for full-scale operation.
- Evaluate an approach that is capable of generating a high-throughput of UV-AOP treated water samples using a multiwell reader.

In order to achieve these objectives, experiments were divided into phases.

**Phase 1** Examined the efficacy of AOP for the removal of geosmin from a natural water source at the bench scale level. This work also included the characterizing of and familiarization with a collimated beam which was used for all bench-scale UV-AOP work.

**Phase 2** Examined the impact of AOP on the  $DBP_{fp}$  for a water source that experiences elevated DBP concentrations after passing through a drinking water treatment facility.

**Phase 3** Develop a code structure that efficiently handles large matrices of data that are generated through the collection of FEEM samples. This work was done in Matlab in order to function in harmony with already published FEEM modelling tools.

**Phase 4** Characterized a multiwell reader for UV emittance and developed code within the user interface to facilitate UV exposure of wells with the ability to customize the AOP protocol for UV exposure and emitted wavelength.

### **1.3 Organization of Thesis**

The chapters of this thesis are arranged in the style of a series of journal papers. Each chapter contains an abstract, introduction, materials and methods, results and discussion. Methods that are repeated in multiple chapters are only described in their initial appearance and subsequent chapters will refer to these instances appropriately.

**Chapter 2** provides a brief overview of the state of UV technologies including references to relevant published material that is pertinent to the topic of this thesis. An overview of the different styles of UV reactors and the emittance capabilities of current UV technologies is provided. This chapter also includes a summary of published work on the utilization of AOP and how it behaves with NOM in a natural water matrix.

**Chapter 3** presents the results of a bench-scale study investigating the efficacy of AOP for the degradation of geosmin within a natural water matrix. This chapter investigates how geosmin is removed via a variety of different AOPs including UV, UV/H<sub>2</sub>O<sub>2</sub>, and UV/ O<sub>3</sub>. The regions of typical fluorescent NOM constituents that are most impacted by each AOP for a natural water matrix is also investigated in this chapter.

**Chapter 4** presents the results of a bench-scale study that investigated how AOPs impact the DBP formation potential of a natural water matrix which historically has had elevated DBP concentrations in finished water when using traditional treatment technologies. Trihalomethanes (THMs) and haloacetic acids (HAAs) were the DBPs investigated. The impact of low molecular weight NOM is also investigated in this chapter as a potential root cause of elevated DBP concentrations.

**Chapter 5** provides the results of the initial stages of this research, which involved modelling NOM components using scripts written in Matlab. The data from this chapter was generated from the bench-scale work outlined in Chapters 3 and 4. AOPs including UV, UV/H<sub>2</sub>O<sub>2</sub>, and UV/O<sub>3</sub> were used for all bench-scale work. A portion of the work in this chapter published in *Environmental Science & Technology*.

**Chapter 6** proposes a novel use of a multiwell reader for the use as a bench-scale UV exposure unit. A commercially available multiwell reader was characterized for its UV emittance and used as a AOP reactor for a selection of UV-C wavelengths. This work has been published in *Environmental Science & Technology: Engineering*.

**Chapter 7** provides a summary and conclusion of the presented work included in this thesis. The primary contributions to the field of UV research are noted and contextualized for the broader research community. This chapter also makes recommendations for future work involving the application of AOP and the monitoring of NOM as a result of AOP exposure.

## 2 Review of Advanced Oxidation Processes, Reactors, and Applications for Natural Organic Matter

This chapter outlines conventional uses of UV AOPs along with emerging technologies being developed for further use of UV technologies in water treatment. UV sources are varied in their emitted wavelengths, power efficiency, and lamp type and all of these factors should be characterized when applying this technology at scale. The typical radical generating chemical pathways are also outlined in this chapter along with examples of applications for each of these AOPs. AOPs have a complex relationship with NOM and several factors must be considered when choosing an AO technology for a water matrix. The final portion of this chapter details the role that radical scavengers have in AO treatments. AO scavengers impact the overall efficiency of oxidation technologies and should be investigated when using natural waters.

### 2.1 Current UV Technologies

UV technology has been a mainstay in both drinking water and wastewater treatment for several decades as a disinfectant. The UV-C wavelength range of the electromagnetic spectrum falls between 200 and 280 nm for UV-C. UV-C light is the primary range of the spectra that is relevant for the oxidation and disinfection of water and is designated by the \* in **Figure 2-1**. Current technologies that are used for full-scale processes focus on the emittance of UV light at 254 nm because of its well-documented bactericidal properties with the first documented deactivation of *E.coli* occurring in the 1950's (Clancy et al., 2000, 2004; Zelle & Hollaender, 1954). Historically, mercury-halogen bulbs have been the main source for generating UV light for bactericidal purposes. Low pressure (LP) mercury-halogen lamps provide robust emittance of UV at 254 nm, and medium pressure (MP) lamps are able to emit UV light in a spectral manner. The peak emittance for MP lamps is typically governed by the quartz sheath that protects the lamp and UV filters that can be applied to emitted light external to the lamp.

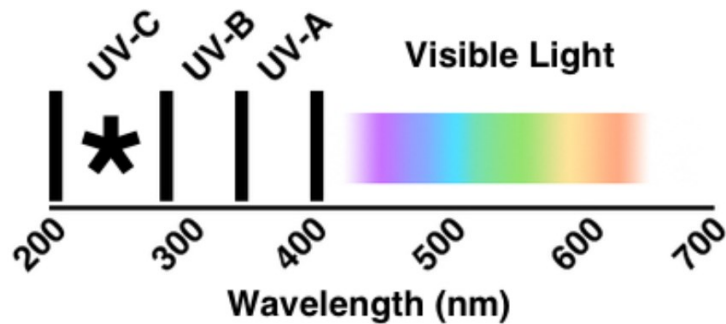


**Figure 2-1** Visible light and UV spectrum. UV-C is the primary range of the UV wavelength spectrum that is used in disinfection and oxidation applications and is noted by the asterisk.

In recent years, a number of emerging technologies have been developed for wider applications of UV treatment. UV light emitting diodes (LEDs), xenon-flash lamps, UV fiber optic filaments, and  $\text{TiO}_2$  / UV photocatalysis are all technologies that are in various stages of development and will drastically expand the design space for UV applications.

### 2.1.1 Mercury Halogen Ballasted UV Emitters

Currently, the most common UV reactor designs still use mercury halogen ballasted lamps for UV-C emittance. Mercury halogen lamps emit UV light via the excitation of mercury vapor via electron flow within the lamp housing (Troue, 1976). A cross-section of a typical mercury-halogen lamp is shown in **Figure 2-2**. Typical fluorescent lamps contain a special coating on the inside of the lamp housing which is excited by UV light and emits pseudo-white light (Coaton & Rees, 1981; Maloney & Clark, 1978; Skwirut & Young, 1989). Mercury lamps that are used for water treatment have lamp housing made from quartz. Mercury is a serious environmental hazard when UV lamps have reached their end of lifecycle (Chatterley & Linden, 2010; Kadam et al., 2019). Mercury lamps are also energy inefficient as they lose much of the input energy via waste heat (Bolton & Stefan, 2002; Martín-Sómer et al., 2017). Despite these

drawbacks, low pressure and medium pressure mercury lamps are a mature technology that is well understood at both the bench-scale and full-scale.

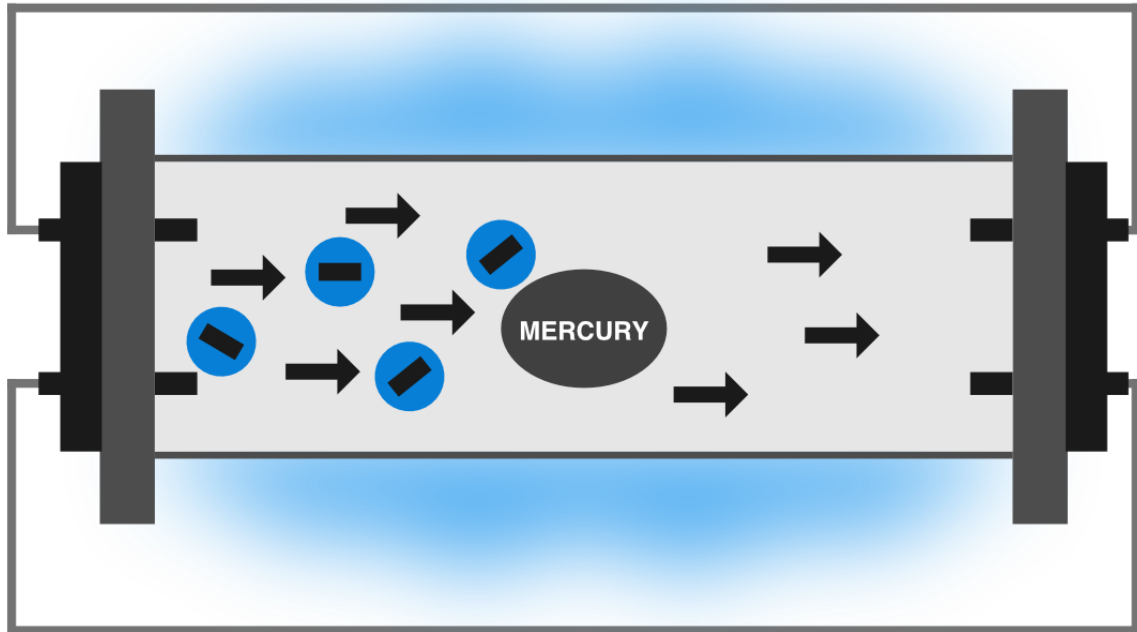


**Figure 2-2** Cross-section of a typical mercury halogen UV lamp

Collimated beams are the most common reactor design for bench-scale work with LP and MP lamps. Collimated beams use a lens and collimator system, which usually surmounts to a quartz shutter and pipe used to direct UV onto an exposure vessel. **Figure 2-3** depicts the typical setup for a bench-scale collimated beam. Collimated beam units must have a collimator that is at least 20cm in length in order to provide sufficient guidance of the light (Bolton & Linden, 2003; Bolton & Stefan, 2002). UV light sources must also be characterized using either a radiometer, spectroradiometer, or integrating sphere before conducting UV experimentation. Collimated beam reactors are time consuming to use despite their ease of use and being a well understood technology for UV researchers. Current experimental setups for both disinfection and AO studies using collimated beams requires a great deal of time because only one sample can be processed at one time. Hence, there is a need for

a high-throughput approach for managing UV exposed samples. A high-throughput approach would expedite bench-scale UV research by orders of magnitude.

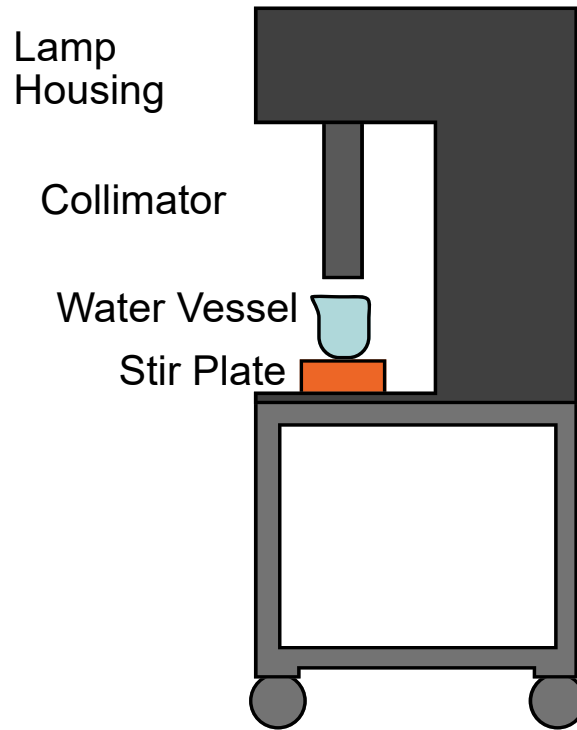


**Figure 2-3:** Collimated beam arrangement for a typical bench-scale UV exposure experiment.

### 2.1.2 Vacuum UV Emitters

Vacuum-UV (VUV) is defined as UV light that is emitted in the wavelength range  $< 200$  nm (Heit et al., 1998). VUV is achieved through the use of excimers or by equipping LP UV lamps with specialized quartz that permits approximately 10% of emitted light at 185 nm (Heit et al., 1998; Imoberdorf & Mohseni, 2011; Szeto et al., 2020). VUV has been demonstrated to be capable of mineralizing TOC with a water matrix at the bench scale with 99% NOM removal after a 180 minute exposure time (translating to a  $34,668 \text{ mJ cm}^{-2}$  fluence at 185 nm and  $405,972 \text{ mJ cm}^{-2}$  at 254 nm) (Imoberdorf & Mohseni, 2011). VUV has also been shown useful in the disinfection of pathogens in air with exposure times ranging from 10-30 min to achieve sufficient log reductions in *E.coli*, influenza, and tuberculosis colonies (Szeto et al., 2020).

### **2.1.3 UV Light Emitting Diode Emitters**

UV LEDs allow for increased flexibility in reactor design because of the modular nature of a ballast-free light source. UV LED chips use aluminium gallium nitride and aluminium nitride for producing ultraviolet light (Oto et al., 2010; Taniyasu et al., 2006). UV LEDs also provide a pseudo-single wavelength emittance, which enables for the construction of tunable reactors that are customized to the targets within a water matrix (Beck et al., 2017). While UV LEDs offer a number of novel options for future applications, they are still a developing technology with drawbacks that must be resolved. There are numerous published studies that examine the efficacy of disinfection and oxidation of UV LED treatments at a variety of different peak wavelengths (Oguma et al., 2016, 2018; Rattanakul & Oguma, 2018; Song et al., 2016).

UV LED treatments typically rely on an array of LEDs to be able to apply a UV fluence suitable for disinfection or oxidation (Muramoto et al., 2014). This means that the power requirements for current UV LED arrays are similar to medium pressure mercury halogen lamps (Ibrahim et al., 2014). In time, LED energy-efficiency is expected to increase as the technology matures (D. H. Chen et al., 2005). The cost of UV LEDs are projected to be < \$0.25 per led chip by the end of 2020 with the lifetime of current-generation LEDs to be 100,000 h (Ibrahim et al., 2014). A drawback of UV LEDs is the variability in quality of LED light sources. There are currently no guidelines or regulations regarding the production of UV LEDs and there is often discrepancies in performance when comparing one UV LED source to another (K. Sholtes et al., 2019; K. A. Sholtes et al., 2016). It is also unclear what wavelengths of light are best for disinfection and oxidation and further research is required to fully understand the complex interactions between NOM and light (Bowker et al., 2011). Gaps in policy regarding UV technology was highlighted during the COVID-19 pandemic where there was an uptick in interest for UV technologies and there are still no EPA-protocols for UV disinfection claims (USEPA, 2020a, 2020b, 2020c). A number of unscrupulous companies quickly developed products that lacked sufficient data or safety factors to ensure appropriate use of UV light and resulted in nearly 30 advisory

letters being administered in order to prevent further sales of these products (Fair, 2020; USEPA, 2020c).

The first full-scale UV LED reactor has recently been validated at flow rates comparable to full-scale pipe flow (Jarvis et al., 2019). This study indicated that UV LEDs perform similarly when compared to mercury-based UV lamps. A more holistic approach of UV reactor design is needed when using UV LEDs because of the many options researchers have in selection of emitted wavelength, reactor geometry, and location of UV sources (Jarvis et al., 2019; Keshavarzfathy et al., 2021). Researchers noted that UV LEDs must be meticulously characterized when designing for full scale due to their modular nature and design space (Beck et al., 2017; Yamato et al., 2017). UV LEDs also have point of use applications for water sources such as fountains and rural settings (Aquisense Technologies, 2020). Point of use UV LED reactors have been proven to behave similarly to LP mercury lamps for disinfecting water (Chatterley & Linden, 2010).

#### **2.1.4 Xenon-Flash Excimers for UV Emittance**

Xenon-flash excimer lamps are also capable of spectral output of UV light. Xenon lamps can be tuned similarly to UV LEDs, however, they require monochromatic filters to block unwanted wavelengths of UV-C light (Coogan, 2005). Excimers produce photons in a narrow and controllable range which can then be used to initiate a variety of reactions (He et al., 1998). The primary application for xenon-based UV applications is currently in the healthcare industry. Xenon has been shown to be effective at disinfecting a variety of hospital instruments and room settings (Hosein et al., 2016; Nagaraja, 2015; Villacís et al., 2019; S.-N. Wang et al., 2019). Typical xenon lamps emit spectral UV light in pulses, thus the spectral emittance and frequency of flashes is important to understand their oxidation and disinfection capabilities (Li et al., 2020). Studies comparing pulsed xenon lamps to LP mercury lamps indicate there is no significant difference in disinfection potential between the two technologies but note that xenon lamps require additional optimization of reactor design in order to

improve efficiencies (Al-Gharabli et al., 2016; Otaki et al., 2003). Pulsed xenon reactors have also been shown to be capable of degrading organic pollutants, such as pesticides and pharmaceuticals with performance similar to traditional UV technologies (Baranda et al., 2012, 2014).

### **2.1.5 UV Side Emitting Optical Fibers**

A major drawback for using any traditional UV technologies in a water matrix or in a common space is the effects of shading between emitted UV light and targeted areas; side emitting optical fibers (SEOFs) are an emerging technology that even further expands design options for UV reactors and presents a partial solution to this challenge. SEOF direct UV light down the filament of an optical fiber and are doped with special nanoparticles that allow for the emittance of UV light perpendicular to the path of the optical fiber (Lanzarini-Lopes et al., 2019). Being able to 'bend' light around corners (such as through the twists and turns of a piping system) resolves a number of the current drawbacks for full-scale UV applications (Lanzarini-Lopes et al., 2017, 2020). A series of SEOF can be applied to supplement traditional technologies by extending UV light into areas that are shaded or difficult to illuminate, aiding in the efficacy of UV disinfection and oxidation.

### **2.1.6 Future Prospects for UV Technologies**

UV technology is also poised for an increase in interest and investment in a post-COVID world. The fundamental processes of UV treatment allow for universal application for disinfection if the fluence of light is properly administered. However, one of the current drawbacks of widespread UV applications is the lack of guidelines or regulations, which has led to a number of unproven or unsafe technologies entering the marketplace, such as for the disinfection of personal items or *in-situ* water treatment reactors for domestic use. The need for UV reactors in full-scale settings is outpacing the capacity of researchers and UV companies. Furthermore, current bench-scale work is time consuming due to the limitations of sample exposure when

using a typical flow-through or collimated beam setup. There is a need, as expressed in literature, for an approach that provides a more efficient approach for exposing bench-scale samples to UV exposure (Betzael et al., 2020).

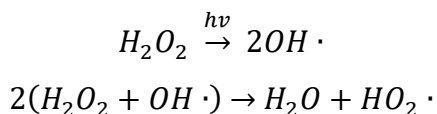
## 2.2 Advanced oxidation processes and pathways

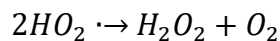
The most promising feature of AO technology is the ability to degrade both legacy and emerging contaminants with a single treatment process (Yang et al., 2014). AOPs have been used for the degradation of a wide variety of targets ranging from taste and odor compounds to pharmaceuticals to antibiotics (Cuerda-Correa et al., 2019; Kutschera et al., 2009; Yuan et al., 2009). The application of AOP results in either complete oxidation or degradation of NOM into lower molecular weight compounds (Lamsal, 2012). Although AOP are capable of degrading any organic compound, the efficiency of AOP is dependent on whether the working oxidants matrix are scavenged by targeted organics or by ambient constituents within a water matrix (Buffle et al., 2006; C.-H. Liao et al., 2001; Sultan & Cho, 2016).

### 2.2.1 Hydrogen Peroxide Based Advanced Oxidation Technologies

Peroxide-based AOP have a more direct chemical pathway for the generation of •OH radicals where a single mole of hydrogen peroxide is catalytically split by UV light into 2 moles of hydroxyl radicals. **Equation 2-1** is adapted from Andreozzi et al. (1999) and summarizes the primary chemical reactions that drive the AOP presented in this thesis. A portion of the generated radicals can non-selectively react with NOM present within the water matrix, whereas the remainder of the produced radicals will reform into H<sub>2</sub>O or react with scavenging ions.

**Equation 2-1** Hydrogen peroxide advanced oxidation pathway.



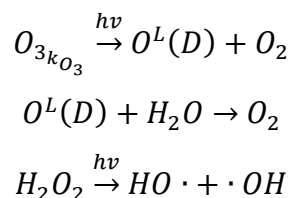


H<sub>2</sub>O<sub>2</sub> based AO technologies have a well-documented history of degrading targeted organic compounds with natural water matrices (Rosenfeldt et al., 2005; Sarathy & Mohseni, 2013; Yuan et al., 2009). Research also suggests that UV / H<sub>2</sub>O<sub>2</sub> technologies are cheaper to apply at full scale for the removal of micro contaminants when compared to other AO technologies (Miralles-Cuevas et al., 2017). H<sub>2</sub>O<sub>2</sub> based AO also outperforms Cl based AO at higher pH at full scale, suggesting that pH control must be considered when applying any AO at scale (C. Wang et al., 2019).

### 2.2.2 Ozone Based Advanced Oxidation Technologies

Ozone follows some of the chemical pathways as hydrogen peroxide when it generates hydroxyl radicals but must first be activated by UV light to initiate the process. **Equation 2-2** details the radical generation pathway for ozone and is adapted from Andreozzi et al. (1999). Ozone is introduced to water matrices in a gaseous state, which can lead to some practical complications when using it at the bench- and full-scale. Ozone must be handled within a fume hood at the bench-scale to limit exposure to off-gassing and at full-scale, additional safety protocols are needed to handle it appropriately (OSHA, 1978).

**Equation 2-2** Ozone advanced oxidation reaction pathway.

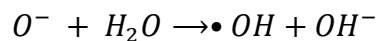
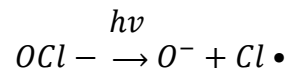
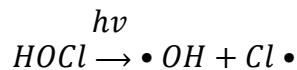


### 2.2.3 Chlorine-Based Advanced Oxidation Technologies

Chlorine-based AOPs are one of the emerging AOP options as it is a very familiar chemical for water utilities to use. The reaction pathway for the generation of radicals

via chlorine based AOPs is shown in **Equation 2-3**. Cl-AOP are also a strong candidate for full-scale AOP use as it could easily be retrofitted into existing drinking water treatment plants because of the prevalence of chlorine as a residual disinfectant technology. Watts and Hoffman (2012) outlined the potential of UV-Cl AOP using water from a facility that typically uses hydrogen peroxide in full-scale processes. UV-Cl treatments exhibited an increase of  $\bullet\text{OH}$  radical generation in the 6-6.5 pH range and performed comparatively to  $\text{H}_2\text{O}_2$  treatments. Chuang et al. (2017) examined the use of chloramine-based AOP as a potential treatment technology for reuse and greywater and concluded that Cl-based AO treatments were comparable to  $\text{H}_2\text{O}_2$  treatments. Both studies also concluded that the excess formation of disinfection byproducts is the primary concern when using Cl as an oxidant.

**Equation 2-3** UV Cl AOP reaction pathway as described by Watts and Hoffman (2012).



Enhancing disinfection byproducts ( $\text{DBP}_{\text{fp}}$ ) in chlorine based AOPs is caused by the high chlorine doses required for oxidation compared to typical disinfection practices and the presence of reactive chlorinated species. The  $\text{DBP}_{\text{fp}}$  of water matrices that have been exposed to AOP were ignored in the early days of AOP studies but have now become one of the primary areas of interest for drinking water treatment researchers (von Gunten, 2018). The same mechanisms that are responsible for the degradation of targeted organic compounds are also linked with increased formation of DBPs (Dong et al., 2017).

#### 2.2.4 Titanium dioxide-based UV AOP

Titanium dioxide ( $\text{TiO}_2$ ) has also been used as a photocatalytic generator of hydroxyl radicals when exposed to UV light (Suzuki et al., 2015).  $\text{TiO}_2$  is typically applied to a surface in the form of a nanotubes or added as a slurry to a water matrix. Each method aim to maximize the surface area of the photocatalyst (P. Huang & Wang, 2019; Nazari et al., 2014).  $\text{TiO}_2$  is considered a good candidate for the removal of targeted organic compounds because it provides three different removal mechanisms for organic removal: oxidation by  $\bullet\text{OH}$ -radicals, reductive dechlorination by superoxide radicals and physical adsorption by  $\text{TiO}_2$  (Gerrity et al., 2009; Matilainen et al., 2011; Wiszniowski et al., 2002). The general photooxidation reaction pathways for  $\text{TiO}_2$  and UV light in a water matrix is outlined in **Figure 2-4**. Nosaka and Nosaka (2017) have detailed several detection methods for quantifying  $\text{TiO}_2$  photocatalytic reactions but note that more work is needed in speciating the reaction pathways for specific compounds, which are currently under debate.

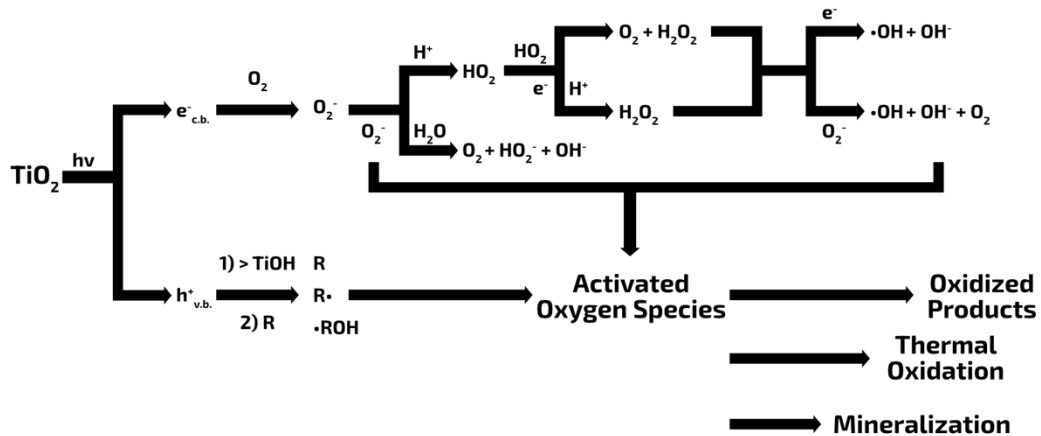


**Figure 2-4** Photoelectrical mechanism for reactions between  $\text{TiO}_2$  and UV light. Adapted from Hoffmann (1995)

The water industry has been on the verge of widescale adoption of novel technologies for several years (Kiparsky et al., 2013; Loeb et al., 2019). The water industry is understandably risk averse and is reluctant to incorporate new technologies until they are fully developed (Kiparsky et al., 2013). A recent review of the state of  $\text{TiO}_2$ -

based AOPs suggests that this technology is a victim of inflated expectations (Loeb et al., 2019). Researchers must reassess the applicability of TiO<sub>2</sub> as more of a niche technology in order to avoid the pitfalls of other overhyped technologies, such as gene therapy, which peaked in interest and investment in the early 1990's but has since settled into niche applications (van Lente et al., 2013).

### **2.3 Scavenging properties of advanced oxidation processes**

Scavenging of oxidative species must be considered to properly understand the efficacy and outcomes of AOP. A number of the reaction pathways and reaction rates for water matrices have been experimentally calculated (Stumm & Morgan, 1996). von Sonntag (2008) details that •OH radicals, while non-selective, primarily undergo three types of reactions:

- i. Addition to C-C, C-N and S-O (in sulfoxides), but not to C-O double bonds
- ii. H-abstraction reactions
- iii. Electron transfer reactions

Addition reactions are considered to be the fastest but are ultimately governed by the electrophilic relationship between •OH and the target compound (von Sonntag, 2008). The H-abstraction rates for H-O, H-C, and H-S are in ascending order with H-O being negligible with reaction rates from other species provided by von Sonntag (2006). Electron transfer reactions are considered energetically unfavourable and are negligible (Fang et al., 2000). Scavenging potential is commonly measured as a bulk parameter due to the range of unknown constituents of a natural water matrix (C. Wang et al., 2020).

Self-scavenging of hydrogen peroxide is another issue when using LP lamps and the dosage must be carefully calibrated to avoid inefficiencies (Matilainen & Sillanpää, 2010). Hydrogen peroxide has a low molar absorbance at 254nm which requires overdosing to sufficiently produce enough •OH for AOP to occur. Overdosing of

hydrogen peroxide causes it to self-react and scavenge itself (Sultan & Cho, 2016). Radical scavenging has also been shown to be enhanced when chloride ions are present. The relationship between radicals and chlorine species is somewhat dependant on pH and the presence of bicarbonate when chloride exceeds a concentration of 250 mM (C.-H. Liao et al., 2001). Overall, the modelling of the scavenging behaviour of a natural water matrix is a useful tool for understanding what may happen as a result of AOP but the complexity of the NOM within a natural water supersedes predictive model abilities (Buffle et al., 2006).

The specific reaction pathways for scavengers are not fully understood or speciated as there are numerous compounds that influence the process. The presence of a variety of radial scavengers in a natural water matrix reduce the quantum yield of chemical oxidants (Watts & Linden, 2007). Despite the abundance of studies that have been published regarding the interactions between AOPs and NOM, there are several gaps when applying this technology to natural water matrices.

## **2.4 Radical Probing for Advanced Oxidation Processes**

The utilization of probe chemicals is vital in characterizing both scavenging pathways and quantifying radical generation within a water matrix during treatment. Several studies have characterized the behavior of compounds such as sucralose, para-chlorobenzoic acid, and coumarin (Jung & Choi, 2006a; Keen & Linden, 2013; Lester et al., 2014; Park et al., 2004; Rosenfeldt et al., 2006a). The UV absorbance via direct photolysis and the vulnerability to chemical oxidation should be considered when selecting a probe chemical as compounds that are susceptible to UV photolysis may not simultaneously be good candidates when reacting with chemical oxidants and vice versa (Wünsch et al., 2021). Probe chemicals are the preferred way for indirectly measuring  $\bullet\text{OH}$  radicals as the lifetime of radical species is too short to practically measure them via other methods (Jing & Chaplin, 2017). Characterization of radical production is also useful in understanding the NOM implications that certain AOPs will have on a water matrix. Recent studies have been able to show the role that

radicals play in the formation of DBPs when they react with NOM that is present within natural waters (Varanasi et al., 2018; Zhang et al., 2021).

## 2.5 Disinfection Byproduct Formation

Recent studies suggest that an increase of formation potential is dependent on the water matrix being used rather than an inherent issue with using AOP (Ike et al., 2019; Metz et al., 2011; von Gunten, 2018). Even UV- and UV-H<sub>2</sub>O<sub>2</sub>-based AOP have shown to increase THM formation potential by as much as 143% when compare to non-AOP treated samples (Dotson et al., 2010). Other studies have shown that AOP can effectively reduce DBP<sub>fp</sub> as much as 77% and 62% for THMs and HAAs respectively (Lamsal et al., 2011). One theory states that that DBP<sub>fp</sub> increases in low intensity and concentration AOPs but DBP<sub>fp</sub> is diminished as AOP intensity and concentration increases (Ike et al., 2019). NOM within a water matrix would be further oxidized into lower molecular weight compounds that are incapable of forming DBPs at higher fluences and oxidant concentrations. Low molecular weight NOM tends to be more hydrophilic in nature and can cause a water matrix to be more prone to THM byproduct formation whereas HAA formation is typically associated with the hydrophobic fractions of a water matrix (Chowdhury et al., 2008; W. Chu et al., 2016; Marhaba & Van, 2000). It is important for water utilities to investigate DBP<sub>fp</sub> outcomes at the bench and pilot scale when considering UV-Cl AOP as a treatment technology. The risk of enhanced DBP<sub>fp</sub> highlights the complex nature of AOPs and additional research is needed to better understand how they interact with NOM.

## **3 Characterization of Geosmin Removal Using Advanced Oxidation Processes on a Natural Water Matrix**

### **3.1 Abstract**

The study outlined in this chapter investigated and characterized the impacts of AOPs on a natural water matrix that has experienced geosmin infiltration as a result of lake recovery. Geosmin was added to a natural water matrix at a concentration of  $20 \text{ ng L}^{-1}$ , which was representative of the peak geosmin concentrations detected by the water utility during this study. UV,  $\text{H}_2\text{O}_2/\text{UV}$ , and  $\text{O}_3/\text{UV}$  AOPs at fluences of  $100 \text{ mJ cm}^{-2}$  and  $1000 \text{ mJ cm}^{-2}$  with chemical concentrations of  $1 \text{ mg L}^{-1}$  and  $10 \text{ mg L}^{-1}$  were used as the treatments for the degradation of geosmin. Peroxide based AOPs were the most effective treatment the degradation of geosmin where  $10 \text{ mg L}^{-1}$  peroxide treatments resulted in residual geosmin concentrations which were below the human detection level. The hydroxyl radical kinetics of the UV light source and AOPs were determined using pCBA as the probe compound. The reaction kinetic results indicated that peroxide-based AO is a major contributor to radical production with peroxide-based AOP generating an order of magnitude more hydroxyl radicals than UV AO at the same fluence. The natural water matrix was also characterized from an NOM perspective by fractionating it into six groups (HOA, HON, HOB, HIA, HIN, HIB) to contextualize which fractions of NOM are most impacted by different AOPs. Fractionation data, coupled with fluorescence excitation-emission matrices indicated that peroxide AO oxidizes the protein-like and aromatic portion of the fluorescent NOM which are linked to the HIA, HIB, and HOB fractions. The HON portion of the NOM oxidized by both peroxide and ozone AOPs. Changes in NOM fractions for Pockwock Lake between 2010 and 2012 indicate that as further brownification occurs, the oxidation of hydrophilic compounds should be monitored, and additional fractionation of Pockwock Lake water is needed to understand how NOM has changed since 2012.

### **3.2 Introduction**

The changing water quality of lakes in Atlantic Canada requires new technologies to be explored to ensure adequately treated drinking water. AOP is a technology that can address these issues via its ability to oxidize any organic compound present within a water matrix. Emergent stressors, such as the brownification of lakes, requires a thorough understanding of how AOP interacts with NOM in a natural water matrix.

This chapter investigated the role that AOP plays in the removal of geosmin, a common taste and odor (T&O) compound, and how AOP interacts with ambient organic material.

The removal of algal metabolites and natural organic matter (NOM) from source waters is an ever-changing issue that water utilities must contend with as the outcomes of climate change assert themselves. AOPs are a next generation treatment technology that are suitable treatment technology for by-products of algal activity, such as taste and odor compounds (Antonopoulou et al., 2014). The presence of geosmin in drinking water gives consumers the impression that a decline in the aesthetic taste of drinking water is equivalent to a decline in the quality and safety of drinking water. Water utilities from a wide range of locations have reported excess complaints when experiencing geosmin outbreaks (Cook et al., 2001).

Studies have shown that several lakes in this region are experiencing lake browning, which is causing changes in the chemistry of the influent water for drinking water treatment plants (Anderson et al., 2017; Williamson et al., 2016). The phenomenon of increasing NOM, color, and taste-and-odor compounds in lakes spells disaster for drinking water treatment facilities that are already constructed (Eikebrokk et al., 2004; Vogt, 2006; Watson, 2003). Source waters that are no longer suitable candidates for the treatment technologies their respective treatment plants were designed for need new technologies to provide safe water. For example, studies have shown there are drinking water treatment facilities within the Halifax Regional Municipality that are projected to not be able to sufficiently coagulate their influent water because of increases in raw water colour (Anderson et al., 2017). AOPs have been shown effective in reducing colour in water via oxidation of humic compounds and therefore could find a suitable application for these plant (Katsumata et al., 2008).

Characterization of NOM within source waters is an important tool for monitoring these changes. One of the common approaches for examining NOM is fractionating it into different families of compounds by absorbing organic compounds onto a high

surface area resin (Thurman & Malcolm, 1979). Previous work from the Centre for Water Resources indicated that in 2010, the raw water NOM of Pockwock Lake was composed of  $\approx 40\%$  hydrophilic material which is not removed via traditional treatment technologies when compared to hydrophobic NOM (Kent et al., 2014; Lamsal et al., 2012; Montreuil, 2011). Fractionation of plant-filtered Pockwock Lake water was conducted in 2012 and captured the state of the NOM during the first detection of geosmin within the watershed. The 2010 and 2012 NOM fractions are compared in this study to assess the changes and state of NOM as a result of early brownification.

Further brownification of source waters may push influent water quality outside of the bounds for reasonable treatment for current facilities. Investigating new technologies that can be retrofitted to existing infrastructure is critical for providing potable water while curbing expenses of treating a changing water matrix (Matilainen & Sillanpää, 2010). AOP have demonstrated the utility as a treatment technology for removing targeted organic compounds within natural water matrices (Matafonova & Batoev, 2018; Wert et al., 2014). Taste and odor compounds, such as geosmin, are one of the primary organic metabolites that are susceptible to oxidative treatments. Typical full-scale water treatment plant removal of geosmin is focused on source waters where geosmin is detected in the order of 100-10,000 ng L<sup>-1</sup> (Ng et al., 2002; Wert et al., 2014).

Low-concentration removal of geosmin in a real water matrix is not well understood because geosmin is not viewed as an aesthetic inconvenience and not a concern to human health. Geosmin is often the canary in the coal mine for serious water quality events such as algal blooms and the infiltration of algal toxins within a source water (Freeman, 2010). Geosmin has been associated with algal species that are also capable of producing toxins (such as microcystin-LR). *Anabaena*, *Aphanizomenon*, *Lyngbya*, *Microcystis*, *Oscillatoria*, *Phormidium*, and *Schizothrix* have been identified as algal species that are both geosmin and toxin producing (Chorus & Bartram, 1999). This

means that for some water sources geosmin is an indicator of much larger issues that will affect public health.

The purpose of the experiments outlined in this chapter was to examine the removal efficacy of geosmin in a real water matrix, quantify the hydroxyl radical production capacity for the AOPs examined in this experimental setup, and quantify the changes in the makeup of natural organic matter within the water matrix as a result of oxidation. This work was accomplished by characterizing the impacts of oxidation using the following tools:

- 1) pCBA reaction kinetics for the production of  $\bullet\text{OH}$  radicals in UV and UV /  $\text{H}_2\text{O}_2$  AOP.
- 2) Compare NOM fractionation of Pockwock Lake water before and after geosmin detection and demonstrate how a changing NOM profile impacts AO.
- 3) Model the fluorescent NOM present in AOPs water matrices using PARAFAC analysis was also used to further characterize the nature of NOM changes as a result of AOP exposure.

### 3.3 Methods

#### 3.3.1 Pockwock Lake Water Quality

The impacts of AOP treatments on the NOM of post-filter lake water was examined via a series of bench-scale experiment using UV, ozone, and peroxide-based oxidation. Pockwock Lake water was collected over the course of 6-months for the bench-scale study. Pockwock Lake is characterized by having low alkalinity, low colour, low DOC, and a NOM profile that is representative of other surface waters in Atlantic Canada. The typical values for post-filter Pockwock Lake water quality are summarized in **Table 3-1**.

**Table 3-1** Typical water quality values for post-filter Pockwock Lake during the experimental timeframe.  $\pm$  values represent a 95% confidence interval about the mean.

<i>Parameter</i>	<i>Value</i>
<i>TOC (mg L<sup>-1</sup>)</i>	1.86 $\pm$ 0.12
<i>UV<sub>254</sub> (cm<sup>-1</sup>)</i>	0.039 $\pm$ 9.06E-03
<i>SUVA (L mg<sup>-1</sup>m<sup>-1</sup>)</i>	1.51 $\pm$ 0.467
<i>Ambient Geosmin (ng L<sup>-1</sup>)</i>	6.487 $\pm$ 3.57

#### 3.3.2 Advanced Oxidation Experimental Design

The low and high levels of the factorial design of the bench-scale UV fluences were 100 and 1000 mJ cm<sup>-2</sup>, whereas hydrogen peroxide and ozone conditions were at a low concentration of 1 mg L<sup>-1</sup> and a high concentration of 10 mg L<sup>-1</sup>. 500 mL of AOP treated water for each experimental condition was collected to prepare total organic carbon (TOC), dissolved organic carbon (DOC), UV<sub>254</sub> absorbance, fluorescent excitation emission matrices (FEEM) and GC-MS-Geosmin samples. H<sub>2</sub>O<sub>2</sub> and O<sub>3</sub> were added to sample beakers immediately before exposure to UV light. A stock solution of 3 mg mL<sup>-1</sup> H<sub>2</sub>O<sub>2</sub> was used to prepare H<sub>2</sub>O<sub>2</sub>-based treatments. H<sub>2</sub>O<sub>2</sub>-based samples were quenched with bovine catalase immediately after UV exposure to ensure residual oxidation did not occur. Ozone samples were prepared using an Azocon

VMUS ozone generator at a rate of 2 L min<sup>-1</sup> and a pressure of 40 psi. The ozone generator was calibrated using the standard indigo method for measuring ozone in aqueous solutions (Baird et al., 2017; Williams & Darby, 1992). A 1000 W, medium-pressure, collimated UV lamp was used for all UV exposures (Calgon Carbon, 2012). UV fluences were calculated using the approach provided by Bolton and Linden (Bolton & Linden, 2003).

### 3.3.3 Hydroxyl Radical Kinetics

The first portion of this study used para-chlorobenzoic acid (pCBA) as a probe compound to quantify the maximum generation of OH• radicals via an array of AO treatments (Lanzarini-Lopes et al., 2017; Pi et al., 2005). pCBA undergoes a first-order reaction when exposed to hydroxyl radicals which can be used to model •OH production (Jung & Choi, 2006b; Park et al., 2004; Pi et al., 2005). pCBA was added to deionized water at a concentration of 50 µM. The pCBA solution was divided into three 1 L amber bottles and pH adjusted to 5.5, 8, and 10 with 0.1M NaOH or 0.1 H<sub>2</sub>SO<sub>4</sub> when appropriate. 125 mL aliquots of pH-adjusted water were then collected in a 250 mL beaker and placed beneath a Calgon Carbon collimated beam unit equipped with a 1000 W medium-pressure UV-C lamp (Calgon Carbon, 2012).

Samples were then exposed to 100, 500, and 1000 mJ cm<sup>-2</sup> fluences and were immediately collected for analysis. UV fluences were calculated in accordance to the method outlined by Linden and Bolton (Bolton & Linden, 2003). pCBA was measured on a Perkin-Elmer Series 200 HPLC using acetonitrile as the mobile phase with a 6-minute runtime for analysis. First order rate constants were calculated for all UV and H<sub>2</sub>O<sub>2</sub> conditions using the method provided by Rosenfeldt (2005). Linear regression was performed on the data (n=3) where the slope of the line is the first order rate constant for each of the AOP conditions. Ozone treatments were omitted from this analysis as they have been shown to not be a suitable probe compound when working in pure water matrices as pCBA promotes ozone decomposition when other scavengers are absent (Park et al., 2004; Pi et al., 2005).

### **3.3.4 Fractionation of Pockwock Lake Water**

Pockwock Lake water was fractionated to assess the changes in NOM makeup when compared to previous work on Pockwock that was conducted in 2010. Post-filter water was used for fractionation and followed the modified Leenheer method described by Marhaba (Leenheer, 1981; Leenheer et al., 2007; Marhaba et al., 2003) that is capable of providing the six NOM fractions provided in **Table 3-2**.

**Table 3-2** Typical NOM fractions and Chemical Groups. Adapted from Edzwald (1993)

<i><b>Fraction</b></i>	<b>Chemical Groups</b>
<b><i>Hydrophobic</i></b>	
<i>Acids</i>	Strong - Humic and fulvic acids, high MW alkyl monocarboxylic and dicarboxylic acids, aromatic acids. Weak - Phenols, tannins, intermediate MW alkyl monocarboxylic and dicarboxylic acids
<i>Bases</i>	Proteins, aromatic amines, high MW alkyl amines
<i>Neutrals</i>	Hydrocarbons, aldehydes, high MW methyl ketones and alkyl alcohols, ethers, furans, pyrrole
<b><i>Hydrophilic</i></b>	
<i>Acids</i>	Hydroxy acids, sugars, sulfonics, low MW alkyl monocarboxylic and dicarboxylic acids
<i>Bases</i>	Amino acids, purines, pyrimidines, low MW alkyl amines
<i>Neutrals</i>	Polysaccharides; low MW alkyl alcohols, aldehydes, and ketones

A series of 5 resin packed Kontes Chromaflex glass columns were used for separating the fractions. DAX-8 resin was used as the adsorbent media for all of the hydrophobic fractions and AG MP-50 resin and Dialon WA-10 resin were used for the HIB and HIA fractions respectively. DOC was measured at the inlet and outlet of each column to determine the proportions of each NOM fraction. Milli-Q was also measured at the outlet of each column before pumping sample water through to ensure that there was not carryover of the resin preparation chemicals used to prepare the different columns.

### 3.3.5 Resin Cleaning Protocols

### 3.3.5.1 *DAX-8 Resin*

Each of the different resins required extensive preparation before adding them to the fractionation columns. New DAX-8 resin was placed in a 500  $\mu\text{m}$  sieve and soaked in 1 N NaOH for 24 hours. Excess NaOH was poured off and the resin was transferred to a Soxhlet apparatus. A boiling flask was filled to the halfway mark with methanol and placed in a heating coil. The assembled Soxhlet apparatus was set to run for 24 h. Methanol was removed and replaced with hexane for another 24 h of sitting in the Soxhlet apparatus. The resin was then removed from the cleaning thimble and rinsed with methanol to remove excess hexane. The resin was then rinsed with Milli-Q to remove any residual methanol. The resin was then transferred to the fractionation columns and rinsed with 0.1 N NaOH and 0.1 N HCl prior to pumping sample water through it.

### 3.3.5.2 *AG MP-50 Resin*

New AG MP-50 resin was transferred to a Soxhlet cleaning thimble. A boiling flask was filled to the halfway mark with methanol and placed in a heating coil. The Soxhlet apparatus was assembled and set to run for 24 h. The resin was removed the following day and rinsed with Milli-Q. The resin was transferred to a column and placed the column in the fume hood. 500 mL of 3 N  $\text{NH}_4\text{OH}$  was then pumped through the column followed by 1 L of Milli-Q. Finally, 500 mL of 2 N HCl was pumped through the column.

### 3.3.5.3 *WA-10 Resin*

New resin WA-10 resin was rinsed with Milli-Q and placed in a Soxhlet thimble. A boiling flask was filled to the halfway mark with acetone and placed in a heating coil to run for 24 h. The resin was then removed from the thimble and placed in a fractionation column in a fume hood. 500 mL of 1 N HCl was then pumped through column followed by 1 L of Milli-Q to remove excess HCl. Finally, 500 mL of 3 N  $\text{NH}_4\text{OH}$  was pumped through the column followed by 1 L of Milli-Q to remove excess  $\text{NH}_4\text{OH}$ .

### **3.3.6 Geosmin Preparation and Addition to Natural Water Matrices**

UV, ozone, and hydrogen peroxide-based oxidation treatments are investigated in this study. Geosmin was spiked into a real water matrix, sourced from Pockwock Lake (Halifax, Nova Scotia). Geosmin was added at a concentration of 20 ng L<sup>-1</sup> to 1 L samples of post-filter water using a stock geosmin solution of 3 mg mL<sup>-1</sup>. Samples and stock solutions were stored in the dark at 4°C when not in use. Samples were kept in headspace-free, amber glass bottles, and were used within 12 hours of creation to minimize losses via geosmin evaporation. Ambient geosmin, which varied seasonally, also contributed to the final geosmin concentration by an average of 6.5 ± 6.04 ng L<sup>-1</sup>. Geosmin samples were processed within 5 days of sample collection in order to avoid geosmin degradation impacting analysis.

Geosmin concentration was measured in plant-filtered water, geosmin spiked plant filtered water, and AOP treated plant-filtered water. This dose was determined through consultation with Halifax water and is based on the maximum geosmin concentration that Halifax Water had observed in their treatment plant. Measuring the geosmin concentration in untreated plant filtered water provided data regarding the algal contribution of geosmin into the water matrix. Geosmin samples were collected immediately after producing 250 mL of AOP-treated water and were stored at 4°C in headspace-free amber bottles while they awaited processing. Geosmin was measured via GC-MS after concentrating geosmin on to solid-phase extraction cartridges using the method described by Wright (Wright et al., 2014). Geosmin samples were passed through solid-phase extraction cartridges (SPE cartridges) using a suction manifold. The SPE cartridges were then eluted with acetone and sodium acetate in order to re-suspend geosmin back into solution. The geosmin/solvent concentrate was then analyzed via a GC-MS.

### **3.3.7 Water Quality Parameter Sample Preparation**

TOC, DOC, and UV<sub>254</sub> absorbance were collected immediately after UV exposure. TOC/DOC was measured using a Shimadzu TOC-V CSH analyzer. DOC samples were

prepared by filtering the treated water through a 0.45-micron polysulfone filter and stabilized with 3 drops of concentrated phosphoric acid. Both TOC and DOC samples were stored at 4°C in 40 mL headspace-free amber bottles prior to analysis. UV<sub>254</sub> absorbance was measured in a 1 cm quartz cuvette using a Hach DR5000 spectrophotometer.

### **3.3.8 Fluorescence Excitation Emission Matrix (FEEM) Preparation**

FEEM samples were analyzed on a Horiba Aqualog fluorometer. First-order and second-order Rayleigh masking, inner-filter effects, and normalization were conducted on FEEM data before exporting datasheets as csv files. The fluorometer was set to a 3 nm bandwidth resolution in both the excitation and emission spectra with a 0.1 s integration time. The excitation spectra ranged from 240 nm to 600 nm and the emission spectra ranged from 213 nm to 620 nm. FEEM samples were processed within one week of collection and were stored in the dark at 4 °C when not in use. A summary of the fluorescent profiles for each of the six NOM fractions are outlined in **Table 3-3**.

**Table 3-3** Typical NOM fractions with corresponding excitation and emission fluorescent regions. Adapted from Marhaba (2000).

<i>Fraction</i>	<b>Major Peak</b>		<b>Minor Peak</b>	
	<i>Excitation (nm)</i>	<i>Emission (nm)</i>	<i>Excitation (nm)</i>	<i>Emission (nm)</i>
<b><i>Hydrophobic</i></b>				
<i>Acid</i>	237-249	417-429	297-309	417-429
<i>Base</i>	225-237	369-381	273-285	369-381
<i>Neutral</i>	225-237	309-321	NA	NA
<b><i>Hydrophilic</i></b>				
<i>Acid</i>	225-237	345-357	273	357-369
<i>Base</i>	225-237	357-369	273-285	357-381
<i>Neutral</i>	225	609-621	NA	NA

### 3.3.9 Parallel Factor Analysis (PARAFAC)

Parallel Factor Analysis (PARAFAC) was used for modelling each of the treatment types used in bench-scale AOP experimentation. The PARAFAC approach uses a trilinear model to generalize FEEM datasets into their underlying signatures (Bro, 1997). A PARAFAC model was generated for untreated samples, UV treated samples, ozone treated samples, and peroxide treated samples. The DomFluor toolbox was used for importing and split-half validation of each of the models to ensure that the appropriate number of components were included in each of the models (Andersen & Bro, 2003). The core DomFluor code by Stedmon was adjusted slightly to accommodate the specific formatting of exported FEEM csv files from the Aqualog device (Stedmon & Bro, 2008). Some small additional changes were also made to the core toolbox code to expedite data exporting to R. Outliers were removed from analysis by identifying them via visual inspection using the guide provided by Stedmon (Stedmon & Bro, 2008). Validated PARAFAC components were exported as vectors to R for further analysis and increased visualization capabilities with ggplot2 (Wickham et al., 2016). RStudio was used for final visualization of PARAFAC models

(*RStudio- Version 1.3.959*, 2020; Hadley et al., 2016). Affinity designer (v. 1.8.3) was used for all final edits of figures and plots (Serif, 2020).

### 3.4 Results

#### 3.4.1 pCBA Kinetics for AOP Conditions

The observed first-order rate constant for each of the UV and UV/H<sub>2</sub>O<sub>2</sub> AO conditions was calculated using the pCBA degradation data at a pH of 5.5, 8, and 10. pCBA data was quantified using a calibration curve ranging from 10 µg L<sup>-1</sup> to 50 µg L<sup>-1</sup>. The slope of ln(pCBA) concentration was plotted against UV fluence to determine the UV fluence-based reaction constant. The plots for each of the observed conditions are shown in **Figure 3-1**.

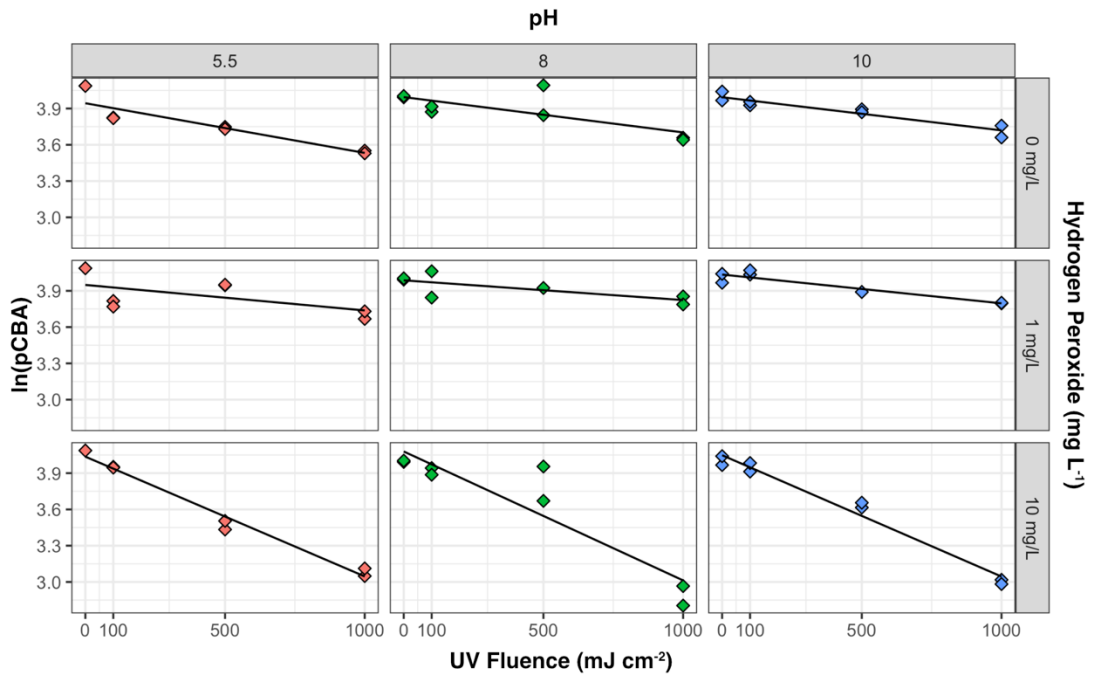


**Figure 3-1** Reaction kinetics of UV and UV/H<sub>2</sub>O<sub>2</sub> based AOPs where the slope of the line represents the fluences based first order reaction constant for •OH radical production

Each of the AOP conditions in **Figure 3-1** exhibited linearity with increasing fluence and chemical oxidant dose vs the degradation of pCBA. First-order rate constants were calculated using the slope of the linear regressions for each of the AOP conditions. The rate of hydroxyl radical production was also calculated by using the equation proposed in previous studies (Rosenfeldt et al., 2005, 2006b). The exposure

rate of •OH radicals per UV fluence ( $\text{mJ cm}^{-2}$ ) for peroxide-based and UV-based AOP are expressed in **Equation 3-1** and **Equation 3-2** and are adapted from Rosenfeldt (2006). The calculated k-values and  $R_{OH,UV}$  values are provided in **Table 3-4** and the code for all the kinetics work is found in **Appendix B**. It is important to note that pCBA is sensitive to both photooxidation and chemical oxidation and it is therefore difficult to fully quantify synergistic effects of UV and  $\text{H}_2\text{O}_2$  AOPs for this given probe chemical.

**Equation 3-1** •OH radical exposure per UV fluence in UV/ $\text{H}_2\text{O}_2$  AOP ( $\text{M s L mJ}^{-1}$ )

$$R_{OH,UV} = \frac{k'_{obs} - k'_d}{k_{OH,pCBA}}$$

**Equation 3-2** •OH radical exposure per UV fluence in UV AOP ( $\text{M s L mJ}^{-1}$ )

$$R_{OH,UV} = \frac{k'_d}{k_{OH,pCBA}}$$

**Table 3-4** Observed pseudo-first order fluence based rate constant for pCBA oxidation ( $L\ mg^{-1}$ )

<i>pH</i>	$H_2O_2$ Concentration ( $mg\ L^{-1}$ )	$k_{obs}^D$ ( $L\ mJ^{-1}$ )	$R_{OH\ UV}$ ( $10^{-13}\ M\ s\ L\ mJ^{-1}$ )
5.5	0	4.11E-04	0.822
	1	2.11E-04	1.242
	10	9.91E-04	2.80
8	0	2.92E-04	0.584
	1	1.63E-04	0.911
	10	1.07E-03	2.717
10	0	2.74E-04	0.548
	1	2.38E-04	1.02
	10	1.00E-03	2.56

The  $\bullet OH$  radical exposure rate for each of the different AO conditions is shown in **Figure 3-2**. These values are similar to those reported by Rosenfeldt (2006) and indicates that production of  $\bullet OH$  radicals is primarily driven by peroxide addition. The  $10\ mg\ L^{-1}$  peroxide conditions produce 3.4 x the amount of  $\bullet OH$  radicals when comparing the pH 5.5 UV photolysis conditions to the pH 5.5 UV +  $10\ mg\ L^{-1}\ H_2O_2$  AOP. The difference in radical production is further exaggerated in the pH 8 and 10 conditions where the  $10\ mg\ L^{-1}\ H_2O_2$  treatment condition produces nearly 10 x the number of radicals when compared to UV photolysis alone.

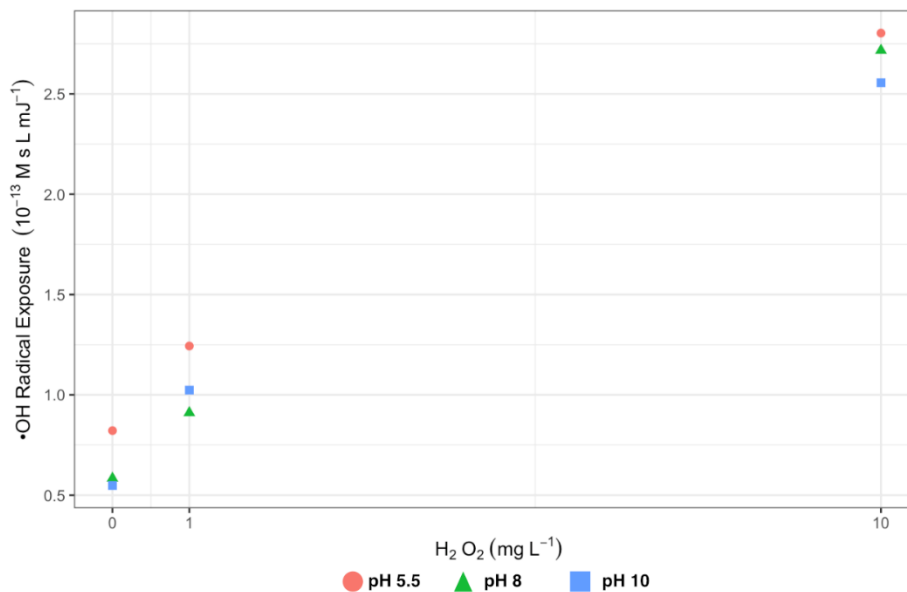


**Figure 3-2**  $R_{OH\ UV}$  values for each of the observed AO conditions in the degradation of pCBA

There does not appear to be a large change in the radical exposure rate per fluence based on changes in pH. Lower pH tends to have a slightly elevated radical production when compared to pH 8 and 10. The radical production and reaction constants calculated in this experiment also represent the maximum number of radicals that can be produce and neglects the effects of scavenging within the water matrix. The overall reaction rates and production of •OH radicals are ultimately dependent on the makeup of the NOM fractions which will compete for the oxidation properties of AOPs. Background NOM has been shown to inhibit the removal of targeted organic compounds by an order of magnitude when the reactive oxidation species are considered (Brame et al., 2015).

### 3.4.2 Geosmin Removal via Advanced Oxidation Processes

AOPs proved to be effective for the degradation of geosmin and altering the NOM within the water matrix. **Error! Reference source not found.** shows the average removal of geosmin for each of the different AOP treatments. Geosmin removal

increases as the dosage of the AOP increases, with high UV and high hydrogen peroxide removing >90% of geosmin. The high UV, high peroxide treatment was the only AOP that was able to degrade geosmin to levels that are below the detection limit for humans. The 95% confidence interval for the high UV high hydrogen peroxide treatment also suggests that the true mean for this treatment is below the detection limit of geosmin for humans. The results indicate that while the synergistic effects between UV and chemical oxidation do improve the removal of target organics, the driving factor of geosmin removal is chemical oxidation. **Error! Reference source not found.** and **Figure 3-4** show that while the ozone-based UV-AOP treatments did not remove as much geosmin as the hydrogen peroxide-based treatments, ozone oxidation is more susceptible to scavenging species present within the water matrix. Low ozone removal efficiencies are driven by the fact that ozone directly reacts with geosmin at a rate orders of magnitude slower than hydrogen peroxide, and ozone-based UV-AOP are entirely reliant on oxidation via hydroxyl radicals (Peter & Von Gunten, 2007). Ozone-refractory organic matter present in the water matrix suppresses the degradation capability of ozone-based UV-AOP (Y. Liu et al., 2015; Pocostales et al., 2010). Hydrogen peroxide-based UV AOP have been reported to have second-order rate constants with geosmin of  $7.8 \times 10^9 \pm 0.24 \text{ M}^{-1}\text{s}^{-1}$  when compared to second-order rate constants for ozone-based UV-AOP and geosmin of  $0.1 \pm 0.03 \text{ M}^{-1}\text{s}^{-1}$  (Peter & Von Gunten, 2007). Hydrogen peroxide has a direct route to produce  $\bullet\text{OH}$  radicals, which explains the vast difference in degradation efficiency when compared to the other AOP treatments.

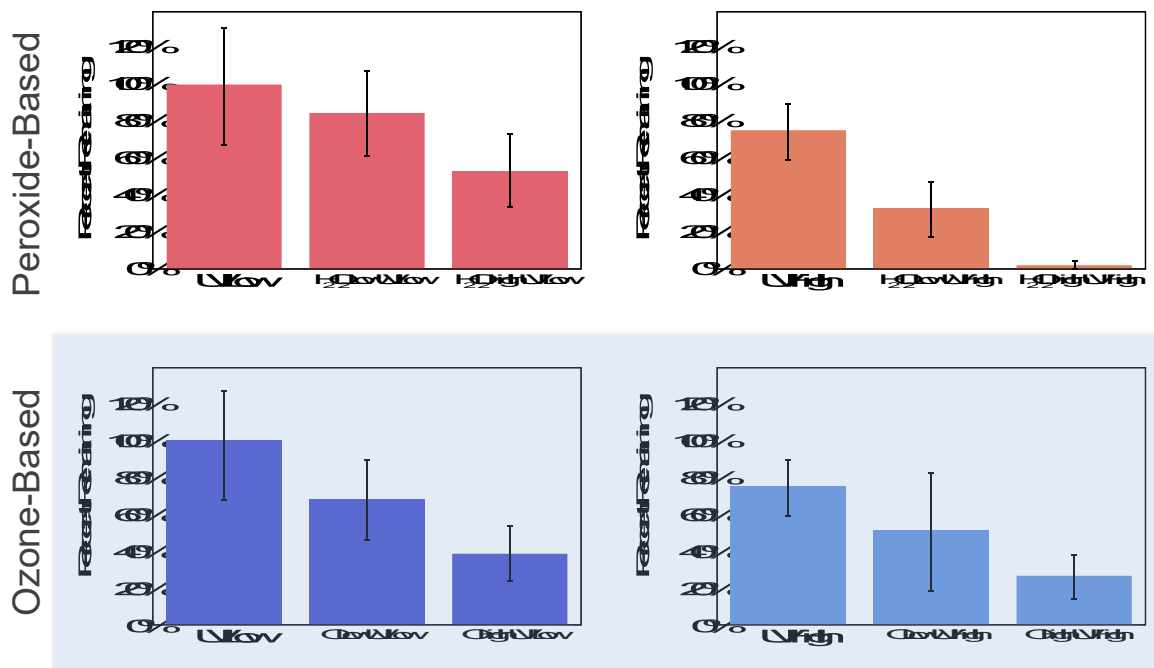


**Figure 3-3** Average geosmin removal for untreated Pockwock Lake water and AOP treated Pockwock Lake water with a 95% confidence interval about the mean.

### 3.4.3 Changes in SUVA After Advanced Oxidation Exposure

SUVA values, shown in **Figure 3-4** provides further insight into the differences between the treatment options. Both 10 mg L<sup>-1</sup> ozone treatments had the lowest SUVA values with means ranging from  $0.83 \pm 0.35$  and  $0.88 \pm 0.36$  L mg<sup>-1</sup> m<sup>-1</sup>. The shift in SUVA from the untreated sample ( $2.17 \pm 0.47$  L mg<sup>-1</sup> m<sup>-1</sup>) to 10 mg L<sup>-1</sup> ozone samples suggests that the nature of the NOM is changing from higher molecular weight compounds to lower molecular weight, aliphatic compounds (Croué, 2004; Hansen et al., 2016). The pattern across AOP treatments in **Figure 3-4** shows that UV fluence alone is a major contributor to the change in the nature of the SUVA for the water matrix.

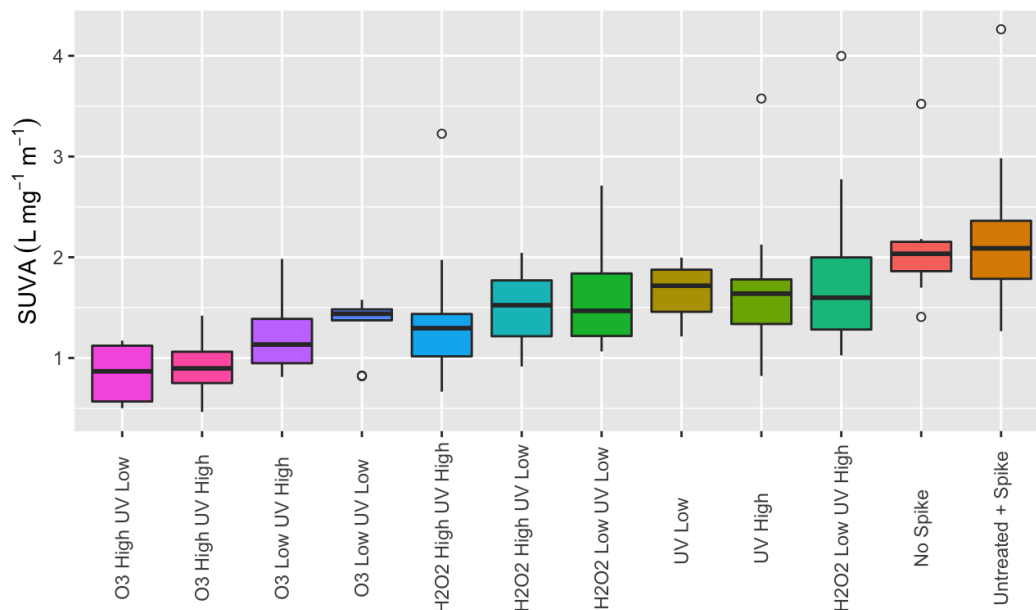


**Figure 3-4** Box and whisker plot of Pockwock Lake SUVA data for each AOP treatment

Ozone samples tend to have lower SUVA values which suggests that high molecular weight compounds, such as humic-like material, are primarily oxidized by ozone treatments. A higher SUVA value in peroxide-based AOPs, coupled with the enhanced degradation of geosmin within the NOM of the water matrix suggests that the reaction pathway between hydrogen peroxide and Pockwock Lake NOM expedites the oxidation of low molecular compounds, such as geosmin, before the oxidation of humic-like material. UV-only AOP treatments tend to demonstrate a mixture in degradation of the humic-like and amino-acid like fluorescence signal. Scavenging of ozone generated radicals and the competing secondary reactions that ozone partakes in when producing radicals in a water matrix are cause of differences in SUVA and geosmin removal. TOC data (located in **Appendix A**) showed no meaningful removal suggesting that complete oxidation (mineralization) is negligible within the water matrix.

### 3.4.4 Comparison of 2010 and 2012 NOM Fractional Distribution

The NOM of Pockwock Lake was characterized in addition to characterizing the AOPs that were used in this study. The proportion of the six NOM fractions present within Pockwock Lake were compared to previous research before brownification impacted lake dynamics. **Figure 3-5** shows the proportional changes in the makeup of NOM with Pockwock Lake and there is an overall increase in DOC in 2012 when compared to 2010. Note that the methods used to fractionate the NOM do so proportionately and the overall DOC recovery is not indicative of method performance (Croué, 2004). Comparing the proportions of the each of the NOM fractions in 2010 and 2012 confirms the changes that have since impacted the overall water quality of Pockwock Lake. Geosmin was first detected in Pockwock Lake the month following the fractionation of the 2012 sample, meaning that the 2012 fractions are capturing the surge in algal activity which led to geosmin detection in Pockwock Lake. The major differences between the 2010 and 2012 fractions are HOA no longer being the dominant hydrophobic fraction with the water matrix and HIB no longer being the dominant hydrophilic fraction. We are instead seeing that the HON and HIN fractions now make up most hydrophobic and hydrophilic compounds.

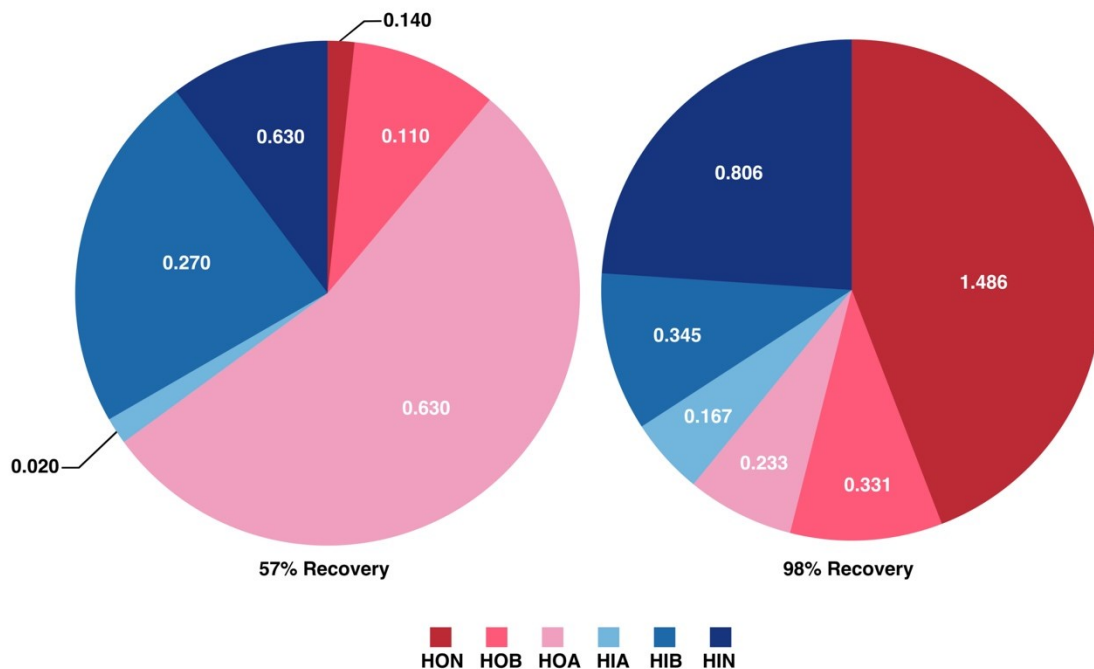


**Figure 3-5** Comparison of NOM fractions for Pockwock Lake from 2010 (left) and 2012 (right). The units are reported as mg L<sup>-1</sup>. 2010 data was gathered from Montreuil (2011)

The shift in NOM from acidified fractions to neutral fractions aligns with the theory that lakes in eastern North America are becoming de-acidified as a result of lowered deposition of sulfurous compounds (Anderson et al., 2017; Keller et al., 1998; MacIsaac et al., 1986). Anderson (2017) describes the increasing colour in lakes across eastern Canada and the increase in the HON fraction (tannic and humic compounds) aligns with this trend. The presence of algal activity has also been shown to negatively impact the efficacy of humic removal during coagulation (Dolejs, 1993). An increase in DBP<sub>fp</sub> is another risk as HON fractions increase. The HON fraction has also been shown to be the most reactive NOM fraction in certain source waters and an increase in the HON fraction may lead to an increase in HAA<sub>fp</sub> as the HON species have been shown to be most reactive in forming HAAs (Marhaba & Van, 2000).

The change in the HIB fraction from 0.270 mg L<sup>-1</sup> to 0.345 mg L<sup>-1</sup> describes the increase in algal activity within the lake. The HIB fraction is associated with amino acids and protein-like material, which is more abundant in the water matrix as algal activity increases (Edzwald, 1993; Marhaba & Van, 2000). Furthermore, an increase in hydrophilic material, which is driven by lake brownification, has been shown to promote algal activity (Leenheer & Croué, 2003; H. Liu et al., 2012). The relative increase in HIN and HIA fractions when compared to 2010 levels causes the proportion of HIB to proportionately decrease.

The proportions of NOM fractions in the 2012 data also highlights potential implications for AO treatments. AOPs tend to oxidize highly aromatic compounds first because of the speed of reactions with and abundance of double bonds (Gligorovski et al., 2015; von Sonntag, 2007, 2008). This means that the hydrophobic fractions will react faster than hydrophilic compounds in natural waters. Changes in the NOM profile for Pockwock Lake also indicate the impact that AOP will have on the water matrix. Ozone has been shown to primarily oxidize all of the hydrophobic fractions with minor changes to hydrophilic fractions (Świetlik et al., 2004). While AOP are often stated that they are non-selective in their reactivity with NOM due to the speed of the reactions some studies show that there are differences when oxidants, such as ozone, react with complex NOM (Sarathy & Mohseni, 2013; Westerhoff et al., 1999). Furthermore, the rate of reaction between advanced oxidants and NOM has some connection with the origin of the NOM in use. Synthetic NOM fractions derived from higher plants have been shown to have significantly different consumptions of radicals when compared to similar synthetic samples that were derived from algal material (Aiken & Cotsaris, 1995; Westerhoff et al., 1999). Seasonality also impacts the nature of the humic material that enters water matrices (Ertel et al., 1984; Rex, 1960).

### 3.4.5 Parallel Factor Analysis (PARAFAC) of AOP Exposed Pockwock Lake Water

FEEM-coupled PARAFAC analysis allows for the deconvolution of fluorophores that describe the nature of fluorescent NOM within a dataset. PARAFAC was used to analyze the impacts of AOP on fluorescent NOM in a real water matrix. The following AOP treatment types were pooled for PARAFAC analysis:

- Untreated (n=44)
- UV (n=46)
- UV + 1 mg L<sup>-1</sup> H<sub>2</sub>O<sub>2</sub> (n=46)
- UV + 10 mg L<sup>-1</sup> H<sub>2</sub>O<sub>2</sub> (n=46)
- UV + 1 mg L<sup>-1</sup> O<sub>3</sub> (n=45)
- UV + 10 mg L<sup>-1</sup> O<sub>3</sub> (n=46)

UV fluences were pooled for PARAFAC analysis as the chemical oxidants are the primary mechanism for changes in fluorescent NOM. Validated *n*-component models were generated using split-half validation and the line plots and contour plots for each model are included in Appendix B. **Figure 3-6** shows the validated model outputs for excitation and emission component wavelengths in the untreated sample dataset. Component 1 depicts the clear presence of fulvic-like fluorophores similar to those detected in Suwannee River Fulvic Acid (1S101F), with peak emissions at 255 nm excitation and 455 nm emission (Sierra et al., 2005). Component 2 is capturing the amino acid-like material in the water matrix with the primary peak located at 250 nm excitation and 450 nm emission wavelengths (Perucho et al., 2015). Component 3 is humic in nature with primary and secondary peaks aligning with those of the Suwannee River humic acid profile (Perucho et al., 2015). This region is also associated with the hydrophobic acidic fraction (HOA) of NOM (Hudson et al., 2007; Marhaba, 2000; Marhaba & Lippincott, 2000). Component 4 indicates the presence of additional biological/protein-like material within the source water with a tyrosine-like peak at

230 nm excitation and 350 nm emission and a tryptophan-like peak at 280 nm excitation and 340 nm emission (Marhaba, 2000; Marhaba & Lippincott, 2000; Markechová et al., 2013).

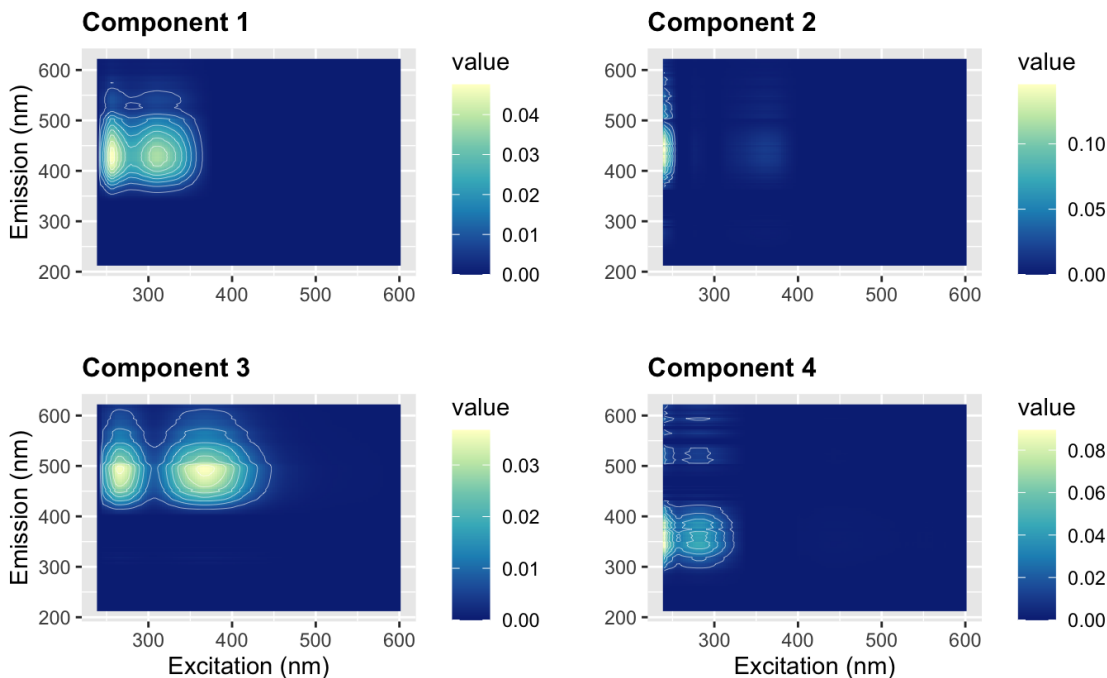


**Figure 3-6** PARAFAC model for untreated post-filter Pockwock Lake water samples. (n=44)

The models for both hydrogen peroxide and ozone based AOPs reinforced the concept that different AOPs maintain a priority with the NOM fractions that they react with. The 10 mg L<sup>-1</sup> hydrogen peroxide AOP model indicated that the protein-like (tyrosine / tryptophan) (**Figure 3-6- Component 4**) and amino acid-like (**Figure 3-6- Component 2**) regions are impacted by peroxide based AOPs. The contour plots in **Figure 3-7** show that the protein-like region is absent in peroxide model and the modelled fulvic and humic-like components are comparable to those in the untreated model. The results indicate that peroxide based AOP is oxidizing the amino acid-like and the protein-like fractions of the fluorescent NOM. Although geosmin does not fluoresce, the changes in similarly structured compounds in the amino acid and

protein-like regions also supports the idea that geosmin has a faster oxidation priority in peroxide AOPs when compared to ozone AOPs.

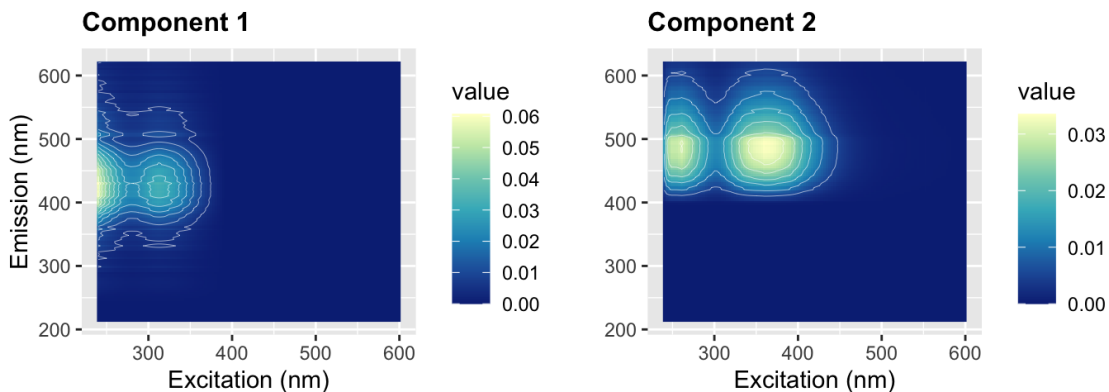


**Figure 3-7** PARAFAC model for UV and 10 mg L<sup>-1</sup> H<sub>2</sub>O<sub>2</sub> treated Pockwock Lake Water. (n=46)

The 10 mg L<sup>-1</sup> ozone treated dataset also exhibited changes in fluorescent NOM composition when compared to the untreated model. **Figure 3-8** shows the contour plots for the 3-component model for the 10 mg L<sup>-1</sup> ozone dataset. Components 1 and 2 in the ozone model correspond with components 1 and 3 in the untreated model and describe the fulvic and humic-like regions of the fluorescent NOM. Component 3 describes the HOB, HIA, and HIB NOM fractions (tyrosine/tryptophan-like) region of the fluorescent NOM.

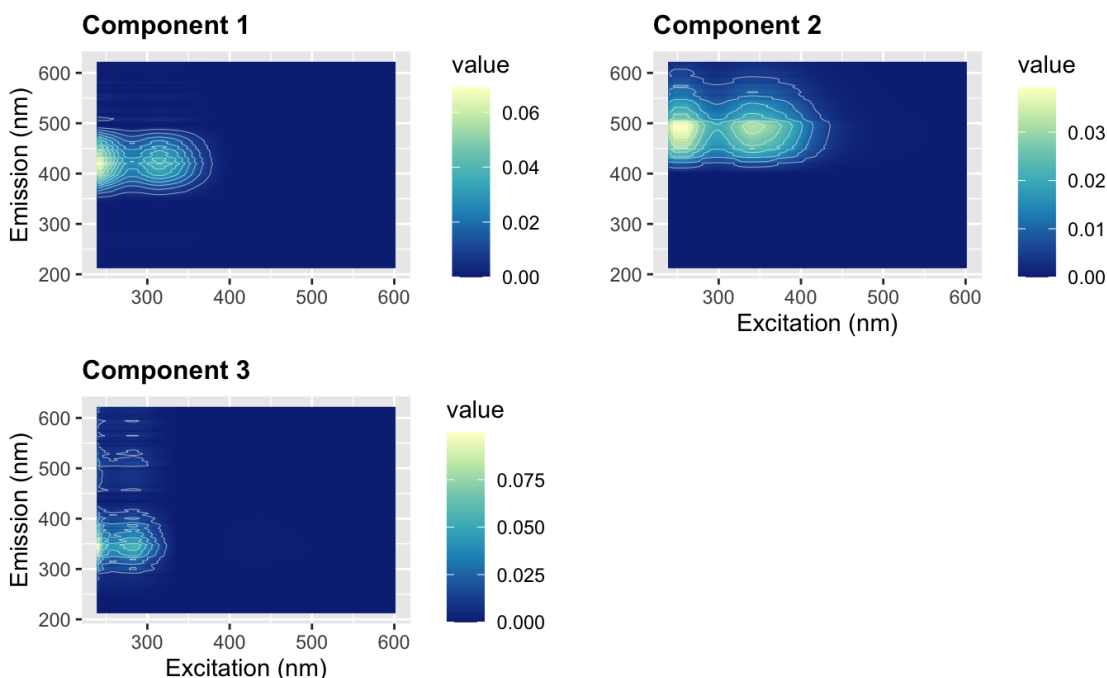


**Figure 3-8** PARAFAC model for UV and 10 mg L<sup>-1</sup> O<sub>3</sub> treated Pockwock Lake Water. (n=46)

A summary of all the PARAFAC models for each of the AOP treatments and the corresponding NOM fraction they describe is provided in **Table 3-5**. The HOA fraction is the primary contributor of fluorescent NOM in the water matrix despite only contributing 7% of the total DOC for Pockwock Lake. The humic and fulvic-like compounds within Pockwock Lake are well defined in all the models which is expected given that fulvic and humic material are the major NOM constituents of surface waters. The HIN fraction, which represents 24% of the total DOC is not well represented in any of the models suggesting that the HIN within Pockwock Lake is non-fluorescing in nature.

The HON fraction that constitutes 44% of the DOC of Pockwock Lake is only represented in the untreated and UV models. These results suggest 2 outcomes:

- 1) The HON within Pockwock Lake is composed of mainly long chain, non-aromatic hydrocarbons and carbohydrates which are non-fluorescing in nature (Edzwald, 1993; Marhaba, 2000; R. T. Williams & Bridges, 1964)

- 2) The portions of the HON fraction that does fluoresce undergoes high priority reactions with both ozone and hydrogen peroxide when they are introduced into the water matrix.

**Table 3-5** Fluorescent NOM regions described by modelled PARAFAC components for AO treatments

	Untreated	UV	UV + 1 mg L <sup>-1</sup> O <sub>3</sub>	UV + 10 mg L <sup>-1</sup> O <sub>3</sub>	UV + 1 mg L <sup>-1</sup> H <sub>2</sub> O <sub>2</sub>	UV + 10 mg L <sup>-1</sup> H <sub>2</sub> O <sub>2</sub>
<i>Component 1</i>	HOA, Fulvic	HOA, Fulvic	HOA, Fulvic	HOA, Fulvic	HOA (Fulvic), HOB, HIB	HOA (Fulvic), HOB
<i>Component 2</i>	Amino Acid-like	HIN, Humic	HOA, HOB, HIA, HIB, Humic	HIN, Humic	HOA, Humic	HIN, Humic
<i>Component 3</i>	HIN, Humic	Amino Acid-like	-	HOB, HIB, HIA	-	-
<i>Component 4</i>	HOA, HOB, HIB, HIA, HON	HON, HIA, HIB, HOA	-	-	-	-

### 3.5 Conclusion

The changes and degradation of NOM in an AO-treated, post-filter, geosmin-containing natural water was analyzed in this chapter. Geosmin was effectively removed below human detection levels in 1000 mJ cm<sup>-2</sup> fluence, 10 mg L<sup>-1</sup> hydrogen peroxide samples suggesting that peroxide-based AOPs are better suited for taste and odor compound removal when compared UV and ozone-based AO. The geosmin removal data shows that AOP treatments are primarily driven by chemical oxidation with UV acting as a supplementary support.

The reaction kinetics between UV and UV-peroxide AO with pCBA were calculated for a range of pH. Hydrogen peroxide AO treatments were shown to produce 10 x the amount of •OH radicals when compared to UV photolysis alone. Differences between peroxide-based and ozone-based AO treatments are explained by coupling SUVA and FEEM data. Ozone-based UV-AOPs primarily oxidizes the humic and fulvic-like portion of the NOM and degrades it into aliphatic, low-molecular weight, non-UV absorbing compounds whereas peroxide-based AOPs oxidize protein-like material faster than humic and fulvic material. Ozone AO treatments had an overall lower SUVA when compared to all other AOPs examined in this study.

The changes in the NOM fractions between pre and post geosmin infiltration into Pockwock Lake were also examined. The NOM of the lake shifted from the HOA fraction being dominant to HON contributing the largest proportion of DOC after geosmin infiltration. FEEM data was modelled for each of the different AOPs. FEEM models revealed the portions of NOM that are most susceptible to chemical and photooxidation. HOA and HOB fractions within Pockwock Lake fall into the category of ozone susceptible compounds. Peroxide-based UV-AOP tends to oxidize the protein-like and aromatic portion of the fluorescent NOM which are linked to the HIA, HIB, and HOB fractions. The HON fraction, which contributed the most to Pockwock Lake DOC, is largely non-fluorescent. The portion of the HON that does fluoresce is

oxidized by both peroxide and ozone AOPs. Changes in NOM fractions for Pockwock Lake between 2010 and 2012 indicate that as further brownification occurs, the oxidation of hydrophilic compounds should be monitored, and additional fractionation of Pockwock Lake water is needed to understand how NOM has changed since 2012.

Overall, peroxide based AOP appear to be the best technology for the degradation of NOM with a water matrix given the volume of radicals that are produced when paired with UV light. The enhanced volume of radicals generated by UV / peroxide processes further supports the oxidation of different NOM fractions when compared to ozone. A higher concentration of radicals produced increase the chance of radicals oxidizing secondary contributors to NOM, such as protein and biological-like fluorescent NOM.

## 4 Assessment of disinfection by-product formation potential in a natural water matrix after exposure to advanced oxidation processes

A portion of the work in this chapter has been published in ACS Environmental Science and Technology: Water Research and Technology

Trueman, B.F., MacIsaac, S.A., Stoddart, A.K., Gagnon, G.A. 2015. Prediction of disinfection by-product formation in drinking water *via* fluorescence spectroscopy. *ACS ES&T WRT*,

### 4.1 Abstract

This chapter assesses the efficacy of AOPs as a treatment technology for the reduction of disinfection byproduct formation potential in a natural water matrix that has historically experienced elevated THM and HAA concentrations in treated water. The impacts of AOPs on the natural organic matter within the water matrix were evaluated using both fluorescent excitation emission matrices and size exclusion chromatography. UV, H<sub>2</sub>O<sub>2</sub>/UV, and O<sub>3</sub>/UV AOPs at fluences of 100 mJ cm<sup>-2</sup> and 1000 mJ cm<sup>-2</sup> with chemical concentrations of 1 mg L<sup>-1</sup> and 10 mg L<sup>-1</sup> were used as the treatments for examining changes in DBPs in this study. Peroxide based AOPs tended to enhance DBP<sub>fp</sub> for both THMs and HAAs. 10 mg L<sup>-1</sup> peroxide treatments exceeding the MACs in both DBP categories. SEC data indicated that both ozone and hydrogen peroxide AOPs form unique, low molecular weight compounds, which are unique to each AO treatment type. Low molecular weight oxidation byproducts are hypothesized to be the source of the additional DBP formation potential when utilizing AOPs. Peroxide based AOPs formed oxidation compounds that were favorable in DBP formation whereas ozone based AOPs did not form DBP favorable oxidation compounds. Enhanced formation of DBPs when using AO highlights the fact that a thorough understanding of the NOM profile of a natural water is necessary before applying this technology. Improper use of AO technology at full scale may inadvertently shift the NOM profile of a water matrix to be more favorable to form DBP<sub>s</sub> after oxidant exposure.

### 4.2 Introduction

Changing water quality in lakes that are experiencing brownification requires new approaches for water treatment. AOP may provide an option for treatment solutions that were previously unavailable. Some studies have shown that while AOP may be useful for the degradation of targeted organic compounds, they may inadvertently enhance DBP formation (Bond et al., 2009; Dong et al., 2019; Ike et al., 2019; Krasner et al., 2006; Nieuwenhuijsen, 2000). Specifically, ozone-based AOP have been linked to excess bromate formation (von Gunten & Oliveras, 1998; von Gunten & Hoigne, 1994). This chapter examines a natural water matrix from a water treatment facility, located in North Sydney, Nova Scotia, that has experienced historic DBP formation problems. A selection of UV-based AOP were applied to post-filter water from the Pottle Lake Water Treatment Plant (PLWTP). The formation of trihalomethanes (THMs) and haloacetic acids (HAAs) is regulated in Canada with maximum allowable concentrations (MACs) for THMs having an MAC of  $100 \mu\text{g L}^{-1}$  and HAAs having an MAC of  $80 \mu\text{g L}^{-1}$  (Federal-Provincial-Territorial Committee on Drinking Water (Canada), 2006; Federal-Provincial-Territorial Committee on Drinking Water (Canada) et al., 2008). THMs and HAAs are two of the most common DBPs and are thought to be carcinogenic in nature (Cotruvo & Amato, 2019; World Health Organization, 2005).

#### **4.2.1 Pottle Lake Water Treatment Plant**

The PLWTP was commissioned in 2010 and serves approximately 19,000 residents in northeastern Cape Breton with a capacity of 4.2 million gallons per day. The plant is equipped with ultrafiltration membranes that serve as the primary removal mechanism of organic material (Cape Breton Regional Municipality, 2015). Pottle Lake is adjacent to a major highway and is also skirted by the town of North Sydney. The proximity to human activity suggests that the NOM within the lake is anthropogenic in nature.

The PLWTP has experienced elevated DBP concentrations since the opening of the plant in 2010. The ability of advanced oxidation to alter the NOM profile of a water

matrix suggests that it is a potential treatment option for DBP precursor removal within Pottle Lake. The typical water quality values for Pottle Lake during experimentation is shown in **Table 4-1**.

**Table 4-1** Typical values for Pottle Lake during the experimentation period.  $\pm$  values represent a 95% confidence interval about the mean.

<i>Parameter</i>	<i>Value</i>
<i>TOC (mg L<sup>-1</sup>)</i>	1.80 $\pm$ 0.167
<i>UV<sub>254</sub> (cm<sup>-1</sup>)</i>	0.057 $\pm$ 5.28E-03
<i>SUVA (L mg<sup>-1</sup>m<sup>-1</sup>)</i>	3.18 $\pm$ 0.176

#### 4.2.2 Disinfection Byproduct Formation Potential

PLWTP filtered water samples were used as the working water matrix for the investigation of disinfection byproduct precursor study. The PLWTP has experienced elevated HAA concentrations in their finished water since the opening of the treatment plant in 2010. AOP samples were collected after UV exposure and prepared for analysis by following the formation potential according to US EPA Methods 552.1 and 552.2 (Hodgeson et al., 2003; Hodgeson & Becker, 1992). The formation potential chlorine dose ranged from 2.8-3.5 mg L<sup>-1</sup> of sodium hypochlorite. The chlorine dose was adjusted over the course of the experiment as the advanced oxidation processes lead to inconsistent residual chlorine in DBP<sub>fp</sub> samples.

DBPs are a well-understood group of organic compounds that are commonly found in treated drinking water (Nieuwenhuijsen, 2000). DBPs form when NOM, typically in the form of broken-down vegetation within a watershed, reacts with chlorine in drinking water treatment plants. DBPs are suspected to be carcinogenic (Villanueva et al., 2004). HAAs are not currently regulated in Canada but have a guideline maximum allowable concentration (MAC) of 100  $\mu$ g L<sup>-1</sup>. THMs are regulated in North America, along with chloroform (a species of THM), with the MAC of 80  $\mu$ g L<sup>-1</sup> (Federal-Provincial-Territorial Committee on Drinking Water (Canada), 2006). There are a growing number of emerging DBPs originating from chloramine and ozone

usage in drinking water treatment including bromate and furanones (Krasner et al., 2006). Recent research suggests that these emerging DBP compounds may be more genotoxic and carcinogenic than currently regulated compounds (Richardson, 2003). Emerging disinfection byproducts, in part, originate from water utilities choosing alternative disinfectants as a means to reduce current regulated DBPs. Some of these emerging DBPs, such as iodinated disinfection byproducts (I-DBPs) have proven to be more toxic when compared to THMs and HAAs (Dong et al., 2019). Variations in treatment technologies and the nature of source water NOM results in the occurrence of new reactions within the water matrix, leading to new compounds being formed (Krasner, 2009).

#### **4.2.3 DBP Precursor Material**

The characterization of disinfection byproduct precursor material is important for the tertiary improvement of drinking water quality. The removal of DBP precursor material results in lower concentrations of THMs and HAAs forming as end products. Advanced oxidation has been hypothesized to have potential to remove this material (Chin & Bérubé, 2005). AOP can also reduce the  $DBP_{fp}$  of a water matrix with reductions in THM and HAA  $DBP_{fp}$  by 77% and 62% respectively (Lamsal et al., 2011).

Oxidation can also inadvertently increase  $DBP_{fp}$  in a water matrix when processes are not properly controlled (Singer, 1999). Oxidation transforms NOM to lower molecular weight states which are more prone to the formation of DBPs (Hammes et al., 2006). Specifically, humic material is connected to higher production of both THMs and HAAs after undergoing oxidation when compared to fulvic-like material within a water matrix (Reckhow et al., 1990). Furthermore, ozone-based AOP have been shown to alter NOM and increase DBP precursor material in certain water matrices (Miltner et al., 1992). Ozone-based AOP are linked with bromate formation whereas hydrogen peroxide-based AOP do not cause bromate formation (Ivančev-Tumbas, 2014; Peter & Von Gunten, 2007). An understanding of the specific natural water matrix is recommended to minimize the side effects of AOP for a water utility if they are

considering employing AOP technology at full scale. Due diligence regarding this issue would require bench scale testing, as is the aim of this study, in order to ensure maintained drinking water quality.

## **4.3 Methods**

Methods detailing how UV exposure was conducted and controlled are described in previous chapters. The specific methods for the different water quality parameters are also described in previous sections. The PARAFAC analysis conducted in this chapter follows the same method outlined in Chapter 3.

### **4.3.1 THM and HAA quantification**

Quantification of THM and HAAs was performed according to US EPA Methods 552.1 and 552.2 (Hodgeson et al., 2003; Hodgeson & Becker, 1992). For THM and HAA analysis, liquid-liquid extraction by pentane and methyl *tert*-butyl ether (MTBE), respectively, were employed prior to detection by gas chromatography with an electron capture detector (GC-ECD). All DBP analysis was performed using a Varian CP-3800 gas chromatograph equipped with a Varian CP-8400 autosampler and an Agilent VF-5ms column of dimensions 30 m × 0.25 mm × 0.25 μm. High purity helium was used as the carrier gas in all separations. Method detection limits for chloroacetic, bromoacetic, dichloroacetic, trichloroacetic, bromochloroacetic, dibromoacetic, tribromoacetic, bromodichloroacetic, and chlorodibromoacetic acids were 4.0, 2.5, 2.0, 1.5, 1.5, 1.0, 8.5, 2.0, and 3.2 μg L<sup>-1</sup>, respectively. Method detection limits for chloroform, dichlorobromomethane, dibromochloromethane, and bromoform were all 1.5 μg L<sup>-1</sup>.

### **4.3.2 Size Exclusion Chromatography Analysis**

Size exclusion chromatography (SEC) samples were collected for all treatments using a Parkin Elmer Series 200 SEC unit. SEC data was exported to R for analysis in R-

Studio (Version 1.3.959). Chromatograms were generated using a custom R script, that has been provided in Appendix D, to ensure consistent and reproducible plotting of NOM data. Chromatograms were normalized to make comparisons between AO treatments obvious and include the range of absorbance data in the visualization portion of the code.

## **4.4 Results and Discussion**

### **4.4.1 Pottle Lake DBP Formation Potential**

Boxplots for the THM AO set of data for Pottle Lake are shown in **Figure 4-1**. The median untreated THM concentration for Pottle lake is  $74.98 \mu\text{gL}^{-1}$ , which is below the guideline threshold of  $100 \mu\text{gL}^{-1}$ . High UV fluence ( $1000 \text{ mJcm}^{-2}$ ) peroxide based AOP tended to increase the  $\text{THM}_{\text{fp}}$  as expected with the  $10 \text{ mgL}^{-1}$  peroxide dose resulting in the largest increases in formation potential. Ozone based AOP did not appreciably increase the formation potential regardless of UV fluence or ozone dose. The high UV fluence and high ozone dose resulted only in marginal increases in  $\text{THM}_{\text{fp}}$  whereas surprisingly, the low UV fluence and high ozone dose resulted, on average, a reduction in the THM formation potential when compared to untreated samples.

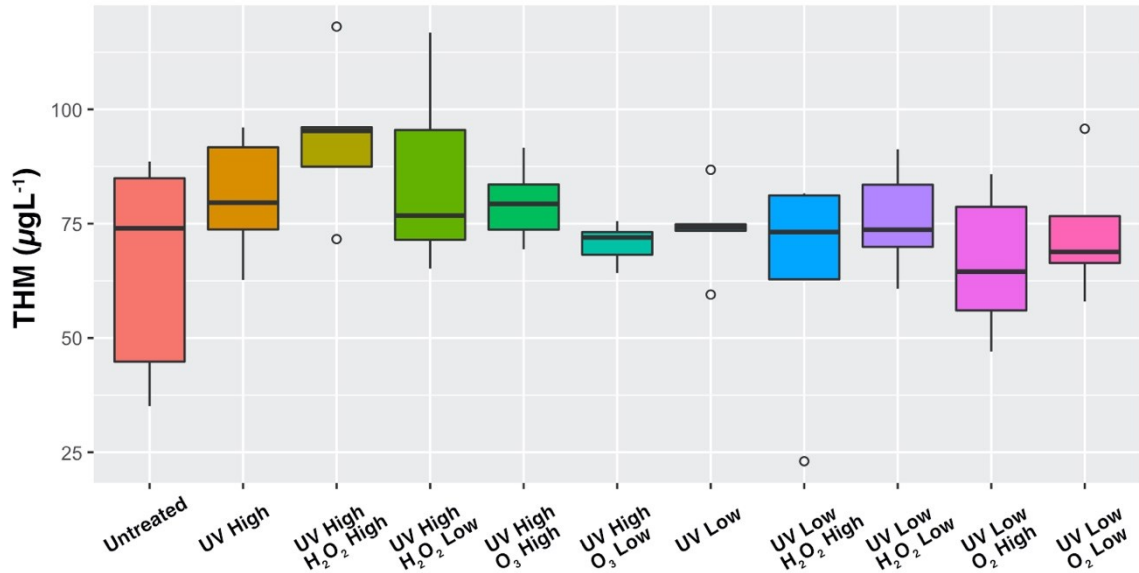


**Figure 4-1** Pottle Lake THM concentration before and after AOP exposure

The HAA results indicate that peroxide based AOP do play a role in the increase of formation potential as shown in **Figure 4-2**. Untreated Pottle Lake water had a median HAA<sub>fp</sub> of 63.9 µg/L<sup>-1</sup>, which is below the 80 µg/L<sup>-1</sup> guideline threshold. The high peroxide and high UV fluence AOP stand out, as the median formation potential concentration is 107.7 µg/L<sup>-1</sup>, which is nearly double when compared to untreated samples and is almost 30 µg/L<sup>-1</sup> above the regulated limit. The high UV and low peroxide treatment resulted in a median formation potential of 87.3 µg/L<sup>-1</sup> which is elevated compared to untreated samples but not above Health Canada guidelines. Low fluence UV treatments did not result in a meaningful increase in formation potential for any treatment, which suggests that the interaction between photooxidation processes and chemical oxidation is the primary driver of changes in NOM in terms of DBP precursor material.

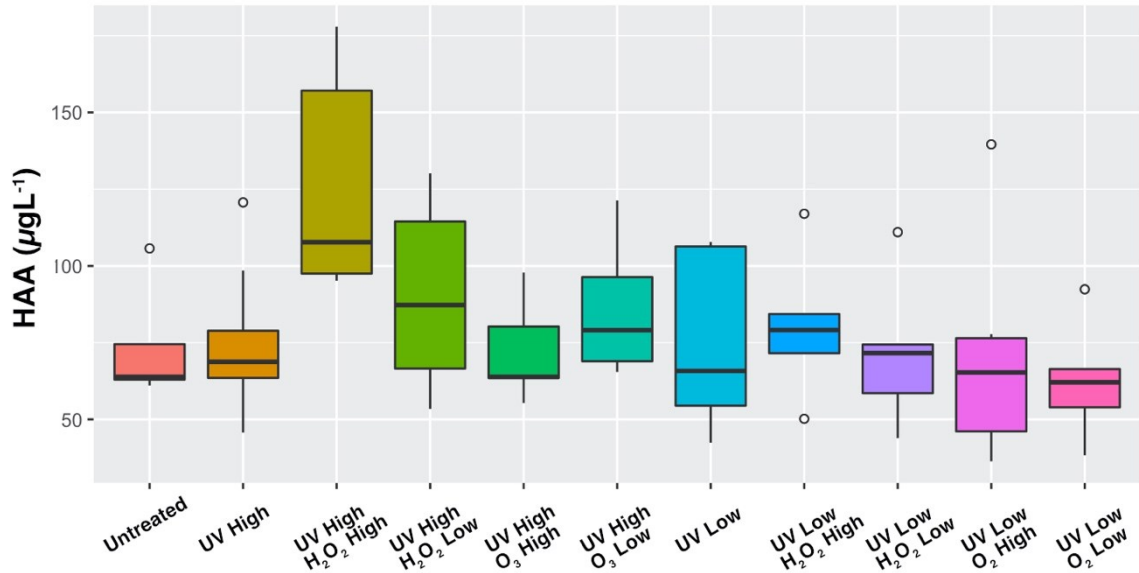


**Figure 4-2** Pottle Lake HAA concentration before and after AOP exposure

#### 4.4.2 Parallel Factor Analysis (PARAFAC) of AOP Exposed Pottle Lake Water

PARAFAC analysis was used to assess portions of the fluorescent NOM for Pottle Lake that are associated with DBP formation. AOP treatments were pooled in a similar fashion as described in Chapter 3. The validated 2-component model for Pockwock Lake is shown in **Figure 4-3**. Component 1 describes the hydrophobic acidic (HOA), hydrophilic neutral (HIN), and fulvic nature of untreated Pottle Lake samples. Component 2 describes the hydrophobic basic (HOB), hydrophilic basic (HIB), and humic nature of the Pottle Lake NOM.

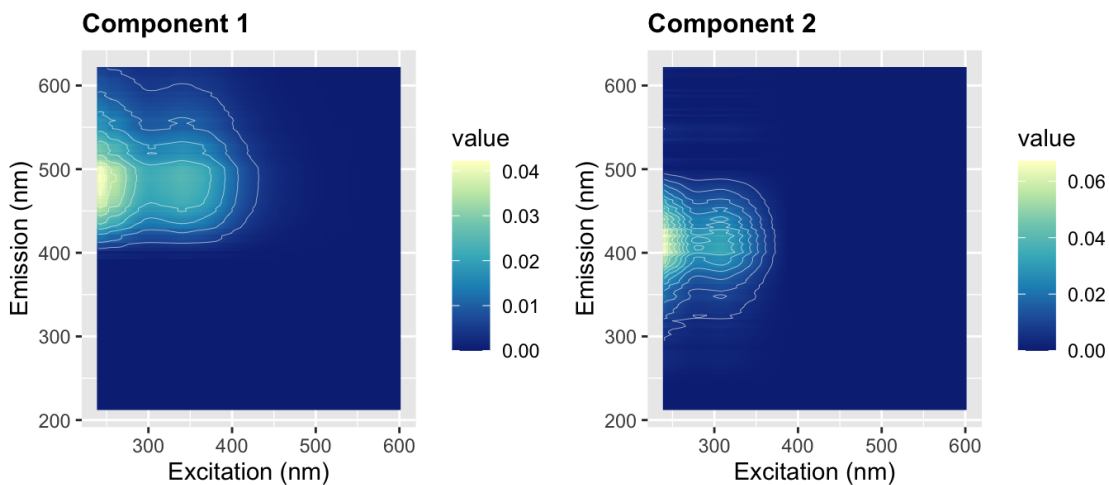


**Figure 4-3** PARAFAC model for untreated post-filter Pottle Lake water samples. (n=24)

The PARAFAC models for each of the AO conditions are further summarized in **Table 4-2**. PARAFAC analysis for this water matrix does not indicate specific changes in Pottle Lake NOM after exposure to AOP. The one notable difference between models is the NOM described by Component 1 and Component 2 in the UV and 10 mg L<sup>-1</sup> H<sub>2</sub>O<sub>2</sub> dataset is exchanged when compared to all other Pottle Lake models. This result suggests that the 10 mg L<sup>-1</sup> peroxide treatment has a slightly greater impact on the HOA and fulvic-like material within the Pottle Lake water matrix compared to the HOB and humic like NOM.

**Table 4-2** Summary of fluorescent NOM PARAFAC models for Pottle Lake

	Untreated	UV	UV + 1 mg L <sup>-1</sup> O <sub>3</sub>	UV + 10 mg L <sup>-1</sup> O <sub>3</sub>	UV + 1 mg L <sup>-1</sup> H <sub>2</sub> O <sub>2</sub>	UV + 10 mg L <sup>-1</sup> H <sub>2</sub> O <sub>2</sub>
<i>Component 1</i>	HOA, HIN, Fulvic	HOA, Humic	HOA, HIN, Fulvic	HOA, HIN, Fulvic	HOA, HIN, Fulvic	HOB, HIN, Humic
<i>Component 2</i>	HOB, HIB, Humic	HOA, HIN, Fulvic	HOA, HOB, Humic	HOB, HIN, Humic	HOB, HIN, Humic	HOA, HIN, Fulvic

**Figure 4-4** shows the contour plots for the UV and high H<sub>2</sub>O<sub>2</sub> model. The difference in modelled components suggests that DBP<sub>fp</sub> is primarily related to the hydrophobic neutral fraction of NOM. Ozone AOPs react with hydrophilic neutral compounds with a low priority and are reported to react with both humic and fulvic substances first (Huang et al., 2004).

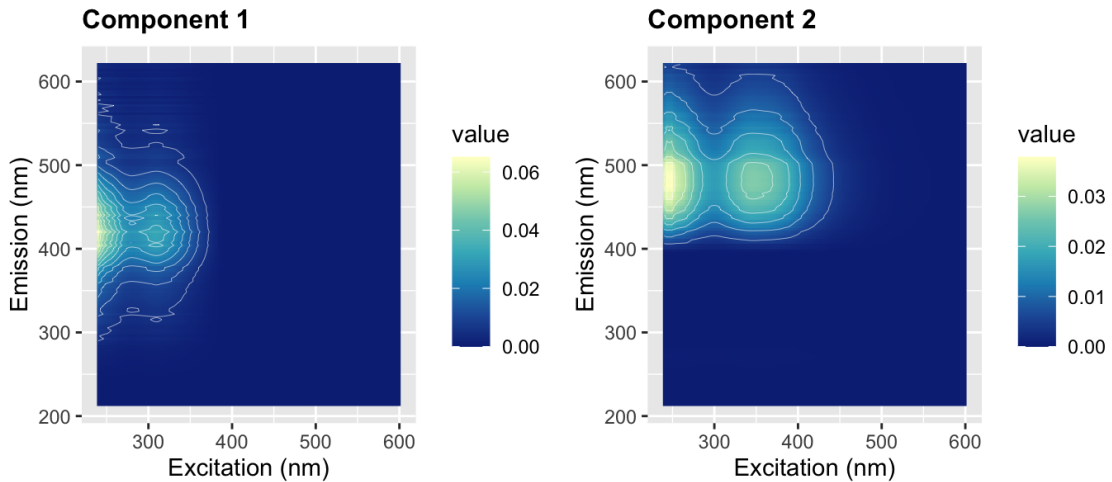


**Figure 4-4** PARAFAC model for UV and 10 mg L<sup>-1</sup> H<sub>2</sub>O<sub>2</sub> post-filter Pottle Lake water samples. (n=45)

SEC data was in alignment with both FEEM and DBP<sub>fp</sub> data in terms of the impacts of AOP on the NOM profile of Pottle Lake water. UV treatments did not cause a reduction or shift in peaks for SEC chromatograms, suggesting that UV based AOP do not initiate

a significant amount of oxidation of NOM. **Figure 4-5** shows the average SEC response for untreated samples compared to the high UV ( $1000 \text{ mJ cm}^{-2}$ ), high  $\text{H}_2\text{O}_2$  ( $10 \text{ mg L}^{-1}$ ), treatment and the high UV ( $1000 \text{ mJ cm}^{-2}$ ), high  $\text{O}_3$   $10 \text{ mg L}^{-1}$ ) treatment. The high  $\text{H}_2\text{O}_2$  treatment indicates that there is formation of a new 10-minute point of elution. There is also shifting of peaks at the 20-minute mark which form low molecular weight compounds later in the elution time. This peak shifting coincides with increased  $\text{DBP}_{\text{fp}}$  for high UV and high  $\text{H}_2\text{O}_2$  AOP is in alignment with previous research that makes this connection (Hammes et al., 2006; Krasner, 2009; Krasner et al., 2006; Nieuwenhuijsen, 2000; Villanueva et al., 2004). The high ozone treatment forms an emergent peak that is detected at the 4-minute elution time and an overall reduction of lower molecular weight compounds later in the elution when compare to untreated samples. Ozone based AOP have also been proven to form DBP precursor material which is potentially capable to form via low molecular weight compounds (Chin & Bérubé, 2005; Chowdhury et al., 2008; Westerhoff et al., 1999). The discrepancy in  $\text{DBP}_{\text{fp}}$  between ozone and peroxide based AO for Pottle Lake water is related to the difference in peak shifting for peroxide and ozone samples as shown in **Figure 4-5**. Supplemental SUVA data in **Appendix C** indicates that both higher concentrations ozone reduced SUVA whereas peroxide treatments at a similar concentration do not change SUVA a significant amount compared to untreated samples when using 95% confidence intervals. Differences in  $\text{DBP}_{\text{fp}}$  for similarly concentrated AO treatments highlights the importance of understanding the nature of the NOM in a water source before applying oxidation technologies at full scale. Additional figures that illustrate the SEC chromatograms for each of the different AOP conditions are provided in Appendix C.

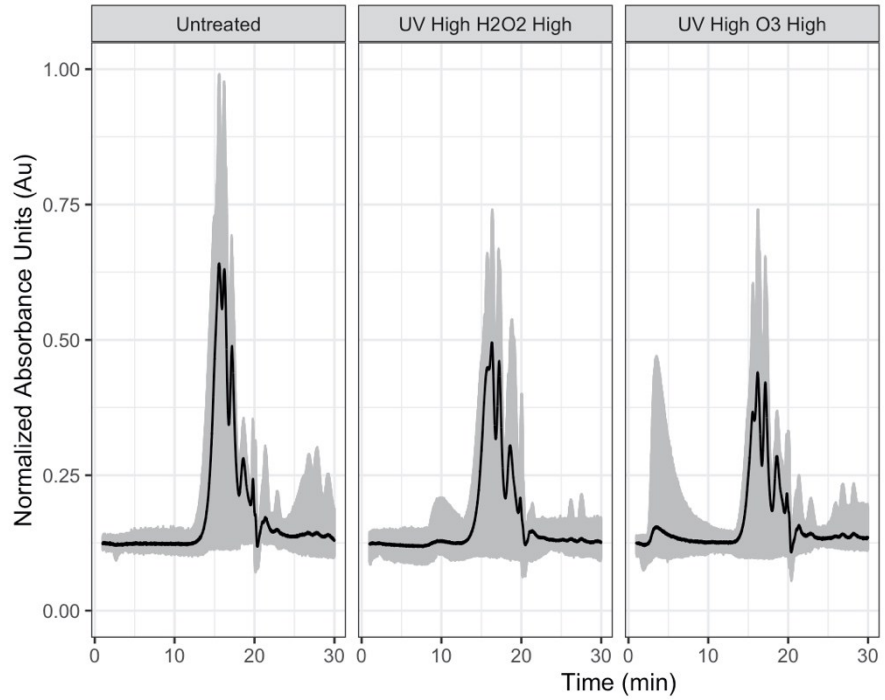


**Figure 4-5** Average SEC chromatogram comparing untreated samples to AOP processes that changed NOM the most. The grey area illustrates the range of SEC response across the dataset and the black line indicated the average.

## 4.5 Conclusion

The application of AOP on a natural water to reduce the  $DBP_{fp}$  was investigated for Pottle Lake, which has a history of finished water with elevated DBPs. The results of this study highlight the fact that although AOP can degrade any type of organic matter, the order and priority of the degradation is notable and requires more research. The experiments outlined in this chapter demonstrates how different types of AO applications result in altering different portions of the NOM profile of a real water matrix. Peroxide based AOP caused an increase of both THM and HAA concentrations that exceeded MACs in some instances. Ozone based AOPs did not cause a notable increase of THM or HAA formation but did generate low molecular weight oxidation byproducts that were detected via SEC. UV AOP also did not cause an increase in THMs or HAAs when compared to untreated samples. The difference in changes in the  $DBP_{fp}$  for peroxide and ozone AOPs of similar concentrations is explained by differences in the post-oxidation NOM as exhibited in SEC chromatograms. Both hydrogen and ozone AO generated low molecular weight compounds, but these compounds differed in size with ozone-based AO treatments forming the smallest compounds. Differences in oxidation byproducts indicates that the portion of the NOM that first reacts with ozone within the Pottle Lake water matrix is able to be fully oxidized when compared to peroxide based AOPs. Partial oxidization of NOM is hypothesized to be the source of additional reactive material for DBPs. In summary, this chapters provides important information for utilities that may be considering the use of AOP as a response changing water quality due to lake recovery. A thorough understanding of the NOM profile of a lake must be understood before choosing an AOP type and dosing regimen. Improper use of oxidation technologies may inadvertently change the NOM profile of a natural water matrix to a state that is more favourable to DBP formation. Further work regarding classification of partially oxidized NOM is recommended in order to better understand the outcomes of AO use in natural waters and to develop an understanding of characteristics of NOM profiles that are conducive to DBP formation.



## **5 Modelling of fluorescent excitation emission matrices to assess the changes in natural organic matter after advanced oxidation treatment**

### **5.1 Abstract**

The study outlined in this chapter provides a tool and framework for characterizing changes in the fluorescent NOM profile of natural and synthetic waters after exposure to AOPs. Both principal component analysis and k-means distancing were used to describe and classify AOP treated water samples based on AOP treatment type and water source. A suite of analysis tools was developed for Matlab that allow for better accessibility of fluorescent excitation emission matrix (FEEM) data. A simple interface was also developed within the Matlab terminal to guide users through the stages of FEEM analysis. Two datasets were used for this study 1) a synthetic water matrix dataset, composed of varying concentrations of common NOM constituents (n= 63) and 2) a natural water matrix dataset, composed of pooled samples from advanced oxidation treated water collected from two source waters within Nova Scotia (n= 531). The PCA and k-means modelling proved to be a useful characterization tool for classifying water samples by fluorescent constituents and by oxidation exposure. k-means distancing for the real water dataset allowed for classification of samples based on lake type. The k-means approach for clustering fluorescent PC score resulted in 84% classification accuracy when classifying HRM source water samples within the same cluster and 71% accurate when classifying CBRM source waters in the sample cluster. Clustering of subsequent PC scores resulted in a 96% grouping of all 10 mg L<sup>-1</sup> hydrogen peroxide, 1000 mJ cm<sup>-2</sup> samples into the same cluster. Utilizing NOM fluorescence data to characterize samples allows for better descriptions of changes that the NOM profile of a natural water goes through as a result of oxidation.

## 5.2 Introduction

AOPs are needed to adequately respond to changing surface waters that are no longer treatable when using traditional technologies. New tools and approaches to examine changes in NOM are needed in order to safely use AOPs. NOM tools that are easily interpreted from a quantitative perspective will provide the proper information for both researchers and water utilities in understand how NOM behaves after exposure to AOP. The need for more simple and efficient tools for understanding changing NOM has been noted by Ivančev-Tumbas (2014). One particular tool in this assessment is Fluorescent excitation emission matrices (FEEMs). FEEMs hold important information regarding the fluorescent natural organic matter (NOM) within a water matrix. FEEMs often consist of thousands of data points, which are easy to interpret qualitatively but are difficult to interpret quantitatively. This inherent barrier within FEEM data results in inefficient utilization of datasets, leading to only understanding the superficial aspects of fluorescent NOM.

Principal Component Analysis (PCA) was used on a selection of two FEEM datasets as a means to address this issue. PCA is a versatile tool which is suited to manage large matrices of data. This approach was inspired by the DomFluor toolbox, developed by Bro, which has been used in numerous studies to assess fluorescent NOM profiles (Bro, 1997). The DomFluor toolbox utilizes parallel factor analysis (PARAFAC) to deconvolute distinct components within fluorescent excitation emission matrices. PARAFAC analysis fits weighted arrays as 'factors' to blindly deconvolute  $n$ -way data in order to reveal interactions or patterns within a dataset (Harshman & Lundy, 1996). Another common method for assessing FEEM data is fluorescence regional integration. Fluorescence regional integration sums the FEEM signal in designated regions that are associated with like compounds, such as, humic material or protein material (W. Chen et al., 2003; Markechová et al., 2013). While fluorescence regional integration is a simple approach, it only describes general changes and shifts in the

fluorescent NOM within a water matrix. The FRI approach does not provide any description of how these changes are represented within a full FEEM dataset.

Previous studies that have examined the application of PCA for FEEM data have used limited datasets and examined a limited band of the fluorescent excitation-emission range (Peleato & Andrews, 2015). FEEM has been used to observe changes in NOM as a result of TiO<sub>2</sub> – UV processes (Valencia et al., 2014). These studies show a potential for the application of this technique on FEEM datasets, as the fluorometer that was used has a boarder excitation-emission range and the dataset used in this study is an order of magnitude larger than previous studies. Also, PCA is ubiquitous in scientific literature and fully implemented in several common programming languages, meaning that numerous resources and studies are available for reference. This makes PCA an attractive third option to PARAFAC and FRI for researchers who may have collected FEEM datasets but have not maximized the information that can be gathered from them. Matlab was used as the programming language for this study and the script has been optimized for handling FEEM from the Horiba Aqualog fluorometer. It should be noted that the overall approach and subsequent application of the core code is applicable for any fluorometer and programming language.

Upon conducting PCA, k-means clustering was applied to principal component scores. K-means clustering blindly takes data points in  $n$ -way dimensions and groups it into  $p$  classifications (Hartigan & Wong, 1979; MacQueen, 1967). This approach has had minimal application thus far in water research, but the study outlined in this paper indicates that k-means clustering is useful in characterizing fluorescent NOM. The goal of this paper is to outline a series of simple visualization and classification tools, which are bundled in a suite of modules (provided in the Supporting Information) that allow a user to interpret large FEEM datasets easily and swiftly. The three-fold visualization approach by using contour plots, scatter plots and k-means clustering gives users a clear visual analysis of what is occurring with the fluorescent NOM in a dataset while still providing quantitative data.

Two different FEEM datasets (i.e., synthetic water, and surface water) were used for assessing the efficacy of PCA for fluorescence data. The synthetic dataset was composed of tryptophan, tyrosine, and Suwanee River humic acid as the contributing compounds to the fluorescent NOM signal. Amino acids are representative of protein-like organics and humic acid is representative of the overall organic fluorescent NOM signal that is dominant in the majority of surface waters (Baghoth et al., 2011b). The surface water dataset was composed of post-filter bed water from two different surface waters from Nova Scotia, Canada. Each of the surface waters were treated with a suite of bench scale advanced oxidation processes to build a dataset of varied NOM fluorescence profiles for each surface water. Advanced oxidation processes alter the NOM makeup of water matrices through the generation of hydroxyl radicals and through direct photo-oxidation (Andreozzi et al., 1999). Hydroxyl radicals ( $\bullet\text{OH}$ ) scavenge and oxidize both inorganic and organic matter within the water matrix and can cause drastic changes in the fluorescent NOM profile (Donham et al., 2014). The advanced oxidation process generated samples provide a dataset where different portions of the FEEM profile have been altered via  $\bullet\text{OH}$  oxidation and scavenging (von Sonntag, 2007). Quantification of changes in the NOM fluorescent expression allows for further insight regarding changes in the overall NOM composition. Previous research conducted by Peleato suggests that FEEM is a suitable analysis for assessing changes in fluorescent organic compounds in a water matrix (Peleato, 2016; Peleato et al., 2017). FEEM has also been used in other studies as a parameter for modelling DOC within a water matrix (W. Chen et al., 2003). Previous research has also shown that using PC scores as predictors for multiple linear regression analysis with a FEEM dataset is a valid approach for modelling parameters such as chlorophyll (Çamdevýren et al., 2005).

One of the major challenges when using FEEM datasets is the overlapping nature of excitation-emission profiles (Bro, 1997). Overlapping fluorescent organic compound profiles causes the degradation of some organic compounds to be masked by other organic compounds that are resistant to the changes that are occurring within the water matrix. The nuanced changes within the FEEM profile requires the usage of an

advanced statistical approach to properly observe these changes. The PARAFAC toolbox addresses this issue by deconvolution of 3D signals into 2D excitation-emission factors. The PCA approach utilized in this study resolves these issues similarly to the DomFluor toolbox, while using a more common and user-friendly algorithm to describe patterns and reduce data.

### **5.3 Principal Component Analysis**

PCA was used as the primary method of analysis for reducing the FEEM datasets because of the robustness of its multivariate approach and the popularity of using PCA within the general scientific community (Abdi & Williams, 2010). The applications of PCA are shown in **Figure 5-1** PCA reduces the dimensionality of data so that a maximum amount of variance is explained by a new orthogonal axis for each of the principal components. This concept was first addressed by Pearson stating that “the line which fits best a system of  $n$  points in  $q$ -fold space passed through the centroid of the system and coincides in direction with the least axis of the ellipsoid of residuals” (Pearson, 1901). Reductions in the dimensionality of the data gleans trends and information from datasets, which are not obvious when data is plotted on an original axis. These trends are typically visualized in the form of biplots where a principal component constitutes each axis. The dimensionality of the data in this study far exceeds the number of samples that make up the dataset. For example, there are >15,000 measurements for each of the 531 samples in the natural water dataset.

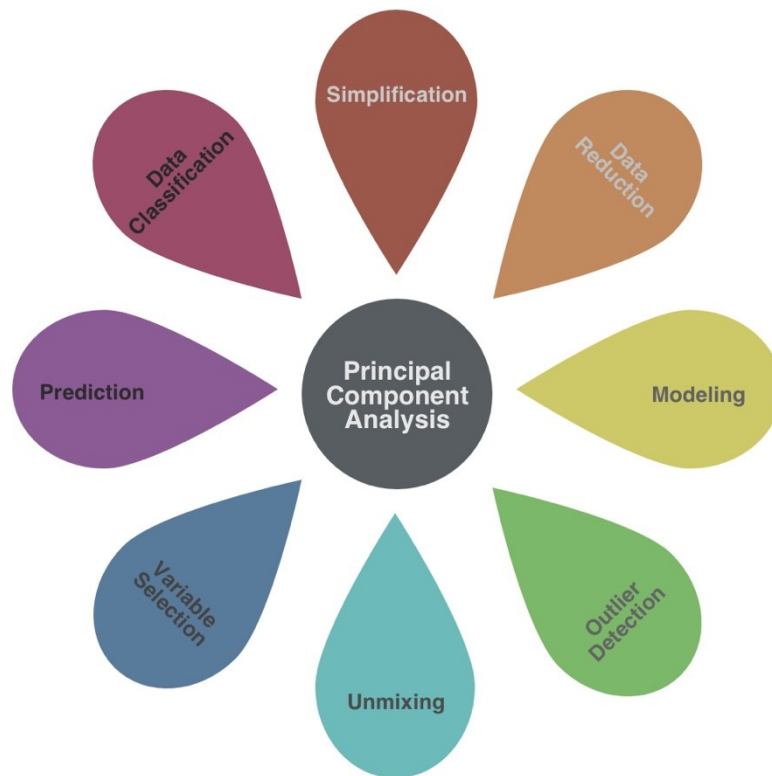


**Figure 5-1** Principal component analysis outcomes. Adapted from (Wold, et al., 1987)

## 5.4 Principal Component Analysis Code Workflow

The code used in this study, included in Appendix E, is structured as a series of functions that are dictated by the user's response to a series of 'Y' or 'N' prompts. Typing 'Y' into the command line will initialize the function that is active in the command line while entering 'N' for a prompt will skip the current function set. Separating each plot and analysis type into different modules allows the user to quickly interpret a fluorescent dataset and to produce a variety of plots that clearly visualize principal components (PCs) in an interpretable way.

The PC Contour functions reshape the vectorized PC loadings back into a matrix where each of the loading values is matched with the corresponding excitation-emission wavelength pairing. The subsequent plots make for an easy comparison

where each of the loadings for each principal component can be compared with the family of fluorescent NOM compounds that the principal component is describing. This visualization is specifically useful for FEEM data as the emission-excitation coordinates on the plot have physical meaning and correspond to organic compounds (Abdi & Williams, 2010; Bro & Smilde, 2014; Wold, et al., 1987).

Biplots are typically used for visualizing PCA results but given the number of variables contained in a FEEM, biplots are not a useful visual tool for interpreting results. Simple scatter plots plotting user-defined PCs were used as an alternative to observe patterns in the data. A secondary method for examining general data patterns was plotting 3 PCs in a three-dimensional scatter plot. Classification of the PC data, where each axis is a different PC, provides quantitative insight regarding the clustering and similarities between the fluorescent NOM in the dataset. For example, classification of samples using fluorescence data has implications for identifying whether or not water quality is being impacted by a contaminant infiltrating a source water (Peleato et al., 2017). Combining the PC loading contour plots with the PC score biplots and k-means clustering data provides a clear picture of what is happening within a given water matrix from a fluorescent NOM perspective.

## **5.5 Methods**

### **5.5.1 Synthetic Water Matrix**

The synthetic water matrix was prepared by adding amino acid (as a representative for protein) and humic acid mixtures to deionized water. Tyrosine, tryptophan, and Suwanee River humic acid were selected as model compounds and spiked, by weight, at 1 mg L<sup>-1</sup>, 5 mg L<sup>-1</sup>, and 10 mg L<sup>-1</sup>. NOM mixtures with two or more amino and humic acids in solution were spiked equal proportion (by weight). TOC and fluorescence samples were simultaneously collected immediately after combining each of the organic mixtures to minimize the impacts of amino acid degradation on fluorescent expression. Ranging the TOC concentrations from 1 mg L<sup>-1</sup> to 10 mg L<sup>-1</sup> provides a

variety of fluorescent single strength within the final dataset. A Shimadzu TOC-V CSH analyzer was used for processing TOC samples. TOC samples were collected and compared to the expected TOC concentration to ensure that the synthetic water was dosed correctly, and the dosed amino acids were consistent in quality.

### **5.5.2 Natural Water Matrix**

Plant-filtered water samples were collected from one drinking water treatment plant within the Halifax Regional Municipality (HRM) and one drinking water treatment plant within the Cape Breton Regional Municipality (CBRM). The collected water samples were used in a series of bench-scale advanced oxidation processes (AOPs) experiments in order to generate a varied NOM composition for each of the known source waters. Samples were UV treated using a 1000W, medium-pressure, Calgon Carbon collimated beam unit and followed the fluence calculation procedure outlined by Bolton and Linden (2003). Low and high UV fluences were 100 and 1000  $\text{mJ cm}^{-2}$  and both ozone and hydrogen peroxide were dosed at a low and high concentration of 1  $\text{mg L}^{-1}$  and 10  $\text{mg L}^{-1}$  respectively. Peroxide stock solutions were prepared to a concentration of 3  $\text{mg mL}^{-1}$  and samples were quenched after UV treatment using bovine catalase. Ozone was applied at a concentration of 1 and 10  $\text{mg L}^{-1}$  using an Azocozon VMUS-4(O<sub>2</sub>) ozone generator at a flow rate of 2  $\text{L min}^{-1}$  and at 40 PSI (exposure time = 6 sec for 1  $\text{mg L}^{-1}$  and 56 sec for 10  $\text{mg L}^{-1}$ ). Both natural water types used in the bench scale experiments are characteristically similar with low DOC (2-3  $\text{mg L}^{-1}$ ), near neutral pH (6.5-7.5), and low colour (<10 ptco).

### **5.5.3 Fluorescence Excitation Emission Matrices (FEEM)**

Fluorescence samples were collected using a Horiba Aqualog fluorometer. Samples were measured every 3 nm over the range of 240-600 nm and 210-610 nm for excitation and emission wavelengths respectively, with a 1 second integration time for each sample. This time was chosen to balance the resolution of the data with the

time required to process each sample. The inner filter effect (IFE), Rayleigh masking (1<sup>st</sup> and 2<sup>nd</sup> order with a 10 nm band width), and normalization of each sample were conducted using the built-in functions that are part of the Aqualog user interface (Horiba Scientific, 2013). After normalization, excitation emission matrices were exported as comma separated value (CSV) files. The list of sample CSV files were imported into Matlab using a method similar to the function contained in the DomFluor toolbox (Bro, 1997). This approach allows the user to easily apply both modelling techniques to the same dataset without having to initialize a new Matlab workspace. The imported fluorescence matrices were then vectorized into a  $15,125 \times n$  working matrix. The core code also gives the user the ability to remove excitation wavelengths at the lower extreme of the detection limit (240nm to 250nm) for the fluorometer. The signal in the 240-250nm portion of the FEEM profile is noisy in some samples and may impact the results for some datasets. The flowchart outlines the major steps from collecting samples, pre-processing data, and finally importing it into the toolbox workflow.

## 5.6 Data Management

The code used for this analysis is structured in a series of user-chosen modules. The user first defines the folder that their samples are located in. Each folder of CSV files is sequentially numerically titled (beginning at 1 and ending at  $n$ ). The sample numbers are indexed with an accompanying data key file which pairs the sample number with the true name of the sample. After importing, each sample was then vectorized so that each excitation-emission wavelength pair were assigned a row of  $p$  variables. The collection of  $n$  vectors was then combined into an  $n$  by  $p$  matrix where each row represented an excitation-emission wavelength pair ( $p$ ) and each column represented a different sample ( $n$ ). The data was then centered ( $\bar{x} = 0$ ) and normalized ( $\sigma = 1$ ) to mitigate the scale of a principal component dominating further analysis. PCA was then conducted on the normalized  $n$  by  $p$  matrix. The principal component loadings were then visualized to reveal patterns regarding what portion

of the fluorescent matrix each of the PCs described. Due to the magnitude of variables that are part of the FEEM measurements, traditional biplots are not appropriate for this dataset and the PC scores were alternatively displayed as a scatterplot. Finally, k-means clustering was applied to the PC scores to further classify the samples with a user-defined number of bins for clustering.

## 5.7 Results and discussion

PCA and k-means clustering was applied to fluorescent NOM data for two different datasets. A synthetic dataset composed of humic and amino acid mixtures was used to test the functionality of the modelling approach when using known NOM profile. A pooled dataset which contained AOP treated samples from two lakes composed the natural water dataset. The raw data was centered and normalized prior to passing it through the PCA algorithm. PCA loading data was visualized in a way to compliment the correlative nature of excitation-emission wavelength pairings. Excitation-emission wavelength pairings are often used as a general method for describing the nature of NOM that they represent. For example, excitation-emission wavelength pairings that fall within the 250-300 nm excitation and 300-350 nm emission region typically coincide with protein-like substances (W. Chen et al., 2003; Stedmon & Bro, 2008). This means that several of the variables that we are considering in this analysis are inherently correlated with each other. The resultant loading data for PCA analysis of this dataset results in numerous variables having the same loading making the true meaning of loading results difficult to grasp.

Excitation-emission matrices for this dataset are composed of >15,000 variables and render biplots, the most common method of visualizing PCA data, uninterpretable. Reshaping PCA loadings back into a matrix form allows for an easily interpretable plot that can simultaneously be compared to both the fluorescence contour plots of a natural water sample and to the PC-*n* vs PC-*m* scatterplot.

The synthetic dataset, composed of humic acid and amino acids, consisted of 63 samples and the pooled natural water dataset consisted of 531 samples. The variance explained by the first four principal components for both the synthetic and natural water matrices is shown in **Table 5-1**. The first component in both water matrices described the majority of the variance in each dataset. In the synthetic water matrix, PC1 (94.22%) encompasses the general protein-like profile, which accounts for the amino acid content. PC1 (84.36%) in the natural water matrix describes the typical humic-like material that is ubiquitous to surface water samples. Although the variance explained by principal components beyond PC1 drastically drops off, the portion of the fluorescent NOM profile that subsequent PCs describe has been shown to be important in developing fluorescent NOM models (Peleato & Andrews, 2015).

**Table 5-1** Variance explained and emission/excitation wavelength peaks for the first 4 principal components

<b>Water Matrix</b>	<b>Principal Component</b>	<b>Variance Explained</b>	<b>Emission Loading Wavelength Absolute Peak (nm)</b>	<b>Excitation Loading Wavelength Absolute Peak (nm)</b>	<b>Explained Region of Fluorescent NOM</b>
<b>Synthetic water</b>	1	94.22%	350	260	Tryptophan-Like
	2	3.40%	475	275	Humic-Like
	3	1.43%	300	275	Protein-Like I
	4	0.66%	300	300	Protein-Like II
<b>Natural water</b>	1	84.36%	443	240	Humic-Like
	2	5.95%	345, 525	350, 430	Protein-Like I
	3	1.52%	335,460	276, 360	Protein-Like II
	4	0.91%	430	270	Fulvic-Like

### 5.7.1 Contour Loading Plots

The contour plots for the synthetic water matrix are shown in **Figure 5-2**. PC 1 and PC 3 describe the region typically associated with protein or biological activity. This result is expected as the dominant compounds that were spiked into the synthetic water matrix are amino acids. Tryptophan and tyrosine are much more fluorescent when compared to humic acid and therefore dominate the fluorescent NOM profile of the synthetic water samples. This result suggests that the internal code of the toolbox is fully functional as PCs 1-4 make physical sense and align with the expected outcome of performing PCA analysis with the synthetic water dataset.

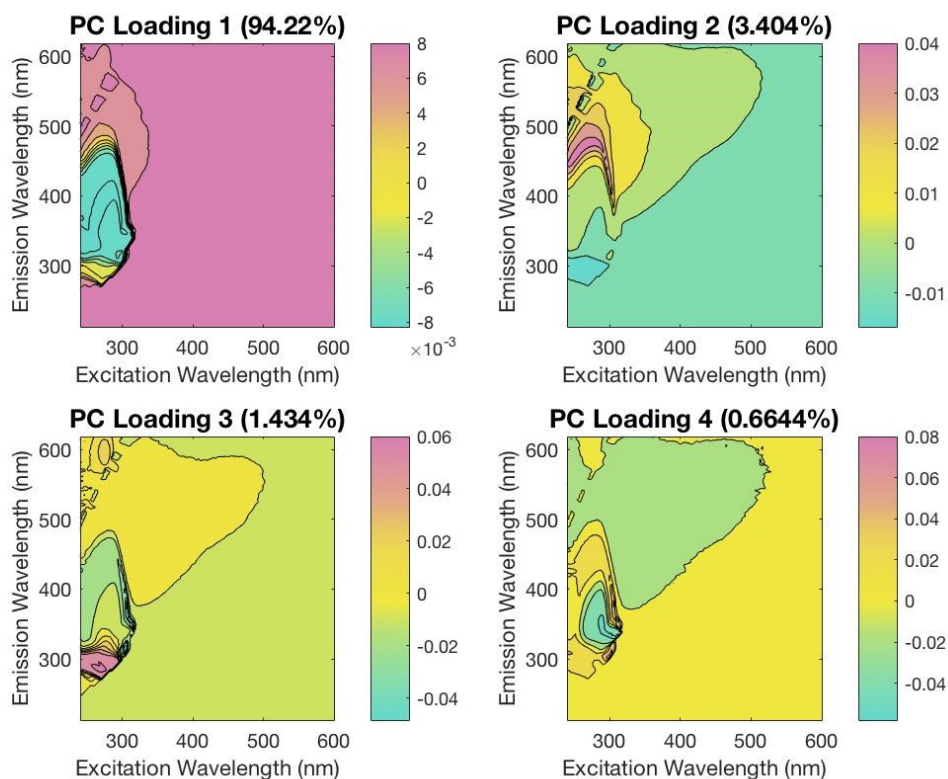


**Figure 5-2** Contour plots for the first four principal component loadings for the synthetic water matrix.

The contour plots for the first four PCs for the natural water dataset are shown in **Figure 5-3**. PC 1 describes the humic-like region of fluorescent expression

(Markechová et al., 2013). PC 2 describes the protein related portion of the fluorescent NOM profile. The protein region of this plot aligns with the components that describe the synthetic water in **Figure 5-2** indicating biological activity in each of the lakes that make up the natural water dataset. The region described in PC 2 has also been shown to have implications for predicting disinfection by-product formation in drinking water (Trueman et al., 2016).

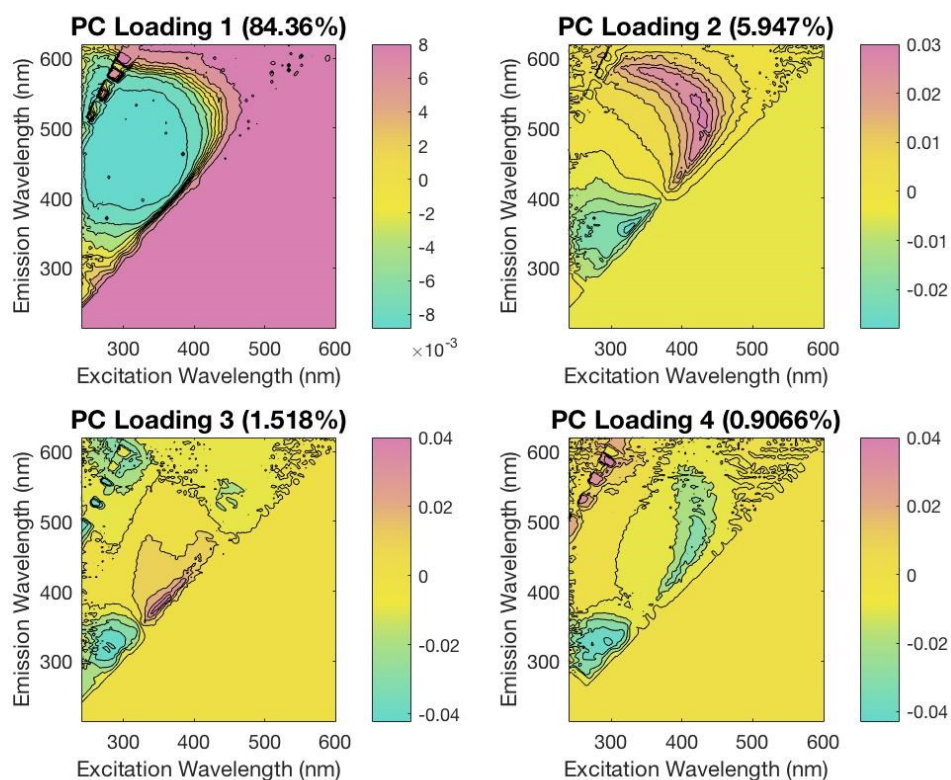


**Figure 5-3** Contour plots for the first four principal component loadings for the natural water matrix.

## 5.7.2 K-means clustering of PCA scores

### 5.7.2.1 *Synthetic water matrix*

K-means clustering was conducted on both the natural and synthetic datasets. Two clusters were chosen for the synthetic water matrix dataset in order to match binary characteristics of humic and amino acids. The results of the k-means clustering are visualized in **Figure 5-4**. Samples that are negative along the PC 1 axis tend to be high in tryptophan, whereas samples that are positive along PC 1 are humic-dominant in nature. **Figure 5-4a** shows that positive PC 2 values are associated with humic samples and negative values are associated with protein tendencies. The PC 3 axis describes the type of amino acid that is in the sample. Negative values are associated with tryptophan and positive values are associated with tyrosine samples. Samples that are dominant in humic acid lie near zero for the PC 3 axis. Combining this result with the contour plot for PC 3 in **Figure 5-2** shows us that the fluorescent region ranging from 250-300 nm excitation and 350-425 nm emission is indicative of tryptophan and the fluorescent region ranging from 240-300 nm excitation and 275-310 nm emission is indicative of tyrosine.

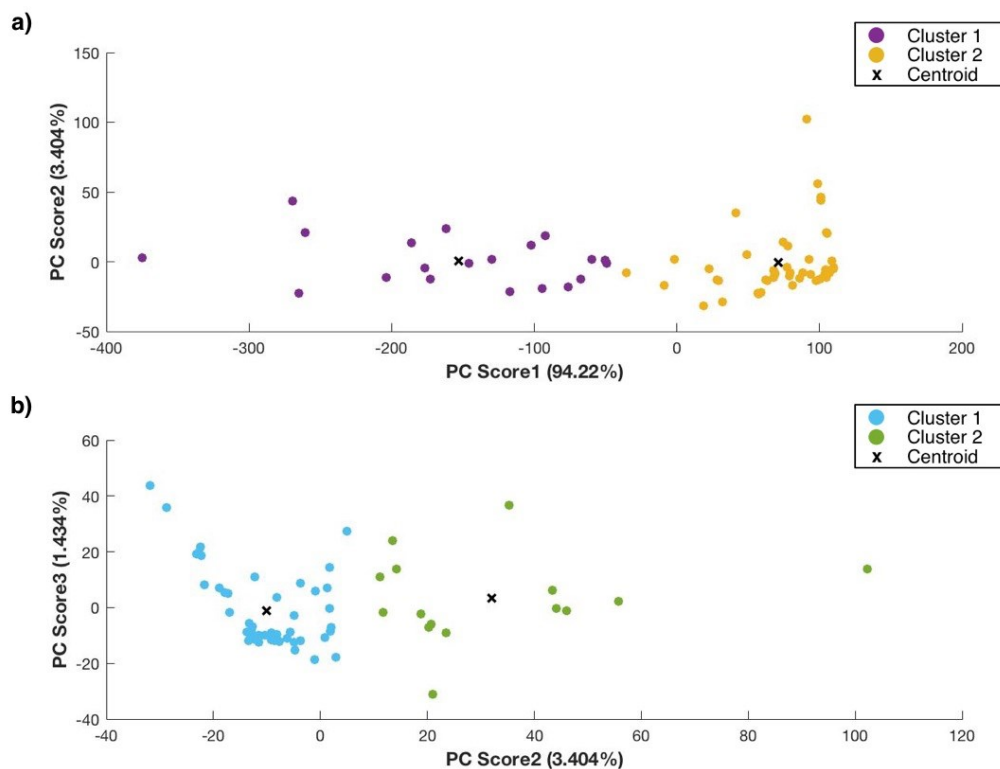


**Figure 5-4** Principal component scores after k-means classification for 2 clusters for the synthetic water matrix dataset.

The k-means clustering data for **Figure 5-4a** shows that 83.3% of the tryptophan samples at a concentration of 5 mg L<sup>-1</sup> and 10 mg L<sup>-1</sup> fall into Cluster 2 (yellow). All samples containing low and medium concentrations of tyrosine, with the exception of the 5 mg L<sup>-1</sup> tyrosine tryptophan mixture, are classified into Cluster 1 (purple). This result shows that the clustering methodology is capable of separating NOM that otherwise is similar in their fluorescent profile and that PC1 described the amount of amino acid content within a water matrix.

Cluster 1 in **Figure 5-4b** is primarily composed of samples that are a mixture of tyrosine-tryptophan and tyrosine-tryptophan-humic acid. **Figure 5-4b** indicates that all samples with humic material at a concentration of 5 mg L<sup>-1</sup> and 10 mg L<sup>-1</sup> are classified as part of Cluster 2 (green). This result indicates that PC2 is describing the humic acid content within a water matrix. These results indicate that the k-means

clustering approach is useful in differentiating between some of the common constituents of fluorescent NOM within a synthetic water matrix and proves proof-of-concept for utilizing this tool in future work.

#### 5.7.2.2 *Natural water matrix*

K-means clustering was also conducted in two dimensions for each of the first three principal components for the natural water matrix dataset. K-means clustering proved useful for classifying the lake origin of samples in the natural water dataset. Plotting the samples using the first three principal components as axes reveals a separation of the data along the PC 1 axis as shown in **Figure 5-5**. The separation along this axis describes the source water of each sample. In **Figure 5-5a**, where PC1 is plotted against PC2, Cluster 1 (purple) tend to be composed of HRM samples whereas Cluster 2 (yellow) tended to be composed of CBRM samples. K-means clustering was 72% accurate when classifying CBRM samples correctly and 83% accurate in classifying HRM samples correctly when using PC 1 and 2 as clustering criteria. **Figure 5-5c** shows the 2-cluster clustering for PC 1 and PC 3. Classification was 84% accurate when classifying HRM source water samples within the same cluster and 71% accurate when classifying CBRM source waters in the sample cluster. The similar results in classification for **Figure 5-5c** when compared to **Figure 5-5a** is due to the influence that PC1 has over the 2-dimensional classification.

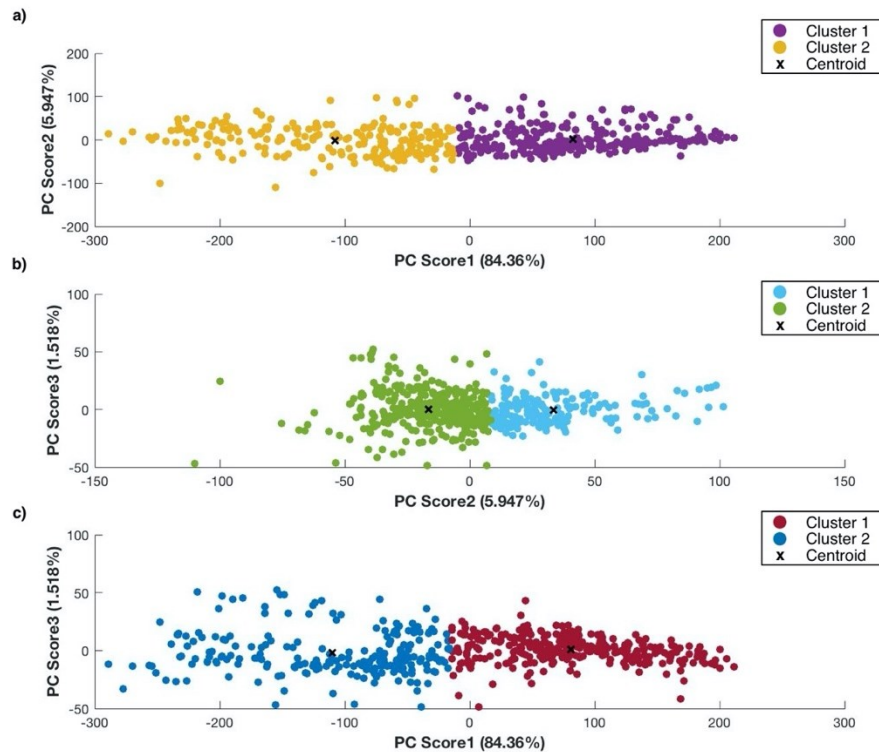


**Figure 5-5** Principal component scores after K-means classification for 2 clusters for the natural water matrix dataset.

**Figure 5-5b** describes treatment type for each sample. All samples for the CBRM and HRM source water that had undergone a UV exposure of  $1000 \text{ mJ cm}^{-2}$  and dosed with  $10 \text{ mg L}^{-1}$  of  $\text{H}_2\text{O}_2$  all fall in Cluster 2 (green). This result suggests that varying combinations of plotted PCs can properly describe subtle similarities within a dataset of treated samples. This also suggests that PC 2 is describing the amount of oxidation that has occurred within the water matrix for each sample. **Table 5-2** shows the distribution of classification for each of the AOP treatments for the natural water dataset. The distributions show that peroxide-based AOP treatments tend to fall into Cluster 2 for **Figure 5-5b**. Untreated and ozone-based treatments tend to fall into Cluster 1 in **Figure 5-5b**. Combining the treatment classification information with the contour plots in **Figure 5-3** shows us that emission-excitation wavelength pairings around the 250 nm excitation and 475 nm emission region is the region that is most impacted by peroxide oxidation. The 250, 475 nm wavelength pair is most commonly

characterized as generally humic-like in nature and is bordering on the fringes of the protein-like region of fluorescence.

**Table 5-2** K-means clustering distribution of PC2 vs PC3 for each of the AOP treatments for the natural water matrix dataset.

<i>Treatment Type</i>	<b>Cluster 1</b>	<b>Cluster 2</b>
<i>Untreated</i>	92%	8%
<i>UV Low (100 mJcm<sup>-1</sup>)</i>	92%	8%
<i>UV High (1000 mJcm<sup>-1</sup>)</i>	68%	32%
<i>UV Low (100 mJcm<sup>-1</sup>) H<sub>2</sub>O<sub>2</sub> Low (1 mgL<sup>-1</sup>)</i>	85%	15%
<i>UV High (1000 mJcm<sup>-1</sup>) H<sub>2</sub>O<sub>2</sub> Low (1 mgL<sup>-1</sup>)</i>	45%	55%
<i>UV Low (100 mJcm<sup>-1</sup>) H<sub>2</sub>O<sub>2</sub> High (10 mgL<sup>-1</sup>)</i>	58%	42%
<i>UV High (1000 mJcm<sup>-1</sup>) H<sub>2</sub>O<sub>2</sub> High (10 mgL<sup>-1</sup>)</i>	4%	96%
<i>UV Low (100 mJcm<sup>-1</sup>) O<sub>3</sub> Low (1 mgL<sup>-1</sup>)</i>	73%	27%
<i>UV High (1000 mJcm<sup>-1</sup>) O<sub>3</sub> Low (1 mgL<sup>-1</sup>)</i>	70%	30%
<i>UV Low (100 mJcm<sup>-1</sup>) O<sub>3</sub> High (10 mgL<sup>-1</sup>)</i>	73%	27%
<i>UV High (1000 mJcm<sup>-1</sup>) O<sub>3</sub> High (10 mgL<sup>-1</sup>)</i>	74%	26%

The results suggests that k-means clustering of PCA scores is robust in identifying differences in water matrices that have similar fluorescent NOM profiles. This approach, when combined with PC loading contour plots, allows us to understand what areas of the FEEM are susceptible to specific AO treatment types for a natural water matrix. Utilizing the k-means and PC loading approach may also be useful for datasets where a water source is suspected to be influenced by external contamination and these results warrant further investigation into these applications. For example, trace pharmaceutical compounds that have a unique fluorescence signature that overlap with the dominant fluorescent NOM would be an interesting area for applying this analysis approach in future work.

PCA and k-means clustering has shown utility for making better use of fluorescent excitation emission matrix datasets. Using contour loading plots, scatter score plots,

and the k-means clustering of PC scores in conjunction with each other gives a clear and interpretable picture of the fluorescent NOM of each of the datasets examined in this study. The provided code is equipped with several functions to give the user options to easily generate these plots. The code is also isolated into user-selected modules, which allow only some portions to be initialized given the users' needs for a dataset. The key advantage of this approach for utilizing FEEM data is the streamlined workflow that allows for a low barrier of entry for those that are hesitant to glean the most information from their FEEM data. While FEEM data does contain data that helps describe the NOM profile of a water matrix, it is important to note that this is strictly fluorescent material and does not fully describe everything that is contained in a water matrix.

Principal component analysis recognized the main fluorescent NOM contributors within each of the analyzed water matrices. Humic-like and fulvic-like compounds dominate much of the FEEM signal of the natural water dataset and therefore were represented overwhelmingly in the first principal component. Additional regions, such as the protein-like and secondary humic-like, were represented in PCs 2, 3, and 4 for the natural water matrix. The primary PCs for the synthetic water dataset described the tryptophan and tyrosine regions of the FEEM profile. This was expected as amino acids are more fluorescently active per milligram DOC when compared to humic and fulvic materials. Positive scores in PC 1 and PC 2 indicate humic material content in the synthetic water matrix. Negative values in PC 1 describe tryptophan content in samples. Negative PC 2 scores tend to describe general protein-like content as samples containing both tryptophan and tyrosine fell within this region. PC 3, while only describing 1.43% of the variance in the dataset, has shown to be key in describing the type of amino acid that is present in a sample. Samples containing the most amount of tryptophan had the most negative scores for PC 3, while samples with the highest scores contained the most tyrosine. Samples that contained only humic acid all fell near the origin for PC 3. This information helps improve in defining the fluorescent region that describes the tyrosine and tryptophan-like region of the FEEM. The fluorescent region of 250-300 nm excitation wavelength and 350-425 nm

emission wavelength is indicative of tryptophan and the fluorescent region ranging from 240-300 nm excitation and 275-310 nm emission is indicative of tyrosine. A better definition of the protein region allows for better interpretations of what protein-like material is present in a natural water matrix from a fluorescent NOM perspective.

## 5.8 Conclusion

This chapter demonstrates the utility of FEEM coupled with PCA and k-means clustering as a useful tool for further characterizing how NOM changes as a result of AO exposure. Furthermore, the PCA / k-means approach has demonstrated utility in characterizing FEEM samples from different sources, such as amino acids. The results of this experiment show proof-of-concept for this approach when utilizing a synthetic water matrix consisting of known constituents and proved to be useful in characterizing fluorescence data when using a real dataset composed of varied and complex water matrices. The k-means distancing approach using natural water matrices was able to classify samples that had undergone the most impactful oxidative treatments ( $1000 \text{ mJ cm}^{-2}$  UV fluence and  $10 \text{ mg L}^{-1}$  peroxide concentration) with 96% accuracy across both source water types, suggesting that peroxide-based oxidation treatments have a signature fluorescent profile. This result further also indicates that this tool and approach could be used for describing changes in a water matrix via other processes such as filtration, coagulation, or seasonal variation.

In summary, PCA analysis, in conjunction with the various visualization tools outlined in this study is an asset for FEEM datasets. The suite of functions provided in the Appendix C allows for FEEM data to be easily interpreted from a quantitative perspective, especially for users who have previously used FEEM for solely qualitative purposes. The approach used in this study was able to better define portions of the fluorescent NOM profile of specific amino acids and also was able to indicate what

portion of the excitation-emission fluorescence spectrum is most vulnerable to specific types of photochemical oxidation.

## 6 Development of a wavelength tunable, high throughput UV exposure tool

"Reproduced with permission from: Instrument Hacking: Repurposing and Recoding a Multiwell Instrument for Automated, High-Throughput Monochromatic UV Photooxidation of Organic Compounds  
Copyright 2020 American Chemical Society."

MacIsaac, S.A., Sweeney, C.L, Gagnon, G.A. 2020. Instrument Hacking: Repurposing and Recoding a Multi-well Instrument for Automated, High-throughput Monochromatic UV Photooxidation of Organic Compounds. *ACS ES&T ENG*.

### 6.1 Abstract

Bench-scale UV experiments are an inefficient and laborious process when using current flow-through and collimated beam technologies. Current technologies are also limited in their ability to customize the emitted wavelength of light. Existing monochromatic UV technologies such as UV-LEDs that are tunable to the full UV-C spectrum are not currently available. The objective of this study was to repurpose a commercially available automated water analysis tool (microplate reader) into a high-throughput, wavelength tunable, proof-of-concept UV-oxidation platform allowing for significant time savings for bench-scale UV experiments. The light source was characterized via actinometry using potassium ferrioxalate, which was combined with fluence equations to control the amount of UV light delivered to microplate wells. Repurposing a microplate reader as an automated, proof-of-concept UV-oxidation platform through the creation of a novel software script resulted in the first reported demonstration of high-throughput bench-scale UV treatment of water samples with unique control over output wavelengths.

## 6.2 Introduction

Natural organic matter (NOM) and synthetic organic contaminants impact water quality is an important area of water research for many reasons – from direct public health impacts to indirect process management concerns. One of the more promising treatment technologies for mitigating organic matter in water is through treatment ultraviolet (UV) light, which may also involve a photocatalyst. Energy from UV light is absorbed by organic compounds and can degrade them into benign derivatives through a process commonly referred to as advanced oxidation processes (AOP). AOP are an emerging technology that uses photo- and chemical-oxidative reactions to form non-selective radical species that drive the degradation of organic compounds present in the water (Esplugas et al., 2007). Traditional AOP utilize either low-pressure (LP) or medium-pressure (MP) UV mercury lamps as the photooxidation source in combination with a chemical oxidant such as hydrogen peroxide, ozone, or titanium dioxide (Esplugas et al., 2002; Hoffmann et al., 1995; Ijpelaar et al., 2010). Emerging AOP treatments also include periodate which when combined with hydrogen peroxide has shown efficacy in the removal of organic pollutants and inactivation of pathogens in water (Sun et al., 2020). The spectral nature of MP lamps allows the emittance of light across several wavelengths, some of which may be beneficial for NOM degradation, while others may be inefficiently released as wasted light. LP lamps emit over 90% of their energy at 254 nm and are specialized in their application in damaging pathogen DNA.

In recent years, UV-LED has emerged as a promising mode of UV treatment that not only mitigates the shortcomings of UV mercury lamps but introduces several benefits<sup>9</sup>. In addition to their environmentally friendliness, smaller footprint, and longer lifetime, UV-LEDs operate at various wavelengths and turn on and off with no warm-up or cool down period. UV-LEDs are pseudo-singular in their emitted wavelength and can be tailored to the water matrix to which they are applied (Song

et al., 2016). Furthermore, UV-LEDs have been shown to be as effective as mercury lamps in water disinfection (K. A. Sholtes et al., 2016). The current drawbacks of utilizing this technology are that UV-LEDs that emit at each wavelength of light within the full UV-C range are not currently available or have severe power inefficiencies, and they are still semi-spectral in their output.

Current technologies for producing bench-scale UV-treated samples are flow-through reactors and collimated beam reactors. Flow-through reactors are challenging to use as it is difficult to calculate accurate fluences (UV doses) within the reactor when using actinometry (the measurement of UV intensity) (Nguyen et al., 2019). Although time-consuming, actinometry is one of few options for measurement in a closed reactor. Furthermore, only a single UV fluence can be applied at a time when using a flow-through reactor and the entire system of the reactor must be kept under subdued orange light when working with actinometer chemicals (Bolton et al., 2011). The limitation of exposing a single sample to only one UV fluence at a time results in laborious bench-scale experimentation that requires constant attention from workers. Collimated beam reactors allow for easy calculation of UV fluence because the light emitted from the reactor can be directly measured through the usage of UV-sensitive spectroradiometers. The drawbacks of collimated beam reactors are that they do not represent reactors at full scale and their operation is also time-consuming, as they traditionally produce low volumes of water per treated batch, requiring several batches of UV treated samples to measure multiple parameters. Collimated beams are also able to treat only a single sample at a time with exposure times ranging from minutes to hours, depending on the required fluence. Collimated beam reactors currently require constant oversight during use as the light must be turned on and off at appropriate times and samples must be manually rotated after each UV treatment. The time required for attending to UV reactors for both flow-through and collimated beam designs adds up over the course of a full experimental trial and is an inefficient use of researcher's time. A device that is capable of automatically treating several samples at a time can potentially accelerate bench-scale experimentation by orders of magnitude.

A major obstacle preventing the timely evolution of UV water treatment technology in full-scale drinking-water treatment systems is the lack of an automated high-throughput UV-emitting instrument that provides insight regarding the optimized conditions for sufficient UV treatment. The utilization of a microplate reader to test several different UV treatments in a single protocol addresses this issue. Some studies have used microplates as a way to physically separate samples when exposing microplate wells to UV light, but this approach still requires manually adjusting the plate throughout experimentation to ensure appropriate UV exposure (Betzael et al., 2020). The development of an automated UV reactor would improve the understanding of how UV light interacts with a range of targeted organic compounds and also reduce the number of person-hours required to conduct bench-scale UV treatment experiments. Bench-scale UV treatment is a time-intensive process that is limited by current technologies, as most reactors only produce a single sample at a time and require manual monitoring to ensure consistency between samples. Inefficiencies in the UV treatment process mean that crucial information for disinfection and oxidation research is currently bottlenecked due to dated laboratory protocols.

Microplate readers are commonly used in the biological and pharmaceutical sciences and utilize low volume, separated wells and can detect or emit light across the UV spectrum. However, as microplate readers are not designed for UV oxidation purposes, the software that is native to the instrument limits the user options regarding light exposure per microplate well, which requires the creation of customized protocol that provide additional light per microplate well that is sufficient for photooxidation. Another recent study explicitly states that microplate readers are ideal candidates for UV exposure work and calls for research into the subject (Betzael et al., 2020). Microplate readers allow for repeatable and rapid replication of experiments but have surprisingly not been used for UV disinfection or oxidation experiments before (Betzael et al., 2020). In considering the capabilities of the microplate reader through the lens of UV oxidation technology research and

development, software protocols within standard microplate reader software can be designed to have the instrument behave as a high-throughput UV oxidation platform for use in proof-of-concept experiments.

The following work establishes a novel, microplate reader-based UV reactor as a high-throughput, automated treatment technology. An existing microplate reader has been used as a surrogate UV reactor in a proof-of-concept demonstration of the proposed platform technology. The experiment setup in this study allowed for unique control over the output wavelengths from the surrogate reactor in addition to the high-throughput nature of automating the UV exposure process. This study proposes a platform for a high-throughput technology for the purpose of automating the treatment of water samples via UV treatment. The work outlined in this study saves hours of work for researchers when comparing it to traditional methods for bench-scale UV research. The study is comprised of three phases: 1) development of a novel software script to repurpose an automated microplate reader into a high-throughput proof-of-concept UV oxidation platform; 2) characterization of the light source within the instrument via actinometry; and 3) performance of the microplate reader light source as an oxidation reactor for the degradation of model targeted organic compounds, as determined via liquid chromatography-mass spectrometry (LC-MS).

### **6.3 Materials and Methods**

A Biotek H1 Synergy microplate reader, adapted to behave as a high-throughput, single-wavelength UV reactor, was used for all experiments. The internal light source was a 20W xenon flash bulb equipped with a series of monochromators, which controlled the wavelength of light that reached wells of the microplate. The relative light output of the xenon bulb is provided in the Appendix E with the UV portion of the output highlighted (BioTek, 2020). The Synergy H1 instrument comes with Gen5

software preinstalled on the PC it is paired with. The Gen5 software allows the user to design and program customized protocols for full control over the amount and wavelength of light. The amino acids used in the oxidation experiments (tryptophan and tyrosine) and caffeine, which was used as an internal standard, were obtained from Millipore Sigma Canada Co. (Oakville, ON, CA). Amino acids were chosen as target compounds as they are stable in the water matrix and are representative of protein-like material that is present in natural waters. Both tryptophan and tyrosine are often used as NOM surrogates within water research, as they have been linked to the formation of disinfection by-products when undergoing oxidation via chlorine exposure (Bond et al., 2009; W.-H. Chu et al., 2010). Affinity Designer was used for all illustrations and for editing figures (Serif, 2020).

### **6.3.1 Light Source Actinometry**

The spectral output of the UV-C source is governed by a series of monochromators and internal UV filters that can be controlled using the instrument software (Gen5). A customized set of protocols were developed to achieve a variety of UV exposure times and fluences across the UV-C spectrum. The instrument software limits the user to selecting the number of light emissions at a wavelength for a given protocol. The amount of light emitted by a protocol was modified to accommodate for extended amounts of exposure time for a wavelength of light. A graphical summary of the customization process for the Gen5 software is included in the Supplementary Material that further outlines the approach that was taken for characterizing the internal light source of the microplate reader. 96-well, 300- $\mu$ L volume, transparent, non-binding microplates were used for the lamp characterization study, while 96-well, 300- $\mu$ L volume, black, non-binding black microplates were used for the UV oxidation study.

Potassium ferrioxalate was used as the actinometer for all light quantification in this work because it has a consistent quantum yield across the UV spectrum (Bolton et al., 2011). The actinometry method is described by Bolton and was followed for

preparing all reagents and calculating the power output of the light source (Bolton et al., 2011). 0.006 M potassium ferrioxalate in 0.1 N H<sub>2</sub>SO<sub>4</sub> (FeOX solution) was prepared in a dark room under subdued red light at 20 ± 1°C. All actinometry chemicals were handled under red light while loading and unloading the plate from the instrument and is outlined in **Figure 6-1**.

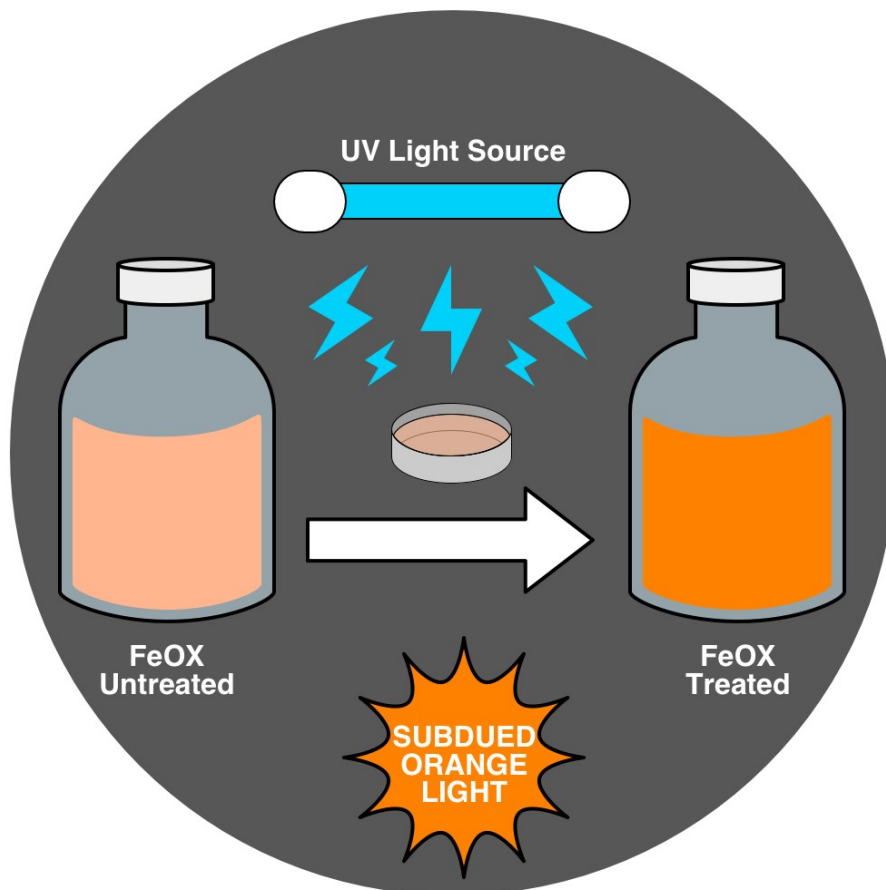


**Figure 6-1** Actinometry handling protocol when exposing microplate wells to UV light.

FeOX solution was added to a sodium acetate buffer solution at pH 4.5 and a 0.2% 1,10 phenanthroline solution. 200 µL of the prepared solution was added to each of the wells on a 96-well plate. The plate was then immediately placed inside of the instrument and exposed to the chosen wavelength of UV light and exposure time. Actinometry response curves were generated from 255 to 290 nm in 5 nm increments across a range of fluences. Microplate wells were exposed to UV light ranging from 5 to 180 seconds of exposure time for the duration of the protocol. This timeline

allowed for the production of a full plate of treated samples to be produced in approximately 5 hours compared to several days of work required to generate a similar number of samples manually working with a collimated beam or flow-through reactor. Absorbance at 510 nm ( $A_{510}$ ) was measured immediately after UV exposure. Non-exposed ('blank') samples were also measured at this time. The resolution of the actinometry curves provided a robust understanding of the spectral output of the internal light source and the necessary information for calculating UV fluence for a given wavelength and exposure time.

### 6.3.2 Calculation of Light Intensity

The equations outlined by Bolton (2011) and quantum yield values developed by Goldstein & Rabani (2007) were used to calculate the fluence at each of the tested wavelengths and exposure times. The quantum yield at a given wavelength determines the UV fluence after exposing the actinometer to light. Equation S1 was used to calculate the moles of  $\text{Fe}^{2+}$  for a given wavelength and exposure time by finding the difference between sample absorbance and blank absorbance at 510 nm ( $A_{510}(\text{Sample})$  and  $A_{510}(\text{Blank})$ , respectively) divided by the molar absorption of Fe(II)-*o*-phenanthroline. The calculated einsteins (energy in one mole of photons) at each exposure time and wavelength were then used to determine UV fluence at each of the data points. The einsteins absorbed at a given wavelength and exposure time was calculated by dividing moles of  $\text{Fe}^{2+}$  by a known quantum yield ( $\phi$ ) at each of the wavelengths examined in this experiment (Equation F2). Quantum yields that were not explicitly calculated in the literature were interpolated with the nearest wavelengths that were available. The maximum difference in quantum yield values when interpolating was 0.01. The energy per einstein at wavelength  $\lambda$  was calculated using Equation F3 where  $h$  is the Planck constant,  $c$  is the speed of light,  $N_A$  is Avogadro's number, and  $\lambda$  is wavelength in meters. Power ( $P(W)$ ) was then calculated according to Equation F4 where  $R$  is the reflection coefficient and  $t$  is time in seconds. Finally, UV fluence was calculated by multiplying  $P(W)$  by  $t(s)$ , a reflection factor

(*Refactor*), and an area factor (*Areafactor*), then dividing by the area of the treated well (Equation F 5).

A simple linear regression was used on fluence curves that was then incorporated into the microplate software to control UV exposure at each of the wavelengths and exposure times. Utilization of the linear regression equations allowed for consistent calculation of fluence for each of the wells of the microplate.

### 6.3.3 Microplate oxidation

A 2<sup>4</sup>-factorial design, outlined in **Figure 6-2**, was used in this experiment with the following factors: amino acid (tryptophan/tyrosine), amino acid concentration (10/100 µg L<sup>-1</sup>), UV wavelength (255/280 nm), and UV fluence (100/400 mJ cm<sup>-2</sup>). Tryptophan and tyrosine were chosen as the targeted organic compounds for applying a UV fluence using the microplate reader as an oxidation reactor. Both amino acids are non-volatile and provide a good representation of biological-like NOM that is present in natural waters (Baghoth et al., 2011b; Peiris et al., 2011). Tyrosine and tryptophan have also been used in several studies as NOM surrogates because of their propensity to behave as precursor material for disinfection by-products (Bond et al., 2009; W. Chu et al., 2016; W.-H. Chu et al., 2010). Each amino acid was added to deionized water to a concentration of 10 and 100 µg L<sup>-1</sup> for a total of four amino acid stock solutions; an amino acid concentration of 10 µg L<sup>-1</sup> represented low-NOM conditions while 100 µg L<sup>-1</sup> represented high-NOM conditions. The solutions were then pipetted onto a 96-well microplate at a volume of 200 µL per well with half of the 96 wells containing 10 µg L<sup>-1</sup> tryptophan solution and the other half holding 10 µg L<sup>-1</sup> tyrosine solution. Samples were then placed into the microplate reader and exposed to UV light to the appropriate UV fluence. This process was repeated for the 100 µg L<sup>-1</sup> solutions.

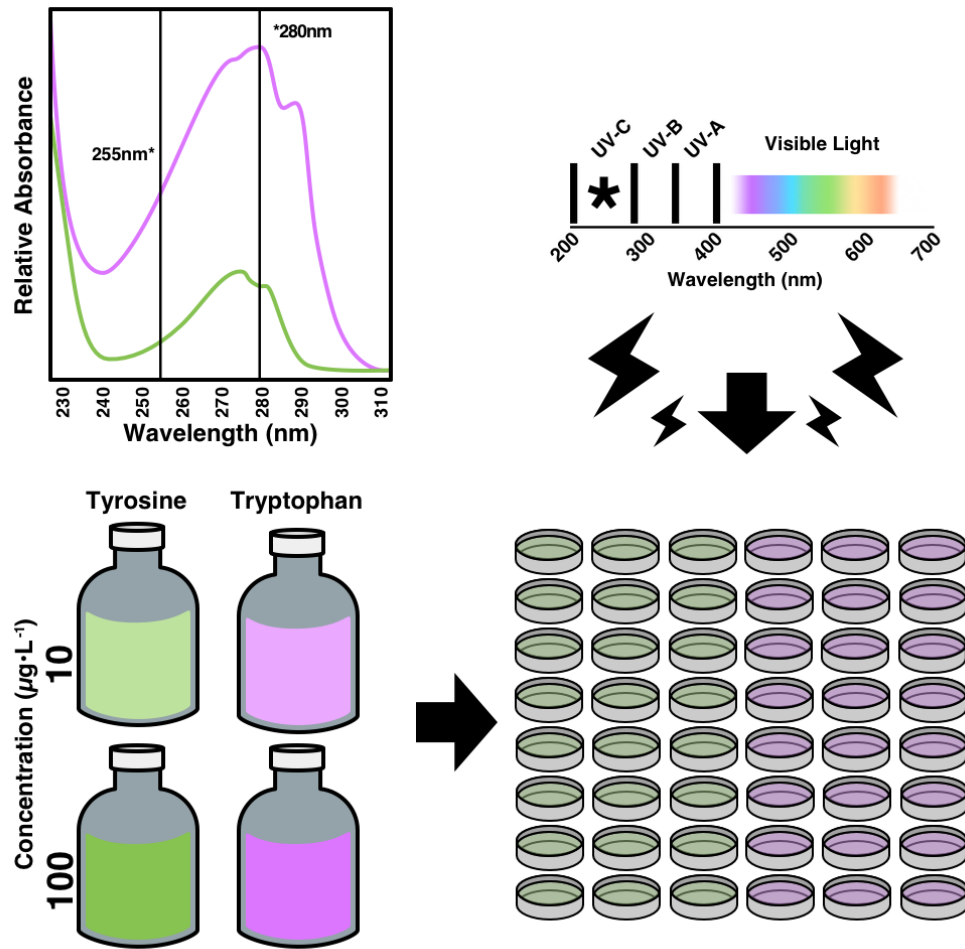


**Figure 6-2** Factorial design of amino acid exposure conditions on multi-well plates.

Customized UV fluence protocols at 255 and 280 nm for both 100 and 400  $\text{mJ cm}^{-2}$  fluences were developed to treat samples appropriately. The two wavelengths of interest were chosen based on work from Beck (2017) that stated that an ideal UV reactor would be capable of emitting light at both 255 and 280 nm (Beck et al., 2017). 255 nm is the wavelength of light that is the primary driver of UV disinfection when using low-pressure UV reactors, and most protein-like material has a peak UV absorbance at 280 nm (Jagger, 1967; Porterfield & Zlotnick, 2010). A reactor capable of emitting at both wavelengths would conceivably damage both DNA and protein-like compounds for biological and organic material.

Tryptophan and tyrosine samples were collected immediately after UV exposure in order to be analyzed via LC-MS. Each sample consisted of 1440  $\mu\text{L}$  of treated water (180  $\mu\text{L}$  of sample from eight identically treated wells from the same microplate column were combined). For a total sample volume of 1.5 mL, 60  $\mu\text{L}$  of internal standard was added to each sample vial prior to LC-MS analysis.

#### **6.3.4 LC-MS analysis**

The Agilent 1260 binary pump LC system coupled to the Agilent 6460 triple quadrupole MS was used for sample analyses. The instrument was operated in positive electrospray ionization (ESI) mode and data acquisition was performed in multiple reaction monitoring (MRM) mode with two transitions yielding a quantifier ion (most abundant product) and qualifier ion. Data analysis was carried out using the Agilent MassHunter Software (Version Rev B.08.00). HPLC separation was achieved using an Agilent Zorbax Eclipse Plus C18 Rapid Resolution High Definition (RRHD) analytical column (50 mm x 2.1 mm, 1.8  $\mu\text{m}$  particle size) at 25  $^{\circ}\text{C}$ .

A sample injection volume of 5  $\mu\text{L}$  was carried by mobile phase consisting of 0.1% formic acid in Milli-Q water (solvent A) and 100% methanol (solvent B) at a flow rate of 300  $\mu\text{L min}^{-1}$ . Solvent B began at 10% and increased to 40% following a linear gradient over 3.7 min followed by a hold time of 3.4 min. The autosampler tray held samples at 4  $^{\circ}\text{C}$ . ESI source parameters operated at the following values: gas temperature, 300  $^{\circ}\text{C}$ ; gas flow rate, 5  $\text{L min}^{-1}$ ; nebulizer pressure, 60 psi; sheath gas temperature, 300  $^{\circ}\text{C}$ ; sheath gas flow rate, 11  $\text{L min}^{-1}$ ; capillary voltage, 4000 V; nozzle voltage, 2000 V; delta EMV cell acceleration voltage, 400. Limits of detection for tyrosine and tryptophan were experimentally determined as 0.1 and 0.2  $\mu\text{g L}^{-1}$ , respectively, and limits of quantitation were calculated as 0.3 and 0.5  $\mu\text{g L}^{-1}$ , respectively (Teale, 1960).

## 6.4 Results and Discussion

### 6.4.1 Actinometry Lamp Characterization

Actinometry experiments resulted in successful characterization of the microplate reader's internal light source. Light output was variable across the UV-C spectrum with less linearity in regions of low relative emittance compared to those of high relative emittance. The combination of a sensitive actinometer and low light intensity at some wavelengths results in non-linearity when wells were exposed to UV-C light. This means that regions with a low relative intensity are not suitable candidates for use as a UV-C oxidation light source (it should be noted that this limitation is specific to this particular light source). **Figure F 1** shows the relative intensity of the UV-C light source for the area of the UV-C spectrum that was examined in this study. Actinometry showed that the light source behaves linearly for wavelengths with a higher relative intensity. Actinometry samples that failed to exhibit linearity with exposure to UV-C wavelengths between 255nm and 290nm were omitted from the further investigation. **Figure 6-3** shows the estimated UV-C fluence for wavelengths where linearity in fluence over exposure time was observed.

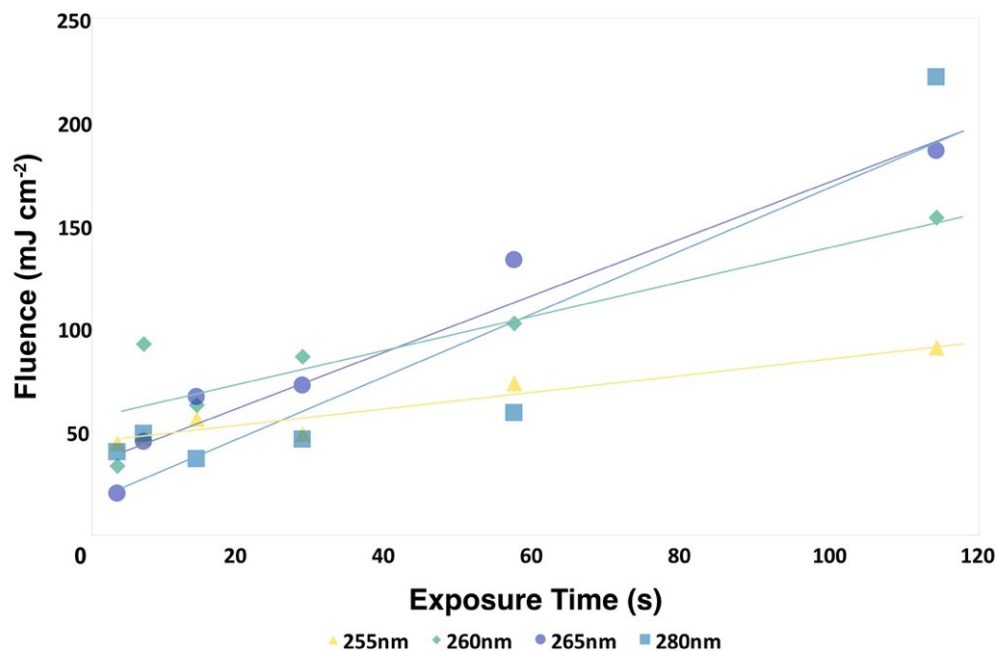


**Figure 6-3** Actinometry-based UV-C fluence curves for wavelengths between 255 and 280nm. Actinometry was conducted using the potassium ferrioxalate method described by Bolton (Bolton et al., 2011).

The fluences expressed in **Figure 6-3** were obtained by calculating the fluence at each of the exposure times as outlined in Section 6.2. The regression equations for each of the curves in **Figure 6-3** were used to calculate UV fluence for a given exposure time for each of the data series in **Figure 6-4**. The terms for each of the fluence curve equations are summarized in **Table F 1**. The regression equations for 255 and 280 nm were used for calculating the oxidation fluence when degrading tryptophan and tyrosine. The characterization of the output of the light source for the microplate reader allows it to be used as an advanced oxidation reactor.

#### 6.4.2 Amino Acid Degradation

Tryptophan and tyrosine were degraded using customized microplate reader protocols for high-throughput UV treated water samples. The protocols were coded in the Gen5 software that is native to the instrument and allows the user to control the amount of UV light delivered to the microplate wells. The user modifies the

exposure time for a selected UV wavelength based on the UV fluence curves generated via actinometry. The program then exposes a selection of microplate wells to the calculated fluence. This protocol allows for UV treatment of a maximum 96 samples in a single run, thus saving several hours of work that would be required using a traditional reactor setup, with typical exposure times ranging from 1-5 mins per well required to achieve a UV fluence in the oxidation range. It is important to note that there is also additional time (in the magnitude of seconds per sample) needed for the internal arm to move from well to well and adjust to a new position on the microplate.

Amino acid-spiked microplate wells were treated with two different oxidation fluences, at two different wavelengths, and at two different initial concentrations. Fluence for each of the protocols was calculated using the fluence response curves generated by actinometry. Exposure times per well ranged from four to fifteen minutes per well for 100 and 400 mJ cm<sup>-2</sup>, respectively. A box and whisker plot for the residual tryptophan and tyrosine concentrations is shown in **Figure 6-4**. The high-NOM condition (100 µg L<sup>-1</sup> amino acid) showed modest degradation in both tryptophan and tyrosine with the 280 nm, 100 mJ cm<sup>2</sup> treatment providing the highest removal. Removal of tryptophan and tyrosine differed in low-NOM conditions (10 µg L<sup>-1</sup> amino acid). While degradation of tyrosine for the 10 µg L<sup>-1</sup> samples was similar to that in 100 µg L<sup>-1</sup> tyrosine samples, the 400 mJ cm<sup>-2</sup> UV treatment of tryptophan for both 255 and 280 nm resulted in 84.66% and 55.17% removal, respectively.

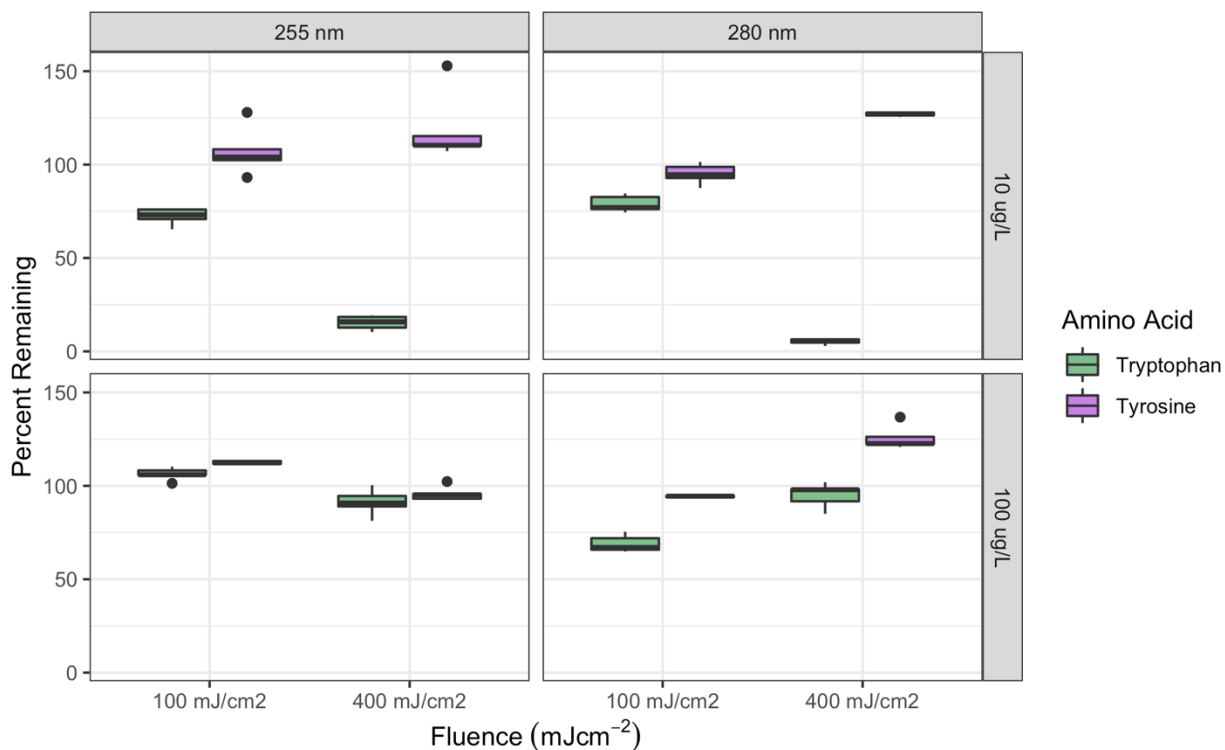


**Figure 6-4** Percentage of residual amino acid after UV exposure for the eight experimental conditions that were tested in this study. Samples with >100% recovery experienced evaporation during the UV exposure process leading to an increased concentration of the analyte.

These results demonstrate that the microplate reader performs advanced oxidation in a high-throughput manner with the added benefit of wavelength selection. Up to 96 individually UV treated samples can be generated in a single run using the protocol developed in this work. Application of this protocol will allow rapid understanding of the absorption and degradation properties of NOM and targeted organic compounds when treated with monochromatic UV-C light.

A limitation of this study was identified in the process of combining eight aliquots of sample from identically treated wells to make up the volume required for LC-MS analysis. Pipetting multiple aliquots of small volumes introduces a degree of uncertainty in amino acid quantitation, as evaporation and concentration of the sample would overestimate analyte response. Slight evaporation was observed in

some wells after UV-C exposure and may be responsible for the apparently higher amino acid concentration in some of the treated samples than in untreated samples, as seen in **Figure 6-4**. Tryptophan and tyrosine were specifically chosen to mitigate potential losses from these effects as they are non-volatile and can be robustly quantified to monitor losses and evaporation. To mitigate this potential source of error, future studies may involve experiments with larger well volumes (to reduce the number of aliquots required) or modification of LC-MS injection parameters to be optimized for low volumes of required treated water per LC-MS sample.

### **6.4.3 Environmental Applications**

This work outlines the steps required to convert an existing technology into a high-throughput UV reactor. The light source within the microplate reader in this study is xenon-flash based but a similar device based on UV-LED light sources is also proposed. UV-LED reactors provide a unique treatment option for providing customized light emittance that could improve degradation efficiency by emitting light only at key absorbance wavelengths specific to targeted compounds. A secondary benefit of this approach would be a reduction of wasted light output by the reactor. This means that the majority of the light output by a tailored UV reactor would be working towards contaminant degradation rather than being wasted, as in the case with medium-pressure UV reactors. Preliminary protocols for LED output standardization and inefficient power output from LED must be improved upon before UV-LEDs are commercially viable (Linden et al., 2019). Customizable UV treatment strategies will have a drastic impact on how water professionals resolve water treatment issues as UV-LED technology expands the design space of where UV treatment can be applied.

A platform that automates the process of applying several different UV treatments across a single protocol of samples would drastically increase the efficiency of bench-scale advanced oxidation studies. A technology that can easily emit a wide variety of UV wavelengths without the constant oversight of a technician provides the

opportunity to design customized UV treatment regimens that are specific to what is being treated. Research is unclear if combining certain wavelengths of light increases disinfection or oxidation capabilities and more work is needed to identify which wavelengths work best in synergy (Yamato Hosoi, Kumiko Oguma, Satoshi Takizawa, 2017). Current studies have examined only a limited combination of wavelengths, and this approach to UV treatment would expand the design space of customized UV treatment research. The platform proposed in this work provides researchers a novel approach to accelerate their understanding of different interactions between UV light and organic material while saving people-hours in the process. In time, UV-LEDs will be able to emit at narrow bandwidth of wavelengths across the UV spectrum, but the current state of the technology does not allow for such use across the full UV spectrum.

Drinking water and wastewater utilities require a firm understanding of potentially harmful organic contaminants and waterborne pathogens, as well as effective methods available to treat them. A high-throughput tunable UV-LED reactor would allow focused and rapid photooxidation experimentation to investigate specific wavelengths that optimally treat individual contaminants and pathogens. Data from these experiments could be utilized by drinking water and wastewater utilities to tailor their treatment strategies, resulting in substantial economic savings. As this technology advances, UV reactors equipped to point-of-use water sources, home appliances, and submersible sensors will soon be a reality for applied water treatment. Moreover, an entirely new branch of UV treatment research investigating the synergistic effects of combining distinct wavelengths of light could be developed. In dire circumstances such as this current global emergency inflicted by the COVID-19 pandemic, call to action associated with UV Treatment have been made and it is conceivable that the proposed high-throughput monochromatic UV treatment platform could be utilized for rapid testing of virus inactivation under multiple water matrices and scenarios (L. Liao et al., 2020).

## 6.5 Conclusions

The research outlined in this study establishes the need for an improved platform for a high-throughput monochromatic UV reactor. A microplate reader was repurposed as a surrogate reactor for a proposed platform technology. The xenon-flash based light source within the reactor was characterized using actinometry and protocols were coded using the instrument software to control the UV fluence applied to wells of microplates. Additional protocols were developed to control both the wavelength emitted from the instrument and the selection of wells treated during instrument operation. This innovative approach was used for the degradation of amino acids that were spiked into deionized water. In the low NOM concentration conditions for 255 and 280 nm, tryptophan was oxidized at a much higher proportion when compared to tyrosine at the 400 mJ cm<sup>-2</sup> fluence. The results indicate that the protocols used for UV exposure are indeed able to tune UV-C light that directs the oxidation of targeted compounds. It also highlights the fact that the wavelength of emitted UV-C light has an impact on the removal efficiency even when the targeted compounds are similar to each other. The oxidation capabilities of the device provided proof-of-concept that a bench-scale UV reactor can be automated to perform rapid, multi-sample treatment protocols. This work also addresses the issue of limited availability of single wavelength emitting reactors through the use of monochromator light source.

This study reveals that a monochromator-based light source may be used as a surrogate for UV-LEDs until the technology evolves to a point when single-wavelength UV LEDs are widely available. The novel approach to use this technology as a proxy reactor will allow for the characterization of the disinfection profile for microorganisms and targeted organic compounds based on emitted UV wavelength. In addition, this platform drastically reduces the person-hours required to conduct a bench-scale UV experiment. Producing 96 UV-treated samples in a few hours is orders of magnitude faster and requires a fraction of the labour required when compared to traditional flow-through or collimated beam bench-scale reactors. The authors

suggest that future work should focus on the development of a solely UV-LED-based automated reactor that functions similarly to the microplate reader but at the bench scale. This reactor would combine the work presented in this study with the work from Betzlal in developing a manual protocol for UV exposure using microplates as a way to separate samples when simultaneously exposing them to UV light (Betzalel et al., 2020).

Another potential function of this technology moving forward is to use it as a screening tool for water utilities to optimize their UV-C treatment conditions. Rapidly producing UV-C treated water at a wide range of UV-C and wavelength conditions would allow for water utilities to easily obtain data that would inform customized water treatment. This functionality would be useful for new and existing water treatment plants that are experiencing seasonality or changes in their influent water quality. The authors propose future work using this high-throughput approach on real water matrices from sources that have issues with known and targeted organic compounds. The use of real environmental samples will provide insight regarding water matrix effects for this experimental setup. Furthermore, the use of real water matrices using the concepts developed in this proof-of-concept study will provide a more robust understanding of how UV-C light interacts with NOM.

The core premise and functionality of the microplate reader can be scaled by using a UV-LED in place of the xenon lamp used in this study. UV-LED reactors are becoming much more selective in their emitted light and have flexible design applications due to their modular nature. A bench-scale device capable of automated, high-throughput exposure of samples to UV light would reduce the people hours required to physically monitor the instrument by orders of magnitude. The inherent flexibility in design of LED centric reactors will expand the design space and practical application of UV treatment by orders of magnitude. UV-LED-based reactors are the future of oxidation and disinfection technology for water treatment.

## 7 Conclusions and Recommendations

### 7.1 Summary and Conclusions

This thesis assesses how AOP impact the NOM of both natural and synthetic water matrices and provides a number of approaches for examining these effects. The work of this thesis gives results that are useful to both the scientific community and to water utilities for their decision making in the face of changing water quality in source waters. The completed thesis objectives focused on better understanding of the relationship between NOM and AOPs and are outlined as follows:

- AOPs were used to degrade targeted, low molecular weight compounds and the side effects of AOP exposure on a natural water matrix were quantified.
  - AOPs caused shifts in humic material to lower molecular weights primarily in H<sub>2</sub>O<sub>2</sub> based conditions.
  - O<sub>3</sub> based AOP tended to initially oxidize protein-like material before humic like material.
  - The results of this phase of experimentation demonstrate that AOP are not entirely non-selective and more research is needed to further quantify oxidation priorities.
- DBP formation in a natural water matrix after exposure to AOP was examined for 10 difference conditions.
  - H<sub>2</sub>O<sub>2</sub> based AOP increased both THM and HAA DBP<sub>fp</sub> while UV and O<sub>3</sub> based AOP did not cause substantial increases in DBP<sub>fp</sub>.
  - The formation of low molecular weight organic compounds was observed in both 10 mg L<sup>-1</sup> peroxide and ozone AO treatments with distinct peaks in SEC data. The difference in these peaks explains the difference in DBP<sub>fp</sub> concentrations in AOP treated datasets.
  - This work highlights the importance of understanding the nature of the NOM of the working water matrix.

- A software package was developed to aid in understanding the changes that occur in large datasets of fluorescent excitation emission matrices when a water matrix is exposed to treatment technologies.
- The dataset used in this study was generated using AOP, but the underlying approach is generic in its assessment of changes in NOM. K-means distancing classification using the PCA loadings showed promise in characterizing changes in the fluorescent profile of natural and synthetic water samples.
- Finally, a commercially available microplate instrument was repurposed and reprogrammed to behave as a high throughput UV exposure unit.
  - Allows for a truly UV tunable and multiwell approach for bench scale UV work and has been proven with a proof-of-concept using model compounds.
  - Increases the rate of data acquisition for AOP samples by orders of magnitude.
  - Also has implications for disinfection studies and the rapid development of tunable UV dose response curves.

The culmination of this thesis contributes to advanced oxidation research by connecting the oxidation properties of AOP with the descriptive nature of fluorescent data. There are currently few studies that examine the role that AOPs may play in the overall change in fluorescent NOM when they are introduced in a water matrix. This thesis also contributes to the UV disinfection and oxidation research community by providing a novel tool for tunable, high throughput UV exposure. There has been a call to action in UV literature for such an approach and the work of this thesis serves this purpose.

## **7.2 Recommendations for Future Work**

This work establishes several options for future research and innovation. The first suggestion is to complete the integration of UV exposure with FEEM measurement on the microplate instrument. The code for this functionality is already written and requires further proof of concept to collect the data reliably. Another recommendation is to incorporate the use of the chemical reservoir pumps that are equipped to the microplate reader instrument. Incorporating these pumps into the high throughput UV exposure approach will allow for additional AOP to be examined in this system. For example, hydrogen peroxide and chlorine based AOP could be examined using this approach and the high throughput methodology would allow for a variety of concentrations and combinations of chemical oxidants to be tested along with UV-C light.

A replication of the geosmin removal study with Pockwock Lake water from present day is also recommended. Replication of this study will allow for a comparison of the nature of the NOM within the lake before and after brownification has occurred. The risk of harmful algal toxins proliferating within the lake is a fear for the water utility each year and a better understanding of NOM is needed to inform decisions that may change water treatment plant processes. Providing a longitudinal study on the changing nature of the NOM of Pockwock Lake would provide useful information as to how AOP may fit into treatment schemes as brownification of lakes impacts water treatment plants.

This work also highlights that an understanding of the NOM profile of a source water is crucial when deciding on an AO treatment type. It is recommended that water utilities consider some of the factors outlined in Chapter 4 when using AOPs at scale. Different AOPs, even when applied at similar dosages results in a vastly different NOM profile after treatment. This outcome is also dependent on the specific water source that is being used. As described in Chapter 4, AOPs can both negatively and positively impact the formation potential of disinfection byproducts. Choosing a treatment type at full scale without this consideration introduces unnecessary risks to the public

health and performance of water treatment plant processes. Changes in NOM can impact coagulation, filtration, and fouling in addition to increase DBP formation.

Fluorescence is recommended as a parameter that can cheaply, non-destructively, and rapidly collect large volumes of NOM data. Although fluorescence cannot specifically quantify compounds within a water matrix, it can be coupled with advanced statistical models and artificial intelligence tools to understand underlying changes in the NOM signature of a water matrix. It is recommended that further research is conducted in this area of study in order to fully realize the potential of excitation-emission matrices for describing the nature of NOM within water matrices.

Finally, the adoption of the high-throughput UV exposure approach is recommended for researchers who need rapid sample generation that is coupled with tuned UV-C light source. In summary, this thesis provides novel research for better understanding the interactions between AOP and NOM. This thesis also establishes a novel framework that expedites the collection of UV exposure data that allows for wider use of AO technologies moving forward.

## References

- Abdi, H., & Williams, L. J. (2010). Principal component analysis: Principal component analysis. *Wiley Interdisciplinary Reviews: Computational Statistics*, 2(4), 433–459. <https://doi.org/10.1002/wics.101>
- Aiken, G., & Cotsaris, E. (1995). Soil and Hydrology: Their effect on NOM. *Journal - American Water Works Association*, 87(1), 36–45.
- Al-Gharabli, S., Engeßer, P., Gera, D., Klein, S., & Oppenländer, T. (2016). Engineering of a highly efficient Xe<sup>2\*</sup>-excilamp (xenon excimer lamp,  $\lambda_{\max}$ = 172 nm,  $\eta$ = 40%) and qualitative comparison to a low-pressure mercury lamp (LP-Hg,  $\lambda$  = 185/254 nm) for water purification. *Chemosphere*, 144, 811–815. <https://doi.org/10.1016/j.chemosphere.2015.09.012>
- Andersen, C. M., & Bro, R. (2003). Practical aspects of PARAFAC modeling of fluorescence excitation-emission data. *Journal of Chemometrics*, 17(4), 200–215. <https://doi.org/10.1002/cem.790>
- Anderson, L. E., Krkošek, W. H., Stoddart, A. K., Trueman, B. F., & Gagnon, G. A. (2017). Lake Recovery Through Reduced Sulfate Deposition: A New Paradigm for Drinking Water Treatment. *Environmental Science & Technology*, 51(3), 1414–1422. <https://doi.org/10.1021/acs.est.6b04889>
- Andreozzi, R., Caprio, V., Insola, A., & Marotta, R. (1999). Advanced oxidation processes (AOP) for water purification and recovery. *Catalysis Today*, 9.

- Antonopoulou, M., Evgenidou, E., Lambropoulou, D., & Konstantinou, I. (2014). A review on advanced oxidation processes for the removal of taste and odor compounds from aqueous media. *Water Research*, *53*, 215–234.  
<https://doi.org/10.1016/j.watres.2014.01.028>
- Aquisense Technologies. (2020). *PEARLAQUA DECA™ UV-C LED POINT-OF-ENTRY SYSTEM*. <https://www.aquisense.com/pearlaqua-deca>
- Baghoth, S. A., Sharma, S. K., & Amy, G. L. (2011a). Tracking natural organic matter (NOM) in a drinking water treatment plant using fluorescence excitation-emission matrices and PARAFAC. *Water Research*.  
<https://doi.org/10.1016/j.watres.2010.09.005>
- Baghoth, S. A., Sharma, S. K., & Amy, G. L. (2011b). Tracking natural organic matter (NOM) in a drinking water treatment plant using fluorescence excitation-emission matrices and PARAFAC. *Water Research*, *45*(2), 797–809.  
<https://doi.org/10.1016/j.watres.2010.09.005>
- Baird, R., Eaton, A., & Rice, E. (2017). *Standard Methods for the Examination of Water and Wastewater*. Standard Methods. <https://www.standardmethods.org>
- Baker, A. (2001). Fluorescence Excitation–Emission Matrix Characterization of Some Sewage-Impacted Rivers. *Environmental Science & Technology*, *35*(5), 948–953.  
<https://doi.org/10.1021/es000177t>
- Baranda, A. B., Barranco, A., & de Marañón, I. M. (2012). Fast atrazine photodegradation in water by pulsed light technology. *Water Research*, *46*(3), 669–678.  
<https://doi.org/10.1016/j.watres.2011.11.034>

- Baranda, A. B., Fundazuri, O., & Martínez de Marañón, I. (2014). Photodegradation of several triazidic and organophosphorus pesticides in water by pulsed light technology. *Journal of Photochemistry and Photobiology A: Chemistry*, *286*, 29–39. <https://doi.org/10.1016/j.jphotochem.2014.03.015>
- Beck, S. E., Ryu, H., Boczek, L. A., Cashdollar, J. L., Jeanis, K. M., Rosenblum, J. S., Lawal, O. R., & Linden, K. G. (2017). Evaluating UV-C LED disinfection performance and investigating potential dual-wavelength synergy. *Water Research*, *109*, 207–216. <https://doi.org/10.1016/j.watres.2016.11.024>
- Betzalel, Y., Gerchman, Y., Cohen-Yaniv, V., & Mamane, H. (2020). Multiwell plates for obtaining a rapid microbial dose-response curve in UV-LED systems. *Journal of Photochemistry and Photobiology B: Biology*, *207*, 111865. <https://doi.org/10.1016/j.jphotobiol.2020.111865>
- BioTek. (2020). *BioTek Synergy H1 Instrument Documentation*. BioTek Instruments, Inc., (Winooski, VT, USA). <https://www.biotek.com/products/detection-hybrid-technology-multi-mode-microplate-readers/synergy-h1-hybrid-multi-mode-reader/>
- Bolton, J. R., & Linden, K. G. (2003). Standardization of Methods for Fluence (UV Dose) Determination in Bench-Scale UV Experiments. *Journal of Environmental Engineering*, *129*(3), 209–215. [https://doi.org/10.1061/\(ASCE\)0733-9372\(2003\)129:3\(209\)](https://doi.org/10.1061/(ASCE)0733-9372(2003)129:3(209))
- Bolton, J. R., & Stefan, M. I. (2002). Fundamental photochemical approach to the concepts of fluence (UV dose) and electrical energy efficiency in photochemical

degradation reactions. *Research on Chemical Intermediates*, 28(7–9), 857–870.

<https://doi.org/10.1163/15685670260469474>

Bolton, J. R., Stefan, M. I., Shaw, P., & Lykke, K. R. (2011). Determination of the quantum yields of the potassium ferrioxalate and potassium iodide – iodate actinometers and a method for the calibration of radiometer detectors. *Photochemistry and Photobiology*, 222, 166–169. <https://doi.org/10.1016/j.jphotochem.2011.05.017>

Bond, T., Henriot, O., Goslan, E. H., Parsons, S. A., & Jefferson, B. (2009). Disinfection Byproduct Formation and Fractionation Behavior of Natural Organic Matter Surrogates. *Environmental Science & Technology*, 43(15), 5982–5989.

<https://doi.org/10.1021/es900686p>

Bowker, C., Sain, A., Shatalov, M., & Ducoste, J. (2011). Microbial UV fluence-response assessment using a novel UV-LED collimated beam system. *Water Research*, 45(5), 2011–2019. <https://doi.org/10.1016/j.watres.2010.12.005>

Brame, J., Long, M., Li, Q., & Alvarez, P. (2015). Inhibitory effect of natural organic matter or other background constituents on photocatalytic advanced oxidation processes: Mechanistic model development and validation. *Water Research*, 84, 362–371. <https://doi.org/10.1016/j.watres.2015.07.044>

Bro, R. (1997). PARAFAC. Tutorial and applications. *Chemometrics and Intelligent Laboratory Systems*, 23.

Bro, R., & Smilde, A. K. (2014). Principal component analysis. *Anal. Methods*, 6(9), 2812–2831. <https://doi.org/10.1039/C3AY41907J>

- Buffle, M.-O., Schumacher, J., Meylan, S., Jekel, M., & von Gunten, U. (2006). Ozonation and Advanced Oxidation of Wastewater: Effect of O<sub>3</sub> Dose, pH, DOM and HO<sup>•</sup> - Scavengers on Ozone Decomposition and HO<sup>•</sup> Generation. *Ozone: Science & Engineering*, 28(4), 247–259. <https://doi.org/10.1080/01919510600718825>
- Calgon Carbon. (2012). *Calgon Carbon Collimated Beam Unit Users Manual*. Calgon Carbon Corporation. <https://www.calgoncarbon.com/products/rayox/>
- Çamdevýren, H., Demýr, N., Kanik, A., & Keskýn, S. (2005). Use of principal component scores in multiple linear regression models for prediction of Chlorophyll-a in reservoirs. *Ecological Modelling*, 181(4), 581–589. <https://doi.org/10.1016/j.ecolmodel.2004.06.043>
- Cape Breton Regional Municipality. (2015). *Pottle Lake Water Treatment Plant*. Pottle Lake Water Treatment Plant. <https://www.cbrm.ns.ca/pottle-lake-water-treatment-plant.html>
- Chatterley, C., & Linden, K. (2010). Demonstration and evaluation of germicidal UV-LEDs for point-of-use water disinfection. *Journal of Water and Health*, 8(3), 479–486. <https://doi.org/10.2166/wh.2010.124>
- Chen, D. H., Ye, X., & Li, K. (2005). Oxidation of PCE with a UV LED Photocatalytic Reactor. *Chemical Engineering & Technology*, 28(1), 95–97. <https://doi.org/10.1002/ceat.200407012>
- Chen, W., Westerhoff, P., Leenheer, J. A., & Booksh, K. (2003). Fluorescence Excitation–Emission Matrix Regional Integration to Quantify Spectra for Dissolved

- Organic Matter. *Environmental Science & Technology*, 37(24), 5701–5710.  
<https://doi.org/10.1021/es034354c>
- Chin, A., & Bérubé, P. R. (2005). Removal of disinfection by-product precursors with ozone-UV advanced oxidation process. *Water Research*, 39(10), 2136–2144.  
<https://doi.org/10.1016/j.watres.2005.03.021>
- Chong, M. N., Sharma, A. K., Burn, S., & Saint, C. P. (2012). Feasibility study on the application of advanced oxidation technologies for decentralised wastewater treatment. *Journal of Cleaner Production*, 9.
- Chorus, I., & Bartram, J. (Eds.). (1999). *Toxic cyanobacteria in water: A guide to their public health consequences, monitoring, and management*. E & FN Spon.
- Chowdhury, F. L., Bérubé, P. R., & Mohseni, M. (2008). Characteristics of Natural Organic Matter and Formation of Chlorinated Disinfection By-Products from Two Source Waters that Respond Differently to Ozonation. *Ozone: Science & Engineering*, 30(5), 321–331. <https://doi.org/10.1080/01919510802169272>
- Chu, W., Li, X., Bond, T., Gao, N., & Yin, D. (2016). The formation of haloacetamides and other disinfection by-products from non-nitrogenous low-molecular weight organic acids during chloramination. *Chemical Engineering Journal*, 285, 164–171. <https://doi.org/10.1016/j.cej.2015.09.087>
- Chu, W.-H., Gao, N.-Y., Deng, Y., & Krasner, S. W. (2010). Precursors of Dichloroacetamide, an Emerging Nitrogenous DBP Formed during Chlorination or Chloramination. *Environmental Science & Technology*, 44(10), 3908–3912.  
<https://doi.org/10.1021/es100397x>

- Chuang, Y.-H., Chen, S., Chinn, C. J., & Mitch, W. A. (2017). Comparing the UV/Monochloramine and UV/Free Chlorine Advanced Oxidation Processes (AOPs) to the UV/Hydrogen Peroxide AOP Under Scenarios Relevant to Potable Reuse. *Environmental Science & Technology*, *51*(23), 13859–13868. <https://doi.org/10.1021/acs.est.7b03570>
- Clancy, J. L., Bukhari, Z., Hargy, T. M., Bolton, J. R., Dussert, B. W., & Marshall, M. M. (2000). Using UV to inactivate *Cryptosporidium*. *Journal - American Water Works Association*, *92*(9), 97–104. <https://doi.org/10.1002/j.1551-8833.2000.tb09008.x>
- Clancy, J. L., Marshall, M. M., Hargy, T. M., & Korich, D. G. (2004). Susceptibility of five strains of *Cryptosporidium parvum* oocysts to UV light. *Journal - American Water Works Association*, *96*(3), 84–93. <https://doi.org/10.1002/j.1551-8833.2004.tb10576.x>
- Coaton, J. R., & Rees, J. M. (1981). *54 INCANDESCENT HALOGEN LAMP WITH* (Patent No. 4,256,988).
- Coogan, J. J. (2005). Pathogen Control in Complex Fluids with Water-coupled Excimer Lamps at 282 and 308 nm. *Photochemistry and Photobiology*, *81*(6), 1511. <https://doi.org/10.1562/2005-05-27-RA-547>
- Cook, D., Newcombe, G., & Sztajn bok, P. (2001). The application of powdered activated carbon for mib and geosmin removal: Predicting pac doses in four raw waters. *Water Research*, *35*(5), 1325–1333. [https://doi.org/10.1016/S0043-1354\(00\)00363-8](https://doi.org/10.1016/S0043-1354(00)00363-8)

- Cotruvo, J. A., & Amato, H. (2019). National Trends of Bladder Cancer and Trihalomethanes in Drinking Water: A Review and Multicountry Ecological Study. *Dose-Response*, 17(1), 155932581880778.  
<https://doi.org/10.1177/1559325818807781>
- Croué, J.-P. (2004). Isolation of Humic and Non-Humic NOM Fractions: Structural Characterization. *Environmental Monitoring and Assessment*, 92(1–3), 193–207.  
<https://doi.org/10.1023/B:EMAS.0000039369.66822.c0>
- Cuerda-Correa, E. M., Alexandre-Franco, M. F., & Fernández-González, C. (2019). Advanced Oxidation Processes for the Removal of Antibiotics from Water. An Overview. *Water*, 12(1), 102. <https://doi.org/10.3390/w12010102>
- Díaz, P. (2016). Shifting paradigms, changing waters: Transitioning to integrated urban water management in the coastal city of Dunedin, USA. *Sustainable Cities and Society*, 13.
- Díaz, P., Morley, K. M., & Yeh, D. H. (2017). Resilient urban water supply: Preparing for the slow-moving consequences of climate change. *Water Practice*, 12(1), 17.
- Dolejs, P. (1993). Influence of Algae and Their Exudates on Removal of Humic Substances and Optimal Dose of Coagulant. *Water Science and Technology*, 27(11), 123–132.  
<https://doi.org/10.2166/wst.1993.0271>
- Dong, H., Qiang, Z., Hu, J., & Qu, J. (2017). Degradation of chloramphenicol by UV/chlorine treatment: Kinetics, mechanism and enhanced formation of halonitromethanes. *Water Research*, 121, 178–185.  
<https://doi.org/10.1016/j.watres.2017.05.030>

- Dong, H., Qiang, Z., & Richardson, S. D. (2019). Formation of Iodinated Disinfection Byproducts (I-DBPs) in Drinking Water: Emerging Concerns and Current Issues. *Accounts of Chemical Research*, 52(4), 896–905.  
<https://doi.org/10.1021/acs.accounts.8b00641>
- Donham, J. E., Rosenfeldt, E. J., & Wigginton, K. R. (2014). Photometric hydroxyl radical scavenging analysis of standard natural organic matter isolates. *Environmental Sciences: Processes and Impacts*. <https://doi.org/10.1039/c3em00663h>
- Dotson, A. D., Keen, V. (Olya) S., Metz, D., & Linden, K. G. (2010). UV/H<sub>2</sub>O<sub>2</sub> treatment of drinking water increases post-chlorination DBP formation. *Water Research*, 44(12), 3703–3713. <https://doi.org/10.1016/j.watres.2010.04.006>
- Edzwald, J. K. (1993). Coagulation in Drinking Water Treatment: Particles, Organics and Coagulants. *Water Science and Technology*, 27(11), 21–35.  
<https://doi.org/10.2166/wst.1993.0261>
- Eikebrokk, B., Vogt, R. D., & Liltved, H. (2004). NOM increase in Northern European source waters: Discussion of possible causes and impacts on coagulation/contact filtration processes. *Water Supply*, 4(4), 47–54.  
<https://doi.org/10.2166/ws.2004.0060>
- Ertel, J. R., Hedges, J. I., & Perdue, E. M. (1984). Lignin Signature of Aquatic Humic Substances. *Science*, 223(4635), 485–487.  
<https://doi.org/10.1126/science.223.4635.485>
- Esplugas, S., Bila, D. M., Krause, L. G. T., & Dezotti, M. (2007). Ozonation and advanced oxidation technologies to remove endocrine disrupting chemicals (EDCs) and

pharmaceuticals and personal care products (PPCPs) in water effluents. *Journal of Hazardous Materials*, 149(3), 631–642.

<https://doi.org/10.1016/j.jhazmat.2007.07.073>

Esplugas, S., Giménez, J., Contreras, S., Pascual, E., & Rodríguez, M. (2002). Comparison of different advanced oxidation processes for phenol degradation. *Water Research*, 36(4), 1034–1042. [https://doi.org/10.1016/S0043-1354\(01\)00301-3](https://doi.org/10.1016/S0043-1354(01)00301-3)

Fair, L. (2020, May 7). 45 more companies get coronavirus warning letters [FTC]. *FTC Business Blog*. <https://www.ftc.gov/news-events/blogs/business-blog/2020/05/45-more-companies-get-coronavirus-warning-letters>

Fang, X., Schuchmann, H.-P., & von Sonntag, C. (2000). The reaction of the OH radical with pentafluoro-, pentachloro-, pentabromo- and 2,4,6-triodophenol in water: Electron transfer vs. addition to the ring. *Journal of the Chemical Society, Perkin Transactions 2*, 7, 1391–1398. <https://doi.org/10.1039/b002191l>

Federal-Provincial-Territorial Committee on Drinking Water (Canada). (2006). *Guidelines for Canadian Drinking Water Quality: Guideline Technical Document* (p. 67).

Health Canada. <https://healthycanadians.gc.ca/publications/healthy-living-vie-saine/water-trihalomethanes-eau/alt/water-trihalomethanes-eau-eng.pdf>

Federal-Provincial-Territorial Committee on Drinking Water (Canada), Canada, Health Canada, & Federal-Provincial-Territorial Committee on Health and the Environment (Canada). (2008). *Guidelines for Canadian drinking water quality: Guideline technical document : haloacetic acids*. Health Canada.

<https://central.bac-lac.gc.ca/.item?id=H128-1-08-548E&op=pdf&app=Library>

- Formation of Reactive Free Radicals in an Aqueous Environment. (2006). In Clemens von Sonntag, *Free-Radical-Induced DNA Damage and Its Repair* (pp. 7–46). Springer Berlin Heidelberg. [https://doi.org/10.1007/3-540-30592-0\\_2](https://doi.org/10.1007/3-540-30592-0_2)
- Freeman, K. S. (2010). HARMFUL ALGAL BLOOMS: Musty Warnings of Toxicity. *Environmental Health Perspectives*, 118(11), A473.
- Gerrity, D., Mayer, B., Ryu, H., Crittenden, J., & Abbaszadegan, M. (2009). A comparison of pilot-scale photocatalysis and enhanced coagulation for disinfection byproduct mitigation. *Water Research*, 43(6), 1597–1610. <https://doi.org/10.1016/j.watres.2009.01.010>
- Gligorovski, S., Strekowski, R., Barbati, S., & Vione, D. (2015). Environmental Implications of Hydroxyl Radicals ( $\cdot\text{OH}$ ). *Chemical Reviews*, 115(24), 13051–13092. <https://doi.org/10.1021/cr500310b>
- Gude, V. G. (2017). Desalination and water reuse to address global water scarcity. *Rev Environ Sci Biotechnol*, 19.
- Hammes, F., Salhi, E., Köster, O., Kaiser, H.-P., Egli, T., & von Gunten, U. (2006). Mechanistic and kinetic evaluation of organic disinfection by-product and assimilable organic carbon (AOC) formation during the ozonation of drinking water. *Water Research*, 40(12), 2275–2286. <https://doi.org/10.1016/j.watres.2006.04.029>
- Hansen, A. M., Kraus, T. E. C., Pellerin, B. A., Fleck, J. A., Downing, B. D., & Bergamaschi, B. A. (2016). Optical properties of dissolved organic matter (DOM): Effects of biological and photolytic degradation: DOM optical properties following

degradation. *Limnology and Oceanography*, 61(3), 1015–1032.

<https://doi.org/10.1002/lno.10270>

Harshman, R. A., & Lundy, M. E. (1996). Uniqueness proof for a family of models sharing features of Tucker's three-mode factor analysis and PARAFAC/candecomp.

*Psychometrika*, 61(1), 133–154. <https://doi.org/10.1007/BF02296963>

Hartigan, J. A., & Wong, M. A. (1979). Algorithm AS 136: A K-Means Clustering

Algorithm. *Applied Statistics*, 28(1), 100. <https://doi.org/10.2307/2346830>

He, Z., Mark A. Prelas, Jon M. Meese, & Li-Te Lin. (1998). Microwave excitation and applications of an elliptical excimer lamp. *Laser and Particle Beams*, 16(3), 509–524.

Heit, G., Neuner, A., Saugy, P.-Y., & Braun, A. M. (1998). Vacuum-UV (172 nm)

Actinometry. The Quantum Yield of the Photolysis of Water. *The Journal of*

*Physical Chemistry A*, 102(28), 5551–5561. <https://doi.org/10.1021/jp980130i>

Henderson, R. K., Baker, A., Murphy, K. R., Hambly, A., Stuetz, R. M., & Khan, S. J. (2009).

Fluorescence as a potential monitoring tool for recycled water systems: A review.

*Water Research*, 43(4), 863–881. <https://doi.org/10.1016/j.watres.2008.11.027>

Hodgeson, J W, Collins, J., Barth, R. E., Fair, P. S., Munch, D. J., & Xie, Y. (2003).

DETERMINATION OF HALOACETIC ACIDS AND DALAPON IN DRINKING WATER BY

LIQUID-LIQUID MICROEXTRACTION, DERIVATIZATION, AND GAS

CHROMATOGRAPHY WITH ELECTRON CAPTURE DETECTION. *US EPA*, 55.

- Hodgeson, Jimmie W, & Becker, D. (1992). Determination of haloacetic acids and dalapon in drinking water by ion-exchange liquid-solid extraction and gas chromatography with an electron capture detector. *US EPA*, 30.
- Hoffmann, M. R., Martin, S. T., Choi, Wonyong., & Bahnemann, D. W. (1995). Environmental Applications of Semiconductor Photocatalysis. *Chemical Reviews*, 95(1), 69–96. <https://doi.org/10.1021/cr00033a004>
- Hosein, I., Madeloso, R., Nagarathnam, W., Villamaria, F., Stock, E., & Jinadatha, C. (2016). Evaluation of a pulsed xenon ultraviolet light device for isolation room disinfection in a United Kingdom hospital. *American Journal of Infection Control*, 44(9), e157–e161. <https://doi.org/10.1016/j.ajic.2016.01.044>
- Huang, P., & Wang, Y. (2019). Carpet-like TiO<sub>2</sub> Nanofiber Interlayer as Advanced Absorber for High Performance Li-S batteries. *Int. J. Electrochem. Sci.*, 14, 7.
- Huang, W.-J., Chen, L.-Y., & Peng, H.-S. (2004). Effect of NOM characteristics on brominated organics formation by ozonation. *Environment International*, 29(8), 1049–1055. [https://doi.org/10.1016/S0160-4120\(03\)00099-0](https://doi.org/10.1016/S0160-4120(03)00099-0)
- Hudson, N., Baker, A., & Reynolds, D. (2007). Fluorescence analysis of dissolved organic matter in natural, waste and polluted waters—A review. *River Research and Applications*, 23(6), 631–649. <https://doi.org/10.1002/rra.1005>
- Ibrahim, M. A. S., MacAdam, J., Autin, O., & Jefferson, B. (2014). Evaluating the impact of LED bulb development on the economic viability of ultraviolet technology for disinfection. *Environmental Technology*, 35(4), 400–406. <https://doi.org/10.1080/09593330.2013.829858>

- Ijpelaar, G. F., Harmsen, D. J. H., Beerendonk, E. F., Leerdam, R. C. van, Metz, D. H., Knol, A. H., Fulmer, A., & Krijnen, S. (2010). Comparison of Low Pressure and Medium Pressure UV Lamps for UV/H<sub>2</sub>O<sub>2</sub> Treatment of Natural Waters Containing Micro Pollutants. *Ozone: Science & Engineering*, 32(5), 329–337.  
<https://doi.org/10.1080/01919512.2010.508017>
- Ike, I. A., Lee, Y., & Hur, J. (2019). Impacts of advanced oxidation processes on disinfection byproducts from dissolved organic matter upon post-chlor(am)ination: A critical review. *Chemical Engineering Journal*, 375, 121929.  
<https://doi.org/10.1016/j.cej.2019.121929>
- Imoberdorf, G., & Mohseni, M. (2011). Degradation of natural organic matter in surface water using vacuum-UV irradiation. *Journal of Hazardous Materials*, 186(1), 240–246. <https://doi.org/10.1016/j.jhazmat.2010.10.118>
- Ivančev-Tumbas, I. (2014). The fate and importance of organics in drinking water treatment: A review. *Environmental Science and Pollution Research*, 21(20), 11794–11810. <https://doi.org/10.1007/s11356-014-2894-8>
- Jagger, J. (1967). *Introduction to research in ultra-violet photobiology*. Prentice-Hall: Englewood Cliffs, N.J.
- Jarvis, Autin, Goslan, & Hassard. (2019). Application of Ultraviolet Light-Emitting Diodes (UV-LED) to Full-Scale Drinking-Water Disinfection. *Water*, 11(9), 1894.  
<https://doi.org/10.3390/w11091894>
- Jing, Y., & Chaplin, B. P. (2017). Mechanistic Study of the Validity of Using Hydroxyl Radical Probes To Characterize Electrochemical Advanced Oxidation Processes.

*Environmental Science & Technology*, 51(4), 2355–2365.

<https://doi.org/10.1021/acs.est.6b05513>

- Jung, H., & Choi, H. (2006a). Catalytic decomposition of ozone and para-Chlorobenzoic acid (pCBA) in the presence of nanosized ZnO. *Applied Catalysis B: Environmental*, 66(3–4), 288–294. <https://doi.org/10.1016/j.apcatb.2006.03.009>
- Jung, H., & Choi, H. (2006b). Catalytic decomposition of ozone and para-Chlorobenzoic acid (pCBA) in the presence of nanosized ZnO. *Applied Catalysis B: Environmental*, 66(3–4), 288–294. <https://doi.org/10.1016/j.apcatb.2006.03.009>
- Kadam, A. R., Nair, G. B., & Dhoble, S. J. (2019). Insights into the extraction of mercury from fluorescent lamps: A review. *Journal of Environmental Chemical Engineering*, 7(4), 103279. <https://doi.org/10.1016/j.jece.2019.103279>
- Katsumata, H., Sada, M., Kaneco, S., Suzuki, T., Ohta, K., & Yobiko, Y. (2008). Humic acid degradation in aqueous solution by the photo-Fenton process. *Chemical Engineering Journal*, 137(2), 225–230. <https://doi.org/10.1016/j.cej.2007.04.019>
- Keen, O. S., & Linden, K. G. (2013). Re-Engineering an Artificial Sweetener: Transforming Sucralose Residuals in Water via Advanced Oxidation. *Environmental Science & Technology*, 47(13), 6799–6805. <https://doi.org/10.1021/es304339u>
- Keller, W., Gunn, J. M., & Yan, N. D. (1998). Acid rain—Perspectives on lake recovery. *Journal of Aquatic Ecosystem Stress and Recovery Volume*, 6, 206–216.
- Kent, F. C., Montreuil, K. R., Stoddart, A. K., Reed, V. A., & Gagnon, G. A. (2014). Combined use of resin fractionation and high performance size exclusion chromatography for characterization of natural organic matter. *Journal of*

*Environmental Science and Health, Part A*, 49(14), 1615–1622.

<https://doi.org/10.1080/10934529.2014.950926>

Keshavarzfathy, M., Hosoi, Y., Oguma, K., & Taghipour, F. (2021). Experimental and computational evaluation of a flow-through UV-LED reactor for MS2 and adenovirus inactivation. *Chemical Engineering Journal*, 407, 127058.

<https://doi.org/10.1016/j.cej.2020.127058>

Khan, S. J., & Cwiertny, D. M. (2020). Editorial Perspectives: What is “safe” drinking water, anyway? *Environmental Science: Water Research & Technology*, 6(1), 12–14. <https://doi.org/10.1039/C9EW90058F>

Kiparsky, M., Sedlak, D. L., Thompson, B. H., & Truffer, B. (2013). The Innovation Deficit in Urban Water: The Need for an Integrated Perspective on Institutions, Organizations, and Technology. *Environmental Engineering Science*, 30(8), 395–408. <https://doi.org/10.1089/ees.2012.0427>

Krasner, S. W. (2009). The formation and control of emerging disinfection by-products of health concern. *Philosophical Transactions of the Royal Society A: Mathematical, Physical and Engineering Sciences*, 367(1904), 4077–4095.

<https://doi.org/10.1098/rsta.2009.0108>

Krasner, S. W., Weinberg, H. S., Richardson, S. D., Pastor, S. J., Chinn, R., Scilimenti, M. J., Onstad, G. D., & Thruston, A. D. (2006). Occurrence of a New Generation of Disinfection Byproducts<sup>†</sup>. *Environmental Science & Technology*, 40(23), 7175–7185. <https://doi.org/10.1021/es060353j>

- Kutschera, K., Börnick, H., & Worch, E. (2009). Photoinitiated oxidation of geosmin and 2-methylisoborneol by irradiation with 254nm and 185nm UV light. *Water Research*, 43(8), 2224–2232. <https://doi.org/10.1016/j.watres.2009.02.015>
- Lamsal, R. (2012). *ADVANCED OXIDATION PROCESSES: ASSESSMENT OF NATURAL ORGANIC MATTER REMOVAL AND INTEGRATION WITH MEMBRANE PROCESSES*. Dalhousie University.
- Lamsal, R., Montreuil, K. R., Kent, F. C., Walsh, M. E., & Gagnon, G. A. (2012). Characterization and removal of natural organic matter by an integrated membrane system. *Desalination*, 303, 12–16. <https://doi.org/10.1016/j.desal.2012.06.025>
- Lamsal, R., Walsh, M. E., & Gagnon, G. A. (2011). Comparison of advanced oxidation processes for the removal of natural organic matter. *Water Research*, 45(10), 3263–3269. <https://doi.org/10.1016/j.watres.2011.03.038>
- Lanzarini-Lopes, M., Garcia-Segura, S., Hristovski, K., Messerly, M., Simon, A. J., & Westerhoff, P. (2019). Particle-modified polymeric cladding on glass optical fibers enhances radial light scattering. *Journal of the Optical Society of America B*, 36(6), 1623. <https://doi.org/10.1364/JOSAB.36.001623>
- Lanzarini-Lopes, M., Garcia-Segura, S., Hristovski, K., & Westerhoff, P. (2017). Electrical energy per order and current efficiency for electrochemical oxidation of p-chlorobenzoic acid with boron-doped diamond anode. *Chemosphere*, 188, 304–311. <https://doi.org/10.1016/j.chemosphere.2017.08.145>

Lanzarini-Lopes, M., Zhao, Z., Perreault, F., Garcia-Segura, S., & Westerhoff, P. (2020).

Germicidal glowsticks: Side-emitting optical fibers inhibit *Pseudomonas aeruginosa* and *Escherichia coli* on surfaces. *Water Research*, *184*, 116191.

<https://doi.org/10.1016/j.watres.2020.116191>

Leenheer, J. A. (1981). Comprehensive approach to preparative isolation and fractionation of dissolved organic carbon from natural waters and wastewaters.

*Environmental Science & Technology*, *15*(5), 578–587.

<https://doi.org/10.1021/es00087a010>

Leenheer, J. A., & Croué, J.-P. (2003). Characterising Dissolved Aquatic Organic Matter.

*Environ. Sci. Technol.*, 19–26.

Leenheer, J. A., Dotson, A., & Westerhoff, P. (2007). *Dissolved Organic Nitrogen*

*Fractionation. 1*, 13.

Lester, Y., Ferrer, I., Thurman, E. M., & Linden, K. G. (2014). Demonstrating sucralose as a monitor of full-scale UV/AOP treatment of trace organic compounds. *Journal of Hazardous Materials*, *280*, 104–110.

*Hazardous Materials*, *280*, 104–110.

<https://doi.org/10.1016/j.jhazmat.2014.07.009>

Li, J.-J., Wang, S.-N., Qiao, J.-J., Chen, L.-H., Li, Y., Wu, Y., Ding, Y.-X., Wang, M.-M., Tian,

Y., Liu, Y.-B., Yan, C., Zhang, C., & Gao, C.-Q. (2020). Portable pulsed xenon

ultraviolet light disinfection in a teaching hospital animal laboratory in China.

*Journal of Photochemistry and Photobiology B: Biology*, *207*, 111869.

<https://doi.org/10.1016/j.jphotobiol.2020.111869>

- Liao, C.-H., Kang, S.-F., & Wu, F.-A. (2001). Hydroxyl radical scavenging role of chloride and bicarbonate ions in the H<sub>2</sub>O<sub>2</sub>/UV process. *Chemosphere*, *44*(5), 1193–1200. [https://doi.org/10.1016/S0045-6535\(00\)00278-2](https://doi.org/10.1016/S0045-6535(00)00278-2)
- Liao, L., Xiao, W., Zhao, M., Yu, X., Wang, H., Wang, Q., Chu, S., & Cui, Y. (2020). Can N95 Respirators Be Reused after Disinfection? How Many Times? *ACS Nano*, *14*(5), 6348–6356. <https://doi.org/10.1021/acsnano.0c03597>
- Linden, K. G., Hull, N., & Speight, V. (2019). Thinking Outside the Treatment Plant: UV for Water Distribution System Disinfection. *Accounts of Chemical Research*, *52*(10), 2707–2715. <https://doi.org/10.1021/acs.accounts.9b00060>
- Liu, H., Jeong, J., Gray, H., Smith, S., & Sedlak, D. L. (2012). Algal Uptake of Hydrophobic and Hydrophilic Dissolved Organic Nitrogen in Effluent from Biological Nutrient Removal Municipal Wastewater Treatment Systems. *Environmental Science & Technology*, *46*(2), 713–721. <https://doi.org/10.1021/es203085y>
- Liu, Y., Jiang, J., Ma, J., Yang, Y., Luo, C., Huangfu, X., & Guo, Z. (2015). Role of the propagation reactions on the hydroxyl radical formation in ozonation and peroxone (ozone/hydrogen peroxide) processes. *Water Research*, *68*, 750–758. <https://doi.org/10.1016/j.watres.2014.10.050>
- Loeb, S. K., Alvarez, P. J. J., Brame, J. A., Cates, E. L., Choi, W., Crittenden, J., Dionysiou, D. D., Li, Q., Li-Puma, G., Quan, X., Sedlak, D. L., David Waite, T., Westerhoff, P., & Kim, J.-H. (2019). The Technology Horizon for Photocatalytic Water Treatment: Sunrise or Sunset? *Environmental Science & Technology*, *53*(6), 2937–2947. <https://doi.org/10.1021/acs.est.8b05041>

MacIsaac, H. J., Keller, W., Hutchinson, T. C., & Yan, N. D. (1986). Natural changes in the planktonic rotifera of a small acid lake near Sudbury, Ontario following water quality improvements. *Water, Air, and Soil Pollution*, 31, 791–797.

MacQueen, J. (1967). SOME METHODS FOR CLASSIFICATION AND ANALYSIS OF MULTIVARIATE OBSERVATIONS. *MULTIVARIATE OBSERVATIONS*, 17.

Maloney, K. M., & Clark, R. E. (1978). (54) ALUMINA COATINGS FOR MERCURY VAPOR LAMPS (Patent No. 4,079,288).

Marhaba, T. F. (2000). Fluorescence Technique for Rapid Identification of DOM Fractions. *Journal of Environmental Engineering*, 126(2), 145–152.  
[https://doi.org/10.1061/\(ASCE\)0733-9372\(2000\)126:2\(145\)](https://doi.org/10.1061/(ASCE)0733-9372(2000)126:2(145))

Marhaba, T. F., & Lippincott, R. L. (2000). Application of Fluorescence Technique for Rapid Identification of DOM Fractions in Source Waters. *Journal of Environmental Engineering*, 126(11), 1039–1044. [https://doi.org/10.1061/\(ASCE\)0733-9372\(2000\)126:11\(1039\)](https://doi.org/10.1061/(ASCE)0733-9372(2000)126:11(1039))

Marhaba, T. F., Pu, Y., & Bengraïne, K. (2003). Modified dissolved organic matter fractionation technique for natural water. *Journal of Hazardous Materials*, 101(1), 43–53. [https://doi.org/10.1016/S0304-3894\(03\)00133-X](https://doi.org/10.1016/S0304-3894(03)00133-X)

Marhaba, T. F., & Van, D. (2000). The variation of mass and disinfection by-product formation potential of dissolved organic matter fractions along a conventional surface water treatment plant. *Journal of Hazardous Materials*, 74(3), 133–147.  
[https://doi.org/10.1016/S0304-3894\(99\)00190-9](https://doi.org/10.1016/S0304-3894(99)00190-9)

- Markechová, D., Tomková, M., & Sádecká, J. (2013). Fluorescence Excitation-Emission Matrix Spectroscopy and Parallel Factor Analysis in Drinking Water Treatment: A Review. *Pol. J. Environ. Stud*, 22(5), 1289–1295.
- Martín-Sómer, M., Pablos, C., van Grieken, R., & Marugán, J. (2017). Influence of light distribution on the performance of photocatalytic reactors: LED vs mercury lamps. *Applied Catalysis B: Environmental*, 215, 1–7.  
<https://doi.org/10.1016/j.apcatb.2017.05.048>
- Matafonova, G., & Batoev, V. (2018). Recent advances in application of UV light-emitting diodes for degrading organic pollutants in water through advanced oxidation processes: A review. *Water Research*, 132, 177–189.  
<https://doi.org/10.1016/j.watres.2017.12.079>
- Matilainen, A., Gjessing, E. T., Lahtinen, T., Hed, L., Bhatnagar, A., & Sillanpää, M. (2011). An overview of the methods used in the characterisation of natural organic matter (NOM) in relation to drinking water treatment. *Chemosphere*, 83(11), 1431–1442. <https://doi.org/10.1016/j.chemosphere.2011.01.018>
- Matilainen, A., & Sillanpää, M. (2010). Removal of natural organic matter from drinking water by advanced oxidation processes. *Chemosphere*, 80(4), 351–365.  
<https://doi.org/10.1016/j.chemosphere.2010.04.067>
- Metz, D. H., Meyer, M., Dotson, A., Beerendonk, E., & Dionysiou, D. D. (2011). The effect of UV/H<sub>2</sub>O<sub>2</sub> treatment on disinfection by-product formation potential under simulated distribution system conditions. *Water Research*, 45(13), 3969–3980.  
<https://doi.org/10.1016/j.watres.2011.05.001>

- Miltner, R., Shukairy, H., & Summers, R. (1992). Disinfection by-product formation and control by ozonation and biotreatment. *Journal - American Water Works Association*, *84*(11), 52–63.
- Miralles-Cuevas, S., Darowna, D., Wanag, A., Mozia, S., Malato, S., & Oller, I. (2017). Comparison of UV/H<sub>2</sub>O<sub>2</sub>, UV/S<sub>2</sub>O<sub>8</sub><sup>2-</sup>, solar/Fe(II)/H<sub>2</sub>O<sub>2</sub> and solar/Fe(II)/S<sub>2</sub>O<sub>8</sub><sup>2-</sup> at pilot plant scale for the elimination of micro-contaminants in natural water: An economic assessment. *Chemical Engineering Journal*, *310*, 514–524. <https://doi.org/10.1016/j.cej.2016.06.121>
- Montreuil, K. R. (2011). *Natural Organic Matter Characterization in Drinking Water*. Dalhousie University.
- Muramoto, Y., Kimura, M., & Nouda, S. (2014). Development and future of ultraviolet light-emitting diodes: UV-LED will replace the UV lamp. *Semiconductor Science and Technology*, *29*(8), 084004. <https://doi.org/10.1088/0268-1242/29/8/084004>
- Nagaraja, A. (2015). Clostridium difficile infections before and during use of ultraviolet disinfection. *American Journal of Infection Control*, *6*.
- Nazari, A., Torabian, S., Montazer, M., Moghadam, M. B., & Shahvaziyan, M. (2014). Spraying Colloidal Nano TiO<sub>2</sub> and Cross-linkable Polysiloxane onto Acrylic Carpet for Self-cleaning. *Research Journal of Textile and Apparel*, *18*(3), 51–60. <https://doi.org/10.1108/RJTA-18-03-2014-B007>
- Ng, C., Losso, J. N., Marshall, W. E., & Rao, R. M. (2002). Freundlich adsorption isotherms of agricultural by-product-based powdered activated carbons in a geosmin–

water system. *Bioresource Technology*, 85(2), 131–135.

[https://doi.org/10.1016/S0960-8524\(02\)00093-7](https://doi.org/10.1016/S0960-8524(02)00093-7)

Nguyen, T. M. H., Suwan, P., Koottatep, T., & Beck, S. E. (2019). Application of a novel, continuous-feeding ultraviolet light emitting diode (UV-LED) system to disinfect domestic wastewater for discharge or agricultural reuse. *Water Research*, 153, 53–62. <https://doi.org/10.1016/j.watres.2019.01.006>

Nieuwenhuijsen, M. J. (2000). Chlorination disinfection byproducts in water and their association with adverse reproductive outcomes: A review. *Occupational and Environmental Medicine*, 57(2), 73–85. <https://doi.org/10.1136/oem.57.2.73>

Nosaka, Y., & Nosaka, A. Y. (2017). Generation and Detection of Reactive Oxygen Species in Photocatalysis. *Chemical Reviews*, 117(17), 11302–11336.

<https://doi.org/10.1021/acs.chemrev.7b00161>

Oguma, K., Kanazawa, K., Kasuga, I., & Takizawa, S. (2018). Effects of UV Irradiation by Light Emitting Diodes on Heterotrophic Bacteria in Tap Water. *Photochemistry and Photobiology*, 94(3), 570–576. <https://doi.org/10.1111/php.12891>

Oguma, K., Kita, R., & Takizawa, S. (2016). Effects of Arrangement of UV Light-Emitting Diodes on the Inactivation Efficiency of Microorganisms in Water. *Photochemistry and Photobiology*, 92(2), 314–317.

<https://doi.org/10.1111/php.12571>

OSHA. (1978). *Occupational Health Guideline for Ozone*. US Dept of Health and Human Services. <https://www.cdc.gov/niosh/topics/ozone/default.html>

- Otaki, M., Okuda, A., Tajima, K., Iwasaki, T., Kinoshita, S., & Ohgaki, S. (2003). Inactivation differences of microorganisms by low pressure UV and pulsed xenon lamps. *Water Science and Technology*, 47(3), 185–190.  
<https://doi.org/10.2166/wst.2003.0193>
- Oto, T., Banal, R. G., Kataoka, K., Funato, M., & Kawakami, Y. (2010). 100 mW deep-ultraviolet emission from aluminium-nitride-based quantum wells pumped by an electron beam. *Nature Photonics*, 4(11), 767–770.  
<https://doi.org/10.1038/nphoton.2010.220>
- Park, J.-S., Choi, H., & Cho, J. (2004). Kinetic decomposition of ozone and para-chlorobenzoic acid (pCBA) during catalytic ozonation. *Water Research*, 8.
- Pearson, Karl. (1901). On Lines and Planes of Closest Fit to Systems of Points in Space. *Philosophical Magazine*, 2, 559–572.
- Peiris, R. H., Budman, H., Moresoli, C., & Legge, R. L. (2011). Identification of humic acid-like and fulvic acid-like natural organic matter in river water using fluorescence spectroscopy. *Water Science and Technology*, 63(10), 2427–2433.  
<https://doi.org/10.2166/wst.2011.439>
- Peleato, Nicolás M. (2016). *Fluorescence spectroscopy for monitoring reduction of natural organic matter and halogenated furanone precursors by biofiltration*. 7.
- Peleato, Nicolás M, & Andrews, R. C. (2015). Contributions of spatial, temporal, and treatment impacts on natural organic matter character using fluorescence-based measures. *Water Supply*, 15(3), 589–598. <https://doi.org/10.2166/ws.2015.013>

- Peleato, Nicolas M., Legge, R. L., & Andrews, R. C. (2017). Investigation of fluorescence methods for rapid detection of municipal wastewater impact on drinking water sources. *Spectrochimica Acta - Part A: Molecular and Biomolecular Spectroscopy*. <https://doi.org/10.1016/j.saa.2016.07.031>
- Peleato, Nicolás M, Legge, R. L., & Andrews, R. C. (2017). Characterization of UF foulants and fouling mechanisms when applying low in-line coagulant pre-treatment. *Water Research*, 126, 1–11. <https://doi.org/10.1016/j.watres.2017.08.064>
- Perucho, J., Gonzalo-Gobernado, R., Bazan, E., Casarejos, M. J., Jiménez-Escrig, A., Asensio, M. J., & Herranz, A. S. (2015). Optimal excitation and emission wavelengths to analyze amino acids and optimize neurotransmitters quantification using precolumn OPA-derivatization by HPLC. *Amino Acids*, 47(5), 963–973. <https://doi.org/10.1007/s00726-015-1925-1>
- Peter, A., & Von Gunten, U. (2007). Oxidation Kinetics of Selected Taste and Odor Compounds During Ozonation of Drinking Water. *Environmental Science & Technology*, 41(2), 626–631. <https://doi.org/10.1021/es061687b>
- Pi, Y., Schumacher, J., & Jekel, M. (2005). The Use of para-Chlorobenzoic Acid (pCBA) as an Ozone/Hydroxyl Radical Probe Compound. *Ozone: Science & Engineering*, 27(6), 431–436. <https://doi.org/10.1080/01919510500349309>
- Pocostales, J. P., Sein, M. M., Knolle, W., von Sonntag, C., & Schmidt, T. C. (2010). Degradation of Ozone-Refractory Organic Phosphates in Wastewater by Ozone and Ozone/Hydrogen Peroxide (Peroxone): The Role of Ozone Consumption by

- Dissolved Organic Matter. *Environmental Science & Technology*, 44(21), 8248–8253. <https://doi.org/10.1021/es1018288>
- Porterfield, J. Z., & Zlotnick, A. (2010). A simple and general method for determining the protein and nucleic acid content of viruses by UV absorbance. *Virology*. <https://doi.org/10.1016/j.virol.2010.08.015>
- Rattanakul, S., & Oguma, K. (2018). Inactivation kinetics and efficiencies of UV-LEDs against *Pseudomonas aeruginosa*, *Legionella pneumophila*, and surrogate microorganisms. *Water Research*, 130, 31–37. <https://doi.org/10.1016/j.watres.2017.11.047>
- Reckhow, D. A., Singer, P. C., & Malcolm, R. L. (1990). Chlorination of humic materials: Byproduct formation and chemical interpretations. *Environmental Science & Technology*, 24(11), 1655–1664. <https://doi.org/10.1021/es00081a005>
- Rex, R. W. (1960). Electron Paramagnetic Resonance Studies of Stable Free Radicals in Lignins and Humic Acids. *Nature*, 188(4757), 1185–1186. <https://doi.org/10.1038/1881185a0>
- Richardson, S. (2003). Disinfection by-products and other emerging contaminants in drinking water. *TrAC Trends in Analytical Chemistry*, 22(10), 666–684. [https://doi.org/10.1016/S0165-9936\(03\)01003-3](https://doi.org/10.1016/S0165-9936(03)01003-3)
- Rosenfeldt, E. J., Linden, K. G., Canonica, S., & von Gunten, U. (2006a). Comparison of the efficiency of OH radical formation during ozonation and the advanced oxidation processes O<sub>3</sub>/H<sub>2</sub>O<sub>2</sub> and UV/H<sub>2</sub>O<sub>2</sub>. *Water Research*, 40(20), 3695–3704. <https://doi.org/10.1016/j.watres.2006.09.008>

- Rosenfeldt, E. J., Linden, K. G., Canonica, S., & von Gunten, U. (2006b). Comparison of the efficiency of OH radical formation during ozonation and the advanced oxidation processes O<sub>3</sub>/H<sub>2</sub>O<sub>2</sub> and UV/H<sub>2</sub>O<sub>2</sub>. *Water Research*, 40(20), 3695–3704. <https://doi.org/10.1016/j.watres.2006.09.008>
- Rosenfeldt, E. J., Melcher, B., & Linden, K. G. (2005). UV and UV/H<sub>2</sub>O<sub>2</sub> treatment of methylisoborneol (MIB) and geosmin in water. *Journal of Water Supply: Research and Technology-Aqua*, 54(7), 423–434. <https://doi.org/10.2166/aqua.2005.0040>
- RStudio- Version 1.3.959 (1.3.959). (2020). [Mac].
- Sarathy, S., & Mohseni, M. (2013). The fate of natural organic matter during UV/H<sub>2</sub>O<sub>2</sub> advanced oxidation of drinking water. *Journal of Environmental Engineering and Science*, 8(1), 36–44. <https://doi.org/10.1680/jees.2013.0004>
- Serif. (2020). *Afinity Designer* (1.8.3) [Computer software]. Serif.  
<https://affinity.serif.com/en-gb/>
- Sharp, E. L., Jarvis, P., Parsons, S. A., & Jefferson, B. (2006). Impact of fractional character on the coagulation of NOM. *Colloids and Surfaces A: Physicochemical and Engineering Aspects*, 286(1–3), 104–111.  
<https://doi.org/10.1016/j.colsurfa.2006.03.009>
- Sholtes, K. A., Lowe, K., Walters, G. W., Sobsey, M. D., Linden, K. G., & Casanova, L. M. (2016). Comparison of ultraviolet light-emitting diodes and low-pressure mercury-arc lamps for disinfection of water. *Environmental Technology*, 37(17), 2183–2188. <https://doi.org/10.1080/09593330.2016.1144798>

- Sholtes, K., Keliher, R., & Linden, K. G. (2019). Standardization of a UV LED Peak Wavelength, Emission Spectrum, and Irradiance Measurement and Comparison Protocol. *Environmental Science & Technology*, *53*(16), 9755–9763.  
<https://doi.org/10.1021/acs.est.9b02567>
- Sierra, M. M. D., Giovanela, M., Parlanti, E., & Soriano-Sierra, E. J. (2005). Fluorescence fingerprint of fulvic and humic acids from varied origins as viewed by single-scan and excitation/emission matrix techniques. *Chemosphere*, *58*(6), 715–733.  
<https://doi.org/10.1016/j.chemosphere.2004.09.038>
- Singer, P. C. (1999). Humic\_substances\_as\_precursors.pdf. *Water Science and Technology*, *40*(9), 25–30.
- Skwirut, H., & Young, R. C. (1989). *US4871944.pdf* (Patent No. 4871944).
- Song, K., Mohseni, M., & Taghipour, F. (2016). Application of ultraviolet light-emitting diodes (UV-LEDs) for water disinfection: A review. *Water Research*, *94*, 341–349.  
<https://doi.org/10.1016/j.watres.2016.03.003>
- Stedmon, C. A., & Bro, R. (2008). Characterizing dissolved organic matter fluorescence with parallel factor analysis: A tutorial: Fluorescence-PARAFAC analysis of DOM. *Limnology and Oceanography: Methods*, *6*(11), 572–579.  
<https://doi.org/10.4319/lom.2008.6.572>
- Stumm, W., & Morgan, J. J. (1996). *Aquatic chemistry: Chemical equilibria and rates in natural waters* (3rd ed.).
- Sultan, T., & Cho, J. (2016). Optimization of a UV/H<sub>2</sub>O<sub>2</sub> AOP System Using Scavenger Radicals and Response Surface Methodology. *Chemical Engineering*

*Communications*, 203(8), 1093–1104.

<https://doi.org/10.1080/00986445.2015.1124097>

Sun, H., He, F., & Choi, W. (2020). Production of Reactive Oxygen Species by the Reaction of Periodate and Hydroxylamine for Rapid Removal of Organic Pollutants and Waterborne Bacteria. *Environmental Science & Technology*, 54(10), 6427–6437. <https://doi.org/10.1021/acs.est.0c00817>

Suzuki, H., Araki, S., & Yamamoto, H. (2015). Evaluation of advanced oxidation processes (AOP) using O<sub>3</sub>, UV, and TiO<sub>2</sub> for the degradation of phenol in water. *Journal of Water Process Engineering*, 7, 54–60.

<https://doi.org/10.1016/j.jwpe.2015.04.011>

Świetlik, J., Dąbrowska, A., Raczyk-Stanisławiak, U., & Nawrocki, J. (2004). Reactivity of natural organic matter fractions with chlorine dioxide and ozone. *Water Research*, 38(3), 547–558. <https://doi.org/10.1016/j.watres.2003.10.034>

Szeto, W., Yam, W. C., Huang, H., & Leung, D. Y. C. (2020). The efficacy of vacuum-ultraviolet light disinfection of some common environmental pathogens. *BMC Infectious Diseases*, 20(1), 127. <https://doi.org/10.1186/s12879-020-4847-9>

Taniyasu, Y., Kasu, M., & Makimoto, T. (2006). An aluminium nitride light-emitting diode with a wavelength of 210 nanometres. *Nature*, 441(7091), 325–328.

<https://doi.org/10.1038/nature04760>

Teale, F. W. J. (1960). The ultraviolet fluorescence of proteins in neutral solution.

*Biochemical Journal*, 76(2), 381–388. <https://doi.org/10.1042/bj0760381>

Thurman, E. M., & Malcolm, R. L. (1979). *Concentration and fractionation of hydrophobic organic acid constituents from natural waters by liquid chromatography.*

<https://doi.org/10.3133/wsp1817G>

Troue, H. H. (1976). *OPERATING AMERCURY WAPOR LAMP* (Patent No. 3,983,385).

Trueman, B. F., MacIsaac, S. A., Stoddart, A. K., & Gagnon, G. A. (2016). Prediction of disinfection by-product formation in drinking water via fluorescence spectroscopy. *Environmental Science: Water Research & Technology*, 2(2), 383–389. <https://doi.org/10.1039/C5EW00285K>

USEPA. (2020a). Why aren't ozone generators, UV lights, or air purifiers on List N? Can I use these or other pesticidal devices to kill the virus that causes COVID-19? [US EPA]. *COVID-19 FAQ*. <https://www.epa.gov/coronavirus/why-arent-ozone-generators-uv-lights-or-air-purifiers-list-n-can-i-use-these-or-other>

USEPA. (2020b, April 3). EPA Administrator Wheeler Talks with Retailers and Third-Party Marketplace Platforms to Discuss Steps to Protect American Consumers from Fraudulent Coronavirus Disinfectant Claims. *News Releases from Headquarters*›*Chemical Safety and Pollution Prevention (OCSPP)*.

<https://www.epa.gov/newsreleases/epa-administrator-wheeler-talks-retailers-and-third-party-marketplace-platforms-discuss>

USEPA. (2020c, October 17). *EPA Takes Action to Protect Public from Coronavirus Protection Scams*. <https://www.epa.gov/newsreleases/epa-takes-action-protect-public-coronavirus-protection-scams>

- Valencia, S., Marín, J. M., Restrepo, G., & Frimmel, F. H. (2014). Evaluation of natural organic matter changes from Lake Hohloh by three-dimensional excitation–emission matrix fluorescence spectroscopy during TiO<sub>2</sub>/UV process. *Water Research*, *51*, 124–133. <https://doi.org/10.1016/j.watres.2013.12.019>
- van Lente, H., Spitters, C., & Peine, A. (2013). Comparing technological hype cycles: Towards a theory. *Technological Forecasting*, *14*.
- Varanasi, L., Coscarelli, E., Khaksari, M., Mazzoleni, L. R., & Minakata, D. (2018). Transformations of dissolved organic matter induced by UV photolysis, Hydroxyl radicals, chlorine radicals, and sulfate radicals in aqueous-phase UV-Based advanced oxidation processes. *Water Research*, *135*, 22–30. <https://doi.org/10.1016/j.watres.2018.02.015>
- Villacís, J. E., Lopez, M., Passey, D., Santillán, M. H., Verdezoto, G., Trujillo, F., Paredes, G., Alarcón, C., Horvath, R., & Stibich, M. (2019). Efficacy of pulsed-xenon ultraviolet light for disinfection of high-touch surfaces in an Ecuadorian hospital. *BMC Infectious Diseases*, *19*(1), 575. <https://doi.org/10.1186/s12879-019-4200-3>
- Villanueva, C. M., Cantor, K. P., Cordier, S., Jaakkola, J. J. K., King, W. D., Lynch, C. F., Porru, S., & Kogevinas, M. (2004). Disinfection Byproducts and Bladder Cancer: A Pooled Analysis. *Epidemiology*, *15*(3), 357–367. <https://doi.org/10.1097/01.ede.0000121380.02594.fc>
- Vogt, R. (2006). *Aluminium – the link between increase in water colour and DOC and reduction in Acid rain.*

- von Gunten, U. (2018). Oxidation Processes in Water Treatment: Are We on Track? *Environmental Science & Technology*, 52(9), 5062–5075.  
<https://doi.org/10.1021/acs.est.8b00586>
- von Gunten, U., & Oliveras, Y. (1998). Advanced Oxidation of Bromide-Containing Waters: Bromate Formation Mechanisms. *Environmental Science & Technology*, 32(1), 63–70. <https://doi.org/10.1021/es970477j>
- von Gunten, Urs., & Hoigne, Juerg. (1994). Bromate Formation during Ozonization of Bromide-Containing Waters: Interaction of Ozone and Hydroxyl Radical Reactions. *Environmental Science & Technology*, 28(7), 1234–1242.  
<https://doi.org/10.1021/es00056a009>
- von Sonntag, C. (2007). The basics of oxidants in water treatment. Part A: OH radical reactions. *Water Science and Technology*, 55(12), 19–23.  
<https://doi.org/10.2166/wst.2007.383>
- von Sonntag, C. (2008). Advanced oxidation processes: Mechanistic aspects. *Water Science and Technology*, 58(5), 1015–1021.  
<https://doi.org/10.2166/wst.2008.467>
- Wang, C., Moore, N., Bircher, K., Andrews, S., & Hofmann, R. (2019). Full-scale comparison of UV/H<sub>2</sub>O<sub>2</sub> and UV/Cl<sub>2</sub> advanced oxidation: The degradation of micropollutant surrogates and the formation of disinfection byproducts. *Water Research*, 161, 448–458. <https://doi.org/10.1016/j.watres.2019.06.033>
- Wang, C., Rosenfeldt, E., Li, Y., & Hofmann, R. (2020). External Standard Calibration Method To Measure the Hydroxyl Radical Scavenging Capacity of Water Samples.

*Environmental Science & Technology*, 54(3), 1929–1937.

<https://doi.org/10.1021/acs.est.9b06273>

Wang, S.-N., Li, J.-J., Liu, Y.-X., Lin, Z., Qiao, J.-J., Chen, L.-H., Li, Y., Wu, Y., Wang, M.-M., Liu, Y.-B., Yan, C., Chen, Z.-H., & Gao, C.-Q. (2019). Pulsed xenon ultraviolet and non-thermal atmospheric plasma treatments are effective for the disinfection of air in hospital blood sampling rooms. *Photodiagnosis and Photodynamic Therapy*, 27, 137–140. <https://doi.org/10.1016/j.pdpdt.2019.05.034>

Watson, S. B. (2003). Cyanobacterial and eukaryotic algal odour compounds: Signals or by-products? A review of their biological activity. *Phycologia* 42 (4), 332e350. *Phycologia*, 42(4), 332–350.

Watts, M. J., Hofmann, R., & Rcdsenfeldt, E. J. (2012). Low-pressure UV/Cl<sub>2</sub> for advanced oxidation of taste and odor. *Journal - American Water Works Association*, 104(1), E58–E65. <https://doi.org/10.5942/jawwa.2012.104.0006>

Watts, M. J., & Linden, K. G. (2007). Chlorine photolysis and subsequent OH radical production during UV treatment of chlorinated water. *Water Research*, 41(13), 2871–2878. <https://doi.org/10.1016/j.watres.2007.03.032>

Wert, E. C., Korak, J. A., Trenholm, R. A., & Rosario-Ortiz, F. L. (2014). Effect of oxidant exposure on the release of intracellular microcystin, MIB, and geosmin from three cyanobacteria species. *Water Research*, 52, 251–259. <https://doi.org/10.1016/j.watres.2013.11.001>

Westerhoff, P., Aiken, G., Amy, G., & Debroux, J. (1999). Relationships between the structure of natural organic matter and its reactivity towards molecular ozone

and hydroxyl radicals. *Water Research*, 33(10), 2265–2276.

[https://doi.org/10.1016/S0043-1354\(98\)00447-3](https://doi.org/10.1016/S0043-1354(98)00447-3)

Wickham, H., Winston Chang, Lionel Henry, Thomas Lin Pedersen, Kohske Takahashi, Claus Wilke, Kara Woo, Hiroaki Yutani, & Dewey Dunnington. (2016). *Elegant Graphics for Data analysis*. Springer-Verlag, New York, 4(43), 1686.

Williams, M. E., & Darby, J. L. (1992). Measuring Ozone by Indigo Method: Interference of Suspended Material. *Journal of Environmental Engineering*, 118(6), 988–993.

[https://doi.org/10.1061/\(ASCE\)0733-9372\(1992\)118:6\(988\)](https://doi.org/10.1061/(ASCE)0733-9372(1992)118:6(988))

Williams, R. T., & Bridges, J. W. (1964). Fluorescence of solutions: A review. *Journal of Clinical Pathology*, 17(4), 371–394. <https://doi.org/10.1136/jcp.17.4.371>

Williamson, C. E., Overholt, E. P., Pilla, R. M., Leach, T. H., Brentrup, J. A., Knoll, L. B., Mette, E. M., & Moeller, R. E. (2016). Ecological consequences of long-term browning in lakes. *Scientific Reports*, 5(1), 18666.

<https://doi.org/10.1038/srep18666>

Wiszniewski, J., Robert, D., Surmacz-Gorska, J., Miksch, K., & Weber, J.-V. (2002).

*Photocatalytic decomposition of humic acids on TiO<sub>2</sub> Part I: Discussion of adsorption and mechanism*. 7.

Wold, Svante, Esbensen, K., & Geladi, Paul. (1987). Principal component analysis.

*Chemometrics and Intelligent Laboratory Systems*, 2(1–3), 37–52.

World Health Organization. (2005). *Trihalomethanes in Drinking-water*. World Health Organization.

[https://www.who.int/water\\_sanitation\\_health/dwq/chemicals/THM200605.pdf](https://www.who.int/water_sanitation_health/dwq/chemicals/THM200605.pdf)

- Wright, E., Daurie, H., & Gagnon, G. A. (2014). Development and validation of an SPE-GC-MS/MS taste and odour method for analysis in surface water. *International Journal of Environmental Analytical Chemistry*, 94(13), 1302–1316.  
<https://doi.org/10.1080/03067319.2014.974586>
- Wünsch, R., Mayer, C., Plattner, J., Eugster, F., Wülser, R., Gebhardt, J., Hübner, U., Canonica, S., Wintgens, T., & von Gunten, U. (2021). Micropollutants as internal probe compounds to assess UV fluence and hydroxyl radical exposure in UV/H<sub>2</sub>O<sub>2</sub> treatment. *Water Research*, 195, 116940.  
<https://doi.org/10.1016/j.watres.2021.116940>
- Yamato, H., Oguma, K., & Takizawa, S. (2017). Evaluation of UV light emitting diode, UV-LED at different wavelengths in the inactivation and photoreactivation of escherichia coli. *Journal of Japan Society of Civil Engineers, Ser. G (Environmental Research)*, 73(7), 337–343.
- Yamato Hosoi, Kumiko Oguma, Satoshi Takizawa. (2017). Evaluation of UV light emitting diode, UV-LED at different wavelengths in the inactivation and photoreactivation of escherichia coli. *Journal of Japan Society of Civil Engineers, Ser. G (Environmental Research)*, 73(7), 337–343.
- Yang, W., Zhou, H., & Cicek, N. (2014). Treatment of Organic Micropollutants in Water and Wastewater by UV-Based Processes: A Literature Review. *Critical Reviews in Environmental Science and Technology*, 44(13), 1443–1476.  
<https://doi.org/10.1080/10643389.2013.790745>

- Yuan, F., Hu, C., Hu, X., Qu, J., & Yang, M. (2009). Degradation of selected pharmaceuticals in aqueous solution with UV and UV/H<sub>2</sub>O<sub>2</sub>. *Water Research*, 43(6), 1766–1774. <https://doi.org/10.1016/j.watres.2009.01.008>
- Zelle, M. R., & Hollaender, A. (1954). *MONOCHROMATIC ULTRAVIOLET ACTION SPECTRA AND QUANTUM YIELDS FOR INACTIVATION OF T<sub>1</sub> AND T<sub>2</sub> ESCHERICHIA COLI BACTERIOPHAGES*. 68, 6.
- Zhang, W., Zhou, S., Wu, Y., Zhu, S., & Crittenden, J. (2021). Computerized Pathway Generator for the UV/Free Chlorine Process: Prediction of Byproducts and Reactions. *Environmental Science & Technology*, 55(4), 2608–2617. <https://doi.org/10.1021/acs.est.0c07080>

## APPENDIX A: Pockwock Lake Water Quality Data and R Code for Plots

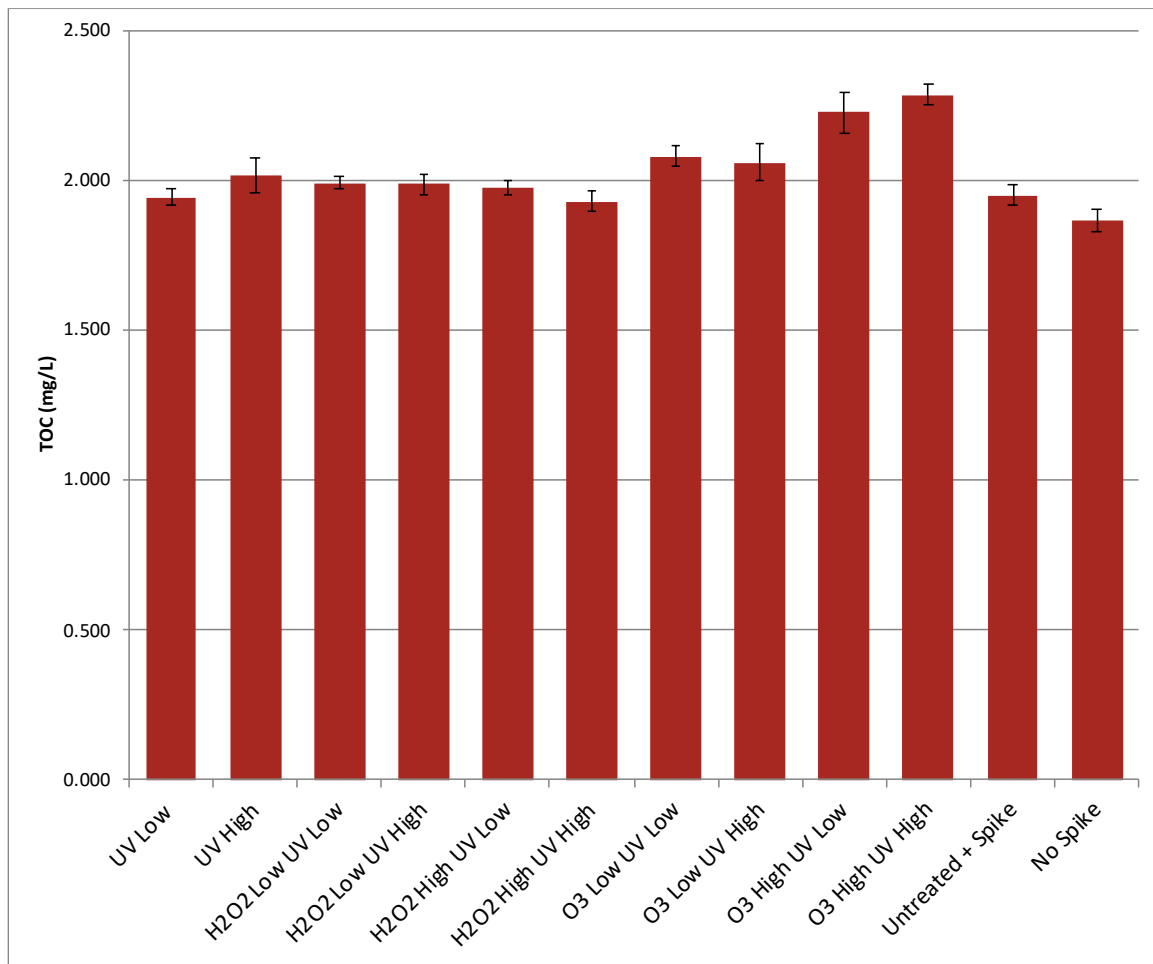


**Figure A-1** Pockwock Lake post plant filtered TOC data. Error Bars indicate standard deviation.

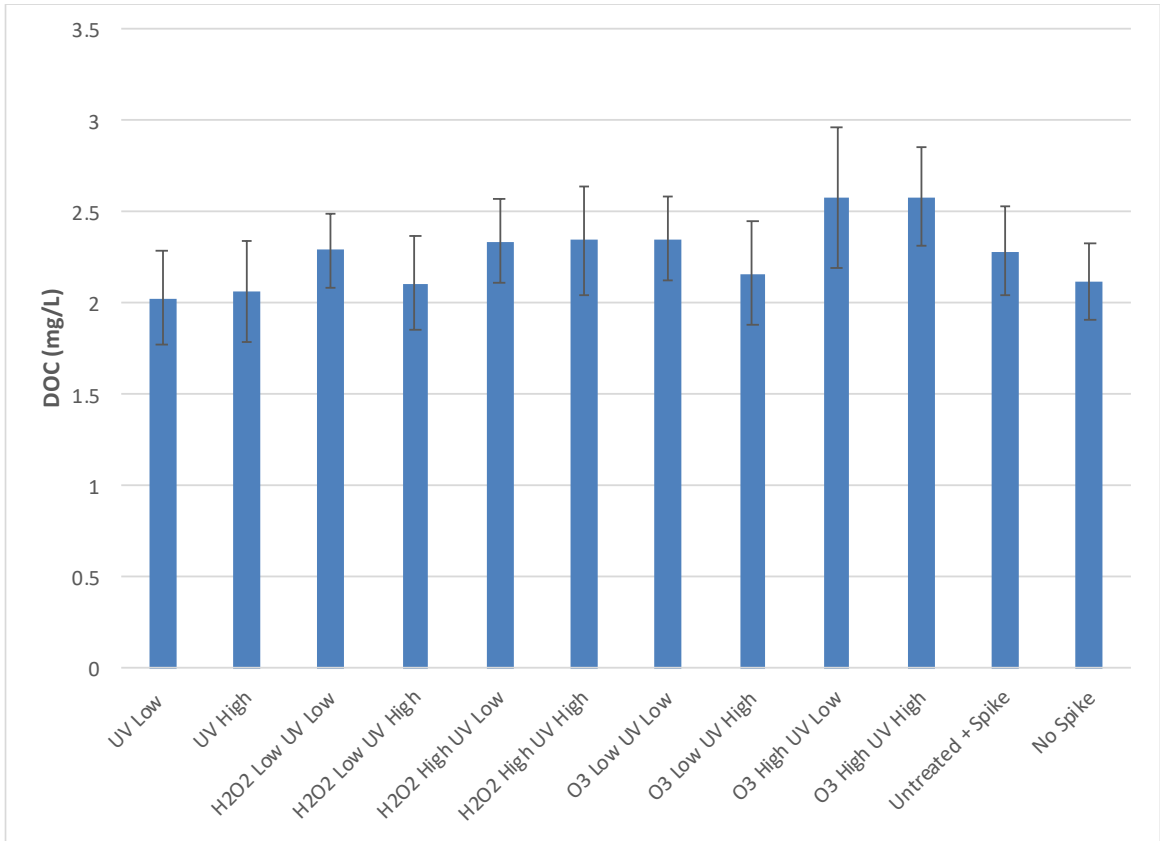


**Figure A-2** Pockwock Lake post plant filtered DOC data. Error Bars indicate standard deviation.

**Table A-1** Summary statistics for Pockwock Lake SUVA

	<b>Average</b>	<b>Median</b>	<b>Standard Deviation</b>	<b>Standard Error</b>	<b>Confidence Interval</b>
<b>UV Low</b>	1.682	1.722	0.250	0.079	0.155
<b>UV High</b>	1.677	1.623	0.540	0.163	0.319
<b>H2O2 Low UV Low</b>	1.631	1.593	0.516	0.163	0.320
<b>H2O2 Low UV High</b>	1.792	1.565	0.628	0.189	0.371
<b>H2O2 High UV Low</b>	1.560	1.547	0.582	0.184	0.361
<b>H2O2 High UV High</b>	1.372	1.274	0.613	0.185	0.362
<b>O3 Low UV Low</b>	1.386	1.452	0.583	0.194	0.381
<b>O3 Low UV High</b>	1.174	1.081	0.576	0.174	0.340
<b>O3 High UV Low</b>	0.881	0.957	0.587	0.186	0.364
<b>O3 High UV High</b>	0.830	0.805	0.593	0.179	0.351
<b>Untreated + Spike</b>	2.156	2.080	0.659	0.199	0.389
<b>No Spike</b>	2.117	2.035	0.673	0.238	0.467

```
---  
title: "Pockwock Lake Box Plot"  
author: "SMI"  
date: "09/11/2020"  
output: html_document  
---
```

```
``{r setup, include=FALSE}  
knitr::opts_chunk$set(echo = TRUE)  
---
```

```
``{r}  
library(tidyverse)  
library(reshape2)  
library(ggthemes)  
library(ggsci)  
library(RColorBrewer)  
library(dplyr)  
  
---
```

```
``{r}  
SUVA_raw <- readxl::read_excel("PockwockSUVA.xlsx", col_names = TRUE, skip = 0)
```

```
SUVA_raw  
---
```

```
``{r}  
SUVA_raw <- readxl::read_excel("PockwockSUVA.xlsx", col_names = TRUE, skip = 0)
```

```

SUVA_raw$Name <- as.factor(SUVA_raw$Name)

SUVA_raw
...

```{r}

SUVA_box <- SUVA_raw

ggplot(SUVA_box, aes(x = reorder(Name,SUVA), y = SUVA, fill = Treatment)) +

  theme(axis.text.x=element_text(angle = 90, vjust = 0.5)) +

  geom_boxplot(outlier.shape = 1, show.legend = FALSE) +

  xlab("")+
  ylab("SUVA" ~ (L~mg^-1 ~m^-1))

...

```

## APPENDIX B: R Code for Kinetics Data

```
---
title: "OH Kinetics"
author: "SMI"
date: "04/08/2020"
output: html_document
---

```{r setup, include=FALSE}
knitr::opts_chunk$set(echo = TRUE)
```

```{r}
library(tidyverse)
library(reshape2)
library(ggthemes)
library(ggsci)
library(RColorBrewer)
library(dplyr)
```

```{r}
kinetics_raw <- readxl::read_excel("Kinetics Data.xlsx", col_names = TRUE, skip = 0)

kinetics_raw

```

```{r}
kinetics_cal <- readxl::read_excel("Calibration Curve Kinetics.xlsx", col_names =
TRUE, skip = 0)

kinetics_cal

```

```{r}
kinetics_curve <- kinetics_cal

ggplot(kinetics_cal, aes(Concentration, Area, fill = "Calibration")) +
  geom_point(size=2, shape=23) +
  geom_smooth(method="lm", se=FALSE) +
  theme(legend.position="none") +
  xlab("Concentration ( $\mu\text{g/L}$ )")
```

```

kin_curve = lm(Concentration ~ Area, data = kinetics_curve)

kin_inter <- kin_curve$coeff[1]
kin_slope <- kin_curve$coeff[2]

kinetics_cal$Final = kinetics_cal$Area * kin_slope + kin_inter

ggplot(kinetics_cal, aes(Concentration, Final, fill = "Calibration")) +
  geom_point(size=2, shape=15, col = "darkcyan") +
  geom_smooth(method="lm", se=FALSE, col = "black", size = 0.5) +
  theme(legend.position="none") +
  xlab("Theoretical Concentration (µg/L)") +
  ylab("Observed Concentration (µg/L)")

ggsave("Kinetics Regressions.png")
```


```

```{r}

kinetics_concentration <- kinetics_raw

kinetics_concentration$Final = kinetics_concentration$Area * kin_slope + kin_inter

kinetics_concentration

```

```{r}
kinetics_cal <- readxl::read_excel("Calibration Curve Kinetics.xlsx", col_names =
TRUE, skip = 0)

kinetics_cal$Final = kinetics_cal$Area * kin_slope + kin_inter

kinetics_cal

```

```{r}
kinetics_unt <- readxl::read_excel("Kinetics Untreated.xlsx", col_names = TRUE, skip
= 0)

kinetics_unt$Final = kinetics_unt$Area * kin_slope + kin_inter

kinetics_unt

```

```


```

```

``{r}

kinetics_factors <- kinetics_concentration %>%
  mutate(
    pH = fct_inorder(paste(pH)),
    H2O2 = fct_inorder(paste(H2O2, "mg/L"))
  )

kinetics_factors
``

``{r}
data <- kinetics_factors

# make ln column for finding k-values

data$ln = log(data$Final)

# plot:

data %>%
  ggplot(aes(UV, Final, fill = pH)) +
  facet_grid(H2O2 ~ pH) +
  geom_point(size=2, shape=23) +
  geom_smooth(method = "lm", se = FALSE, col = "black", size = 0.5) +
  theme_bw()+
  ylab("Measured pCBA Concentration (µM)")+
  xlab("UV Fluence " ~ (mJ ~ cm^2)) +
  scale_x_continuous(breaks=c(1000,500,100, 0))+
  theme(legend.position="none")

# extract linear model coefficients:

data %>%
  group_by(H2O2, pH) %>%
  nest() %>%
  ungroup() %>%
  mutate(
    model = map(data, ~ lm(Final ~ UV, data = .x)),
    tidied = map(model, broom::tidy)
  ) %>%
  unnest(tidied)

ggsave("Kinetics Regressions.png")

```

```

# plot II

data %>%
  ggplot(aes(UV, ln, fill = pH)) +
  facet_grid(H2O2 ~ pH) +
  geom_point(size=2, shape=23) +
  geom_smooth(method = "lm", se = FALSE, col = "black", size = 0.5) +
  theme_bw()+
  ylab("ln(pCBA)")+
  xlab("UV Fluence "~(mJ~cm^2)))+
  scale_x_continuous(breaks=c(1000,500,100, 0))+
  theme(legend.position="none")

#now we have the coefficients for the slopes in each condition.

data %>%
  group_by(H2O2, pH) %>%
  nest() %>%
  ungroup() %>%
  mutate(
    model = map(data, ~ lm(ln ~ UV, data = .x)),
    tidied = map(model, broom::tidy)
  ) %>%
  unnest(tidied)

ggsave("ln Kinetics.png")

...
```{r}

#R oh values made from the slopes (k values) and the known k-values from
literature

kinetics_Roh <- readxl::read_excel("Roh.xlsx", col_names = TRUE, skip = 0)
kinetics_Roh$pH <- as.factor(kinetics_Roh$pH)
kinetics_Roh$Roh <- kinetics_Roh$Roh*10e12

kinetics_Roh %>%
  ggplot(aes(H2O2, Roh, colour = pH, shape = pH)) +
  geom_point(size=2) +
  theme_bw()+
  guides(fill = guide_legend(title.theme = element_text(angle = 0)))+

  ylab("•OH Radical Exposure "~(10^-13 ~M ~s ~L ~mJ^-1)))+
  xlab(~H[2]~O[2] ~(mg ~L^-1)))+

```

```
scale_x_continuous(breaks=c(10,1,0))+  
theme(legend.position="none")
```

```
'''
```

## APPENDIX C: Additional Data for Pottle Lake

**Table C-1** Summary Statistics for Pottle Lake SUVA Data

	Average	Standard Deviation	Standard Error	Confidence Interval (95%)
<b>Untreated</b>	3.182	0.221	0.090	0.176
<b>UV Low</b>	2.703	0.726	0.297	0.581
<b>UV High</b>	1.921	0.947	0.358	0.701
<b>H2O2 Low UV Low</b>	2.303	1.194	0.451	0.885
<b>H2O2 Low UV High</b>	1.801	1.036	0.463	0.908
<b>H2O2 High UV Low</b>	2.302	1.338	0.598	1.172
<b>H2O2 High UV High</b>	1.555	0.812	0.332	0.650
<b>O3 Low UV Low</b>	2.403	0.276	0.113	0.221
<b>O3 Low UV High</b>	1.787	0.484	0.242	0.474
<b>O3 High UV Low</b>	1.831	0.448	0.183	0.359
<b>O3 Low UV High</b>	1.629	0.505	0.206	0.404

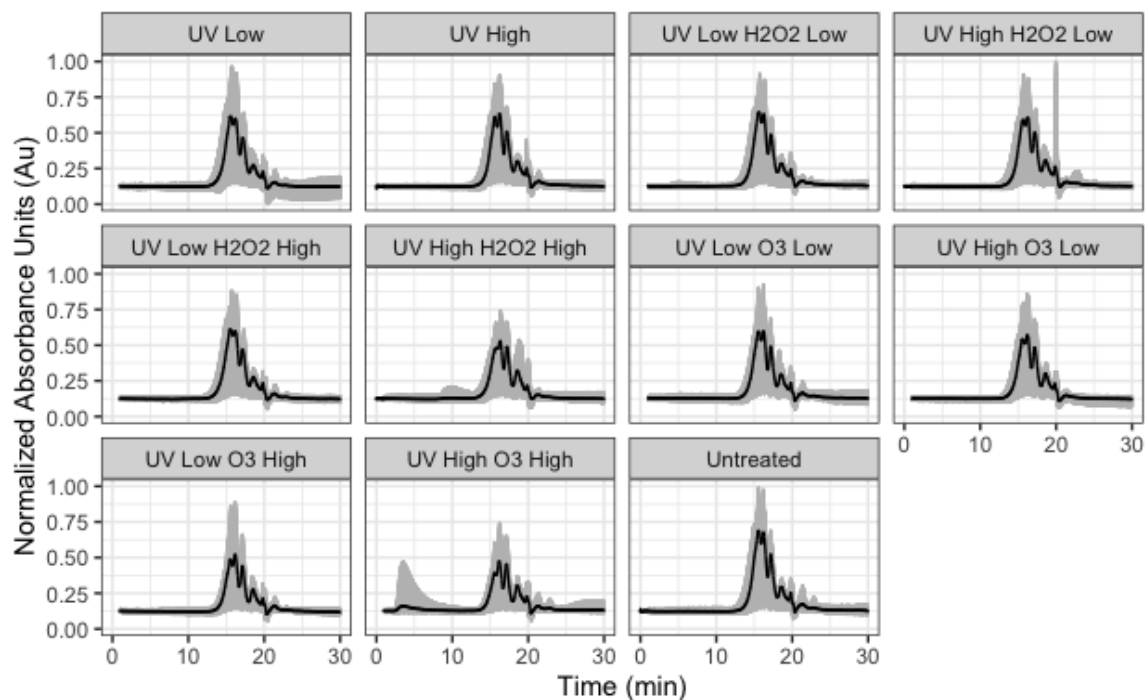


**Figure C-1** Normalized chromatograms for each AOP treatment for Pottle Lake water. Grey shading depicts the range of the data and the black line indicated the average response.

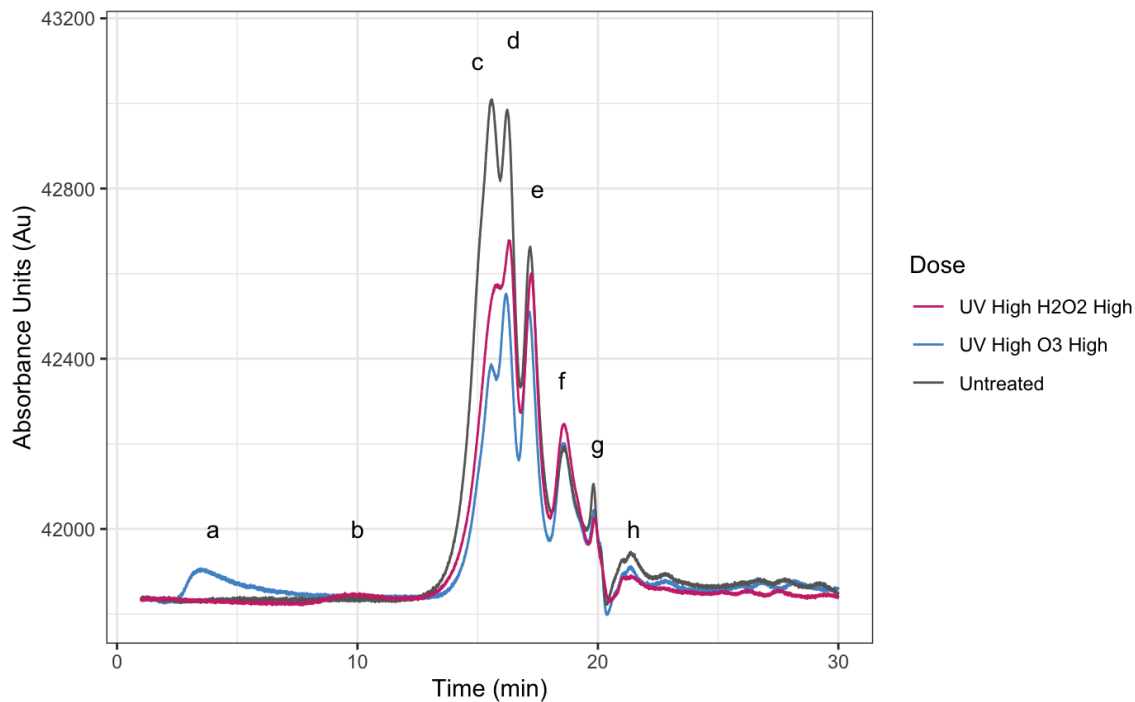


**Figure C-2** Comparison of peroxide and ozone AOP treatments to untreated NOM profile. Note the formation of peak A in ozone samples and peak B in peroxide samples.

## APPENDIX D: R Code for Contour plots

```
---
title: "Contour Matrices"
author: "SMI"
date: "11/11/2020"
output: html_document
---

```{r setup, include=FALSE}
knitr::opts_chunk$set(echo = TRUE)
```

```{r}
library(tidyverse)
library(reshape2)
library(ggthemes)
library(ggsci)
library(RColorBrewer)
library(readxl)
library(patchwork)
library(pracma)
```

```{r}

Excitation = read_excel('PARAFAC Components.xlsx', sheet = 'Excitation', col_names
= TRUE, col_types = NULL, na = "", skip = 0)

Emission = read_excel('PARAFAC Components.xlsx', sheet = 'Emission', col_names =
TRUE, col_types = NULL, na = "", skip = 0)

...

```{r}

UV_Comp1_Contour <- Excitation$`UV Component 1` %*% t(Emission$`UV
Component 1`)

colnames(UV_Comp1_Contour) <- Emission$`Emission Wavelength`

UV_Comp1_Contour %>%
  as_tibble() %>%
  mutate(excitation = Excitation$`Excitation Wavelength`) %>%
```

```

pivot_longer(-excitation, names_to = "emission") %>%
mutate(emission = as.numeric(emission)) %>%
arrange(excitation, emission) %>%
# next three lines sets up a regular grid of emission values
# make sure to check that the differences between emission and emission_corr are
small
group_by(excitation) %>%
mutate(emission_corr = seq(min(emission), max(emission), length.out =
length(emission))) %>%
ungroup() %>%
ggplot(aes(excitation, emission_corr, fill = value, z = value)) +
geom_raster() +
geom_contour(col = "white")

```

---

```

---
title: "Contour Matrices"
author: "Sean MacIsaac & Benjamin Trueman"
date: "11/11/2020"
output: html_document
---

```

```

```${r setup, include=FALSE}
knitr::opts_chunk$set(echo = TRUE)
```

```

```

```${r}
library(tidyverse)
library(reshape2)
library(ggthemes)
library(ggsci)
library(RColorBrewer)
library(readxl)
library(patchwork)
```

```

```

```${r}

```

```

Excitation = read_excel('PARAFAC Components PTL.xlsx', sheet = 'Excitation',
col_names = TRUE, col_types = NULL, na = "", skip = 0)

```

```

Emission = read_excel('PARAFAC Components PTL.xlsx', sheet = 'Emission',
col_names = TRUE, col_types = NULL, na = "", skip = 0)

```

...

```
``{r}
```

```
UV_Comp1_Contour <- Excitation$`UV Component 1` %>% t(Emission$`UV  
Component 1`)
```

```
colnames(UV_Comp1_Contour) <- Emission$`Emission Wavelength`
```

```
p1 <- UV_Comp1_Contour %>%  
  as_tibble() %>%  
  mutate(excitation = Excitation$`Excitation Wavelength`) %>%  
  pivot_longer(-excitation, names_to = "emission") %>%  
  mutate(emission = as.numeric(emission)) %>%  
  arrange(excitation, emission) %>%  
  # next three lines sets up a regular grid of emission values  
  # make sure to check that the differences between emission and emission_corr are  
  small  
  group_by(excitation) %>%  
  mutate(emission_corr = seq(min(emission), max(emission), length.out =  
length(emission))) %>%  
  ungroup() %>%  
  ggplot(aes(excitation, emission_corr, fill = value, z = value)) +  
  geom_raster() +  
  scale_fill_distiller(palette = "YlGnBu", direction = -1) +  
  geom_contour(col = "white", size = .1) +  
  xlab("Excitation (nm)") +  
  ylab("Emission (nm)") +  
  ggtitle("Component 1") +  
  theme(plot.title = element_text(size = 12, face = "bold"))
```

```
UV_Comp2_Contour <- Excitation$`UV Component 2` %>% t(Emission$`UV  
Component 2`)
```

```
colnames(UV_Comp2_Contour) <- Emission$`Emission Wavelength`
```

```
p2 <- UV_Comp2_Contour %>%  
  as_tibble() %>%  
  mutate(excitation = Excitation$`Excitation Wavelength`) %>%  
  pivot_longer(-excitation, names_to = "emission") %>%  
  mutate(emission = as.numeric(emission)) %>%  
  arrange(excitation, emission) %>%  
  # next three lines sets up a regular grid of emission values  
  # make sure to check that the differences between emission and emission_corr are  
  small
```

```

group_by(excitation) %>%
mutate(emission_corr = seq(min(emission), max(emission), length.out =
length(emission))) %>%
ungroup() %>%
ggplot(aes(excitation, emission_corr, fill = value, z = value)) +
geom_raster() +
scale_fill_distiller(palette = "YlGnBu", direction = -1) +
geom_contour(col = "white", size = .1) +
xlab("Excitation (nm)") +
ylab("Emission (nm)") +
ggtitle("Component 2") +
theme(plot.title = element_text(size = 12, face = "bold"))

p1 <- p1 + coord_fixed()
p2 <- p2 + coord_fixed()

colnames(UV_Comp2_Contour) <- Emission$`Emission Wavelength`

p1 + p2
```

```{r}

Excitation = read_excel('PARAFAC Components PTL.xlsx', sheet = 'Excitation',
col_names = TRUE, col_types = NULL, na = "", skip = 0)

Emission = read_excel('PARAFAC Components PTL.xlsx', sheet = 'Emission',
col_names = TRUE, col_types = NULL, na = "", skip = 0)

```

```{r}
#UNTREATED COMPONENT CONTOURS

UT_Comp1_Contour <- Excitation$`Untreated Component 1` %>%
t(Emission$`Untreated Component 1`)

colnames(UT_Comp1_Contour) <- Emission$`Emission Wavelength`

p1 <- UT_Comp1_Contour %>%
as_tibble() %>%
mutate(excitation = Excitation$`Excitation Wavelength`) %>%

```

```

pivot_longer(-excitation, names_to = "emission") %>%
mutate(emission = as.numeric(emission)) %>%
arrange(excitation, emission) %>%
# next three lines sets up a regular grid of emission values
# make sure to check that the differences between emission and emission_corr are
small
group_by(excitation) %>%
mutate(emission_corr = seq(min(emission), max(emission), length.out =
length(emission))) %>%
ungroup() %>%
ggplot(aes(excitation, emission_corr, fill = value, z = value)) +
geom_raster() +
scale_fill_distiller(palette = "YlGnBu", direction = -1) +
geom_contour(col = "white", size = .1) +
xlab("Excitation (nm)") +
ylab("Emission (nm)") +
ggtitle("Component 1") +
theme(plot.title = element_text(size = 12, face = "bold"))

```

```

UT_Comp2_Contour <- Excitation$`Untreated Component 2` %*%
t(Emission$`Untreated Component 2`)

```

```

colnames(UT_Comp2_Contour) <- Emission$`Emission Wavelength`

```

```

p2 <- UT_Comp2_Contour %>%
as_tibble() %>%
mutate(excitation = Excitation$`Excitation Wavelength`) %>%
pivot_longer(-excitation, names_to = "emission") %>%
mutate(emission = as.numeric(emission)) %>%
arrange(excitation, emission) %>%
# next three lines sets up a regular grid of emission values
# make sure to check that the differences between emission and emission_corr are
small
group_by(excitation) %>%
mutate(emission_corr = seq(min(emission), max(emission), length.out =
length(emission))) %>%
ungroup() %>%
ggplot(aes(excitation, emission_corr, fill = value, z = value)) +
geom_raster() +
scale_fill_distiller(palette = "YlGnBu", direction = -1) +
geom_contour(col = "white", size = .1) +
xlab("Excitation (nm)") +
ylab("Emission (nm)") +
ggtitle("Component 2") +
theme(plot.title = element_text(size = 12, face = "bold"))

```

```

p1 <- p1 + coord_fixed()
p2 <- p2 + coord_fixed()

wrap_plots(p1,p2,ncol = 2,nrow = 1)
```

```{r}
#OZONE LOW COMPONENT CONTOURS

Ozone_Comp1_Contour <- Excitation$`Ozone Low Component 1` %>%
t(Emission$`Ozone Low Component 1`)

colnames(Ozone_Comp1_Contour) <- Emission$`Emission Wavelength`

p1 <- Ozone_Comp1_Contour %>%
  as_tibble() %>%
  mutate(excitation = Excitation$`Excitation Wavelength`) %>%
  pivot_longer(-excitation, names_to = "emission") %>%
  mutate(emission = as.numeric(emission)) %>%
  arrange(excitation, emission) %>%
  # next three lines sets up a regular grid of emission values
  # make sure to check that the differences between emission and emission_corr are
  small
  group_by(excitation) %>%
  mutate(emission_corr = seq(min(emission), max(emission), length.out =
length(emission))) %>%
  ungroup() %>%
  ggplot(aes(excitation, emission_corr, fill = value, z = value)) +
  geom_raster() +
  scale_fill_distiller(palette = "YlGnBu", direction = -1) +
  geom_contour(col = "white", size = .1) +
  xlab("Excitation (nm)") +
  ylab("Emission (nm)") +
  ggtitle("Component 1") +
  theme(plot.title = element_text(size = 12, face = "bold"))

Ozone_Comp2_Contour <- Excitation$`Ozone Low Component 2` %>%
t(Emission$`Ozone Low Component 2`)

colnames(Ozone_Comp2_Contour) <- Emission$`Emission Wavelength`

p2 <- Ozone_Comp2_Contour %>%
  as_tibble() %>%

```

```

mutate(excitation = Excitation$`Excitation Wavelength`) %>%
pivot_longer(-excitation, names_to = "emission") %>%
mutate(emission = as.numeric(emission)) %>%
arrange(excitation, emission) %>%
# next three lines sets up a regular grid of emission values
# make sure to check that the differences between emission and emission_corr are
small
group_by(excitation) %>%
mutate(emission_corr = seq(min(emission), max(emission), length.out =
length(emission))) %>%
ungroup() %>%
ggplot(aes(excitation, emission_corr, fill = value, z = value)) +
geom_raster() +
scale_fill_distiller(palette = "YlGnBu", direction = -1) +
geom_contour(col = "white", size = .1) +
xlab("Excitation (nm)") +
ylab("Emission (nm)") +
ggtitle("Component 2") +
theme(plot.title = element_text(size = 12, face = "bold"))

```

```

p1 <- p1 + coord_fixed()
p2 <- p2 + coord_fixed()
wrap_plots(p1,p2,ncol = 2,nrow = 1)
```

```

```

```{r}
#OZONE HIGH COMPONENT CONTOURS

```

```

Ozone_Comp1_Contour <- Excitation$`Ozone High Component 1` %*%
t(Emission$`Ozone High Component 1`)

```

```

colnames(Ozone_Comp1_Contour) <- Emission$`Emission Wavelength`

```

```

p1 <- Ozone_Comp1_Contour %>%
as_tibble() %>%
mutate(excitation = Excitation$`Excitation Wavelength`) %>%
pivot_longer(-excitation, names_to = "emission") %>%
mutate(emission = as.numeric(emission)) %>%
arrange(excitation, emission) %>%
# next three lines sets up a regular grid of emission values
# make sure to check that the differences between emission and emission_corr are
small
group_by(excitation) %>%

```

```

mutate(emission_corr = seq(min(emission), max(emission), length.out =
length(emission))) %>%
  ungroup() %>%
  ggplot(aes(excitation, emission_corr, fill = value, z = value)) +
  geom_raster() +
  scale_fill_distiller(palette = "YlGnBu", direction = -1) +
  geom_contour(col = "white", size = .1) +
  xlab("Excitation (nm)") +
  ylab("Emission (nm)") +
  ggtitle("Component 1") +
  theme(plot.title = element_text(size = 12, face = "bold"))

```

```

Ozone_Comp2_Contour <- Excitation$`Ozone High Component 2` %*%
t(Emission$`Ozone High Component 2`)

```

```

colnames(Ozone_Comp2_Contour) <- Emission$`Emission Wavelength`

```

```

p2 <- Ozone_Comp2_Contour %>%
  as_tibble() %>%
  mutate(excitation = Excitation$`Excitation Wavelength`) %>%
  pivot_longer(-excitation, names_to = "emission") %>%
  mutate(emission = as.numeric(emission)) %>%
  arrange(excitation, emission) %>%
  # next three lines sets up a regular grid of emission values
  # make sure to check that the differences between emission and emission_corr are
  small
  group_by(excitation) %>%
  mutate(emission_corr = seq(min(emission), max(emission), length.out =
length(emission))) %>%
  ungroup() %>%
  ggplot(aes(excitation, emission_corr, fill = value, z = value)) +
  geom_raster() +
  scale_fill_distiller(palette = "YlGnBu", direction = -1) +
  geom_contour(col = "white", size = .1) +
  xlab("Excitation (nm)") +
  ylab("Emission (nm)") +
  ggtitle("Component 2") +
  theme(plot.title = element_text(size = 12, face = "bold"))

```

```

p1 <- p1 + coord_fixed()
p2 <- p2 + coord_fixed()

```

```

wrap_plots(p1,p2,ncol = 2,nrow = 1)
```

```

```

``{r}
#H2O2 Low COMPONENT CONTOURS

H2O2_Comp1_Contour <- Excitation$`H2O2 Low Component 1` %>%
t(Emission$`H2O2 Low Component 1`)

colnames(H2O2_Comp1_Contour) <- Emission$`Emission Wavelength`

p1 <- H2O2_Comp1_Contour %>%
  as_tibble() %>%
  mutate(excitation = Excitation$`Excitation Wavelength`) %>%
  pivot_longer(-excitation, names_to = "emission") %>%
  mutate(emission = as.numeric(emission)) %>%
  arrange(excitation, emission) %>%
  # next three lines sets up a regular grid of emission values
  # make sure to check that the differences between emission and emission_corr are
  small
  group_by(excitation) %>%
  mutate(emission_corr = seq(min(emission), max(emission), length.out =
length(emission))) %>%
  ungroup() %>%
  ggplot(aes(excitation, emission_corr, fill = value, z = value)) +
  geom_raster() +
  scale_fill_distiller(palette = "YlGnBu", direction = -1) +
  geom_contour(col = "white", size = .1) +
  xlab("Excitation(nm)") +
  ylab("Emission (nm)") +
  ggtitle("Component 1") +
  theme(plot.title = element_text(size = 12, face = "bold"))

H2O2_Comp2_Contour <- Excitation$`H2O2 Low Component 2` %>%
t(Emission$`H2O2 Low Component 2`)

colnames(H2O2_Comp2_Contour) <- Emission$`Emission Wavelength`

p2 <- H2O2_Comp2_Contour %>%
  as_tibble() %>%
  mutate(excitation = Excitation$`Excitation Wavelength`) %>%
  pivot_longer(-excitation, names_to = "emission") %>%
  mutate(emission = as.numeric(emission)) %>%
  arrange(excitation, emission) %>%
  # next three lines sets up a regular grid of emission values

```

```

# make sure to check that the differences between emission and emission_corr are
small
group_by(excitation) %>%
mutate(emission_corr = seq(min(emission), max(emission), length.out =
length(emission))) %>%
ungroup() %>%
ggplot(aes(excitation, emission_corr, fill = value, z = value)) +
geom_raster() +
scale_fill_distiller(palette = "YlGnBu", direction = -1) +
geom_contour(col = "white", size = .1) +
xlab("Excitation (nm)") +
ylab("Emission (nm)") +
ggtitle("Component 2") +
theme(plot.title = element_text(size = 12, face = "bold"))

p1 <- p1 + coord_fixed()
p2 <- p2 + coord_fixed()

wrap_plots(p1,p2,ncol = 2,nrow = 1)
```



```

```{r}
#H2O2 High COMPONENT CONTOURS

H2O2_Comp1_Contour <- Excitation$`H2O2 High Component 1` %*%
t(Emission$`H2O2 High Component 1`)

colnames(H2O2_Comp1_Contour) <- Emission$`Emission Wavelength`

p1 <- H2O2_Comp1_Contour %>%
as_tibble() %>%
mutate(excitation = Excitation$`Excitation Wavelength`) %>%
pivot_longer(-excitation, names_to = "emission") %>%
mutate(emission = as.numeric(emission)) %>%
arrange(excitation, emission) %>%
# next three lines sets up a regular grid of emission values
# make sure to check that the differences between emission and emission_corr are
small
group_by(excitation) %>%
mutate(emission_corr = seq(min(emission), max(emission), length.out =
length(emission))) %>%
ungroup() %>%
ggplot(aes(excitation, emission_corr, fill = value, z = value)) +
geom_raster() +
scale_fill_distiller(palette = "YlGnBu", direction = -1) +

```


```

```

geom_contour(col = "white", size = .1) +
xlab("Excitation (nm)") +
ylab("Emission (nm)") +
ggtitle("Component 1") +
theme(plot.title = element_text(size = 12, face = "bold"))

H2O2_Comp2_Contour <- Excitation`H2O2 High Component 2` %*%
t(Emission`H2O2 High Component 2`)

colnames(H2O2_Comp2_Contour) <- Emission`Emission Wavelength`

p2 <- H2O2_Comp2_Contour %>%
  as_tibble() %>%
  mutate(excitation = Excitation`Excitation Wavelength`) %>%
  pivot_longer(-excitation, names_to = "emission") %>%
  mutate(emission = as.numeric(emission)) %>%
  arrange(excitation, emission) %>%
  # next three lines sets up a regular grid of emission values
  # make sure to check that the differences between emission and emission_corr are
  small
  group_by(excitation) %>%
  mutate(emission_corr = seq(min(emission), max(emission), length.out =
length(emission))) %>%
  ungroup() %>%
  ggplot(aes(excitation, emission_corr, fill = value, z = value)) +
  geom_raster() +
  scale_fill_distiller(palette = "YlGnBu", direction = -1) +
  geom_contour(col = "white", size = .1) +
  xlab("Excitation (nm)") +
  ylab("Emission (nm)") +
  ggtitle("Component 2") +
  theme(plot.title = element_text(size = 12, face = "bold"))

p1 <- p1 + coord_fixed()
p2 <- p2 + coord_fixed()

wrap_plots(p1,p2,ncol = 2,nrow = 1)
...

```

## APPENDIX E: Matlab Code for PCA Analysis of FEEM Data

```
ImportFEEM_PCA

prompt = 'Remove 240nm-250nm? (Y/N): ';
YesNoRemove = input(prompt, 's');
check = strcmp(YesNoRemove, 'Y');
%Here I want to remove 121 120 119 118 from the analysis
%Will need to remove the first 4 columns of cleanData, exWave and shift
%data over. Create new variables for this in order to preserve the
%originals

if check == 1
    Data = cleanData(1:125,4:121,1:numsamples);
    NewExWave = exWave(4:121);
    [~,WavelengthNames,~] = xlsread('Wavelength Pairs
Removed.xlsx', 'Sheet1');
else
    Data = cleanData;
    [~,WavelengthNames,~] = xlsread('Wavelength Pairs.xlsx', 'Sheet1');
end

permute(Data, [3 2 1]);
X = reshape(Data, [], size(Data,3), 1)';

%Ask the user if they want their dataset centered and scaled
prompt = 'Center and scale data? (Y/N): ';
YesNo = input(prompt, 's');
check = strcmp(YesNo, 'Y');

if check == 1
    %Center our imported data%
    X(:, :) = X(:, :) - mean(X, 2);
    %Scale our imported data%
    X(:, :) = X(:, :) ./ std(X(:, :));
    %Replace NaN in the event that you have a column of zeros that you
    %divided by
    X(isnan(X))=0;
end

[coeff, score, latent, tsquared, explained, mu] = pca(X);

%This gives the option to plot the Variance Explained
prompt = 'Plot VarExplained? (Y/N): ';
YesNo = input(prompt, 's');

check = strcmp(YesNo, 'Y');

if check == 1
    figure
    VEx = explained(1:10);
    pcxaxis = (1:10);
    bar(pcxaxis, VEx);
    ylim([0 100]);
```

```

        title('Variance explained by first ten principal
components','FontSize',14,'Fontname','Helvetica');
        ylabel('Percentage of Variance
Explained','FontSize',12,'FontName','Helvetica','FontWeight','Bold');
        xlabel('Principal
Component','FontSize',12,'FontName','Helvetica','FontWeight','Bold');
end

%We need to reshape our coeff and plot each of them as a contour plot.
%The first column of coeff will make a PC Contour plot for the First
%Principal Component

prompt = 'Plot PC Contour?(Y/N): '; %This gives the option to plot the
PC Contour
YesNo = input(prompt,'s');
check = strcmp(YesNo,'Y');

if check == 1
    prompt = 'Plot Single Contour or Multiple?(S/M): '; %This gives the
option to plot the PC Contour
    YesNo = input(prompt,'s');
    check = strcmp(YesNo,'S');
    if check == 1
        Con_PCA_Plot
    else
        PlotConBy4
    end
end

prompt = 'Plot 3-space PC?(Y/N): '; %This gives the option to plot PCs
in three-space
YesNo = input(prompt,'s');
check = strcmp(YesNo,'Y');

if check == 1
    PCA_3Space
end

prompt = 'Plot 2D PC?(Y/N): '; %This gives the option to plot PCs in
three-space
YesNo = input(prompt,'s');
check = strcmp(YesNo,'Y');

if check == 1
    FlatPCA
end

%K-means clustering

prompt = 'Calculate K-means Distances?(Y/N): '; %Will bin the samples
into groups
YesNo = input(prompt,'s');
check = strcmp(YesNo,'Y');

if check == 1

```

```

    KMean3D
end

prompt = 'Pair Data With Subset?(Y/N): '; %Provides the ability to match
parameters with FEEM data
YesNo = input(prompt, 's');
check = strcmp(YesNo, 'Y');

if check == 1
    DataPairing
end

prompt = 'Plot Linear Fit to Paired Parameter?(Y/N): '; %Incorporates a
linear regression model to the PC data
YesNo = input(prompt, 's');
check = strcmp(YesNo, 'Y');

if check == 1
    LinearFEEM
end

```

### External functions:

```

%Import Data

foldercheck = exist('fldr', 'var');

if foldercheck == 1
    rmpath(fldr);
end

prompt = 'Enter folder name: ';
prompt1 = 'Enter data key filename: ';
prompt2 = 'Enter number of samples: ';

fldr = input(prompt, 's');
addpath(fldr);

str = input(prompt1, 's');
numsamples = input(prompt2);

[cleanData, names, exWave, emWave] = importCleanData(numsamples, str);

```

```

%Component Plotting

prompt3 = 'Which PC do you want plotted?: '; %This gives the option to
plot the PC Contour
PCPrompt = input(prompt3);
PCData = coeff(:,PCPrompt);
load('FEEMRamp.mat','FEEMMap')
colormap(FEEMMap)

if YesNoRemove == 'Y'
    if check == 1

        PCAPlot = reshape(PCData,[length(emWave),length(NewExWave')]);
        %PCAPlot (PCAPlot<0.00001) = 0;
        figure
        contourf(NewExWave, emWave, PCAPlot)
        xlabel('Excitation Wavelength (nm)')
        ylabel('Emission Wavelength (nm)')
        caxis auto
        kk = num2str(PCPrompt);
        titlestr = ['PC Loading ' , kk, ' (' ,num2str(VEx(PCPrompt(1)),4),
'%)'];
        title(titlestr)
        colormap(FEEMMap)
        colorbar
        end
    elseif YesNoRemove == 'N'
        if check == 1

            PCAPlot = reshape(PCData,[length(emWave),length(exWave')]);
            %PCAPlot (PCAPlot<0.00001) = 0;
            figure
            contourf(exWave, emWave, PCAPlot)
            xlabel('Excitation Wavelength (nm)')
            ylabel('Emission Wavelength (nm)')
            caxis auto
            kk = num2str(PCPrompt);
            titlestr = ['PC Score ' , kk, ' (' ,num2str(VEx(PCPrompt(1)),4),
'%)'];
            title(titlestr)
            colorbar
            end
        end

clear ConPlot1 ConPlot2 ConPlot3 ConPlot4

prompt6 = 'Which PCs do you want to view as a contour?[use square
brackets]: '; %This gives the option to plot the PC Contour
ConPlot = input(prompt6);

ConPlot1(:,1) = coeff(:,ConPlot(:,1));
ConPlot2(:,1) = coeff(:,ConPlot(:,2));
ConPlot3(:,1) = coeff(:,ConPlot(:,3));
ConPlot4(:,1) = coeff(:,ConPlot(:,4));

```

```

load('FEEMRamp.mat','FEEMMap')

if YesNoRemove == 'Y'
    figure
    hold on
    subplot(2,2,1)
    Contour1 = reshape(ConPlot1,[length(emWave),length(NewExWave')]);
    %Contour1 (Contour1<0.00001) = 0;
    contourf(NewExWave, emWave, Contour1)
    xlabel('Excitation Wavelength
(nm) ','FontSize',12,'FontName','Helvetica')
    ylabel('Emission Wavelength
(nm) ','FontSize',12,'FontName','Helvetica')
    caxis auto
    kk = num2str(ConPlot(:,1));
    titlestr = ['PC Loading ', kk, ' (',num2str(VEx(ConPlot(1)),4),
'%)'];
    title(titlestr, 'FontSize',13, 'FontName','Helvetica')
    colorbar
    colormap(FEEMMap)

    subplot(2,2,2)
    Contour2 = reshape(ConPlot2,[length(emWave),length(NewExWave')]);
    %Contour2 (Contour2<0.00001) = 0;
    contourf(NewExWave, emWave, Contour2)
    xlabel('Excitation Wavelength
(nm) ','FontSize',12,'FontName','Helvetica')
    ylabel('Emission Wavelength
(nm) ','FontSize',12,'FontName','Helvetica')
    caxis auto
    kk = num2str(ConPlot(:,2));
    titlestr = ['PC Loading ', kk, ' (',num2str(VEx(ConPlot(2)),4),
'%)'];
    title(titlestr,'FontSize',13, 'FontName','Helvetica')
    colorbar
    colormap(FEEMMap)

    subplot(2,2,3)
    Contour3 = reshape(ConPlot3,[length(emWave),length(NewExWave')]);
    %Contour3 (Contour3<0.00001) = 0;
    contourf(NewExWave, emWave, Contour3)
    xlabel('Excitation Wavelength
(nm) ','FontSize',12,'FontName','Helvetica')
    ylabel('Emission Wavelength
(nm) ','FontSize',12,'FontName','Helvetica')
    caxis auto
    kk = num2str(ConPlot(:,3));
    titlestr = ['PC Loading ', kk, ' (',num2str(VEx(ConPlot(3)),4),
'%)'];
    title(titlestr,'FontSize',13, 'FontName','Helvetica')
    colorbar
    colormap(FEEMMap)

```

```

subplot(2,2,4)
Contour4 = reshape(ConPlot4,[length(emWave),length(NewExWave')]);
%Contour4 (Contour4<0.00001) = 0;
contourf(NewExWave, emWave, Contour4)
xlabel('Excitation Wavelength
(nm)', 'FontSize',12, 'FontName', 'Helvetica')
ylabel('Emission Wavelength
(nm)', 'FontSize',12, 'FontName', 'Helvetica')
caxis auto
kk = num2str(ConPlot(:,4));
titlestr = ['PC Loading ', kk, ' (', num2str(VEx(ConPlot(4)),4),
'%)'];
title(titlestr, 'FontSize',13, 'FontName', 'Helvetica')
colorbar
colormap(FEEMMap)
hold off
end

if YesNoRemove == 'N'

figure
hold on
subplot(2,2,1)
Contour1 = reshape(ConPlot1,[length(emWave),length(exWave')]);
%Contour1 (Contour1<0.00001) = 0;
contourf(exWave, emWave, Contour1)
xlabel('Excitation Wavelength (nm)')
ylabel('Emission Wavelength (nm)')
caxis auto
kk = num2str(ConPlot(:,1));
titlestr = ['PC Loading ', kk, ' (', num2str(VEx(ConPlot(1)),4),
'%)'];
title(titlestr, 'FontSize',13, 'FontName', 'Helvetica')
colorbar
colormap(FEEMMap)

subplot(2,2,2)
Contour2 = reshape(ConPlot2,[length(emWave),length(exWave')]);
%Contour2 (Contour2<0.00001) = 0;
contourf(exWave, emWave, Contour2)
xlabel('Excitation Wavelength (nm)')
ylabel('Emission Wavelength (nm)')
caxis auto
kk = num2str(ConPlot(:,2));
titlestr = ['PC Loading ', kk, ' (', num2str(VEx(ConPlot(2)),4),
'%)'];
title(titlestr, 'FontSize',13, 'FontName', 'Helvetica')
colorbar
colormap(FEEMMap)

subplot(2,2,3)
Contour3 = reshape(ConPlot3,[length(emWave),length(exWave')]);
%Contour3 (Contour3<0.00001) = 0;
contourf(exWave, emWave, Contour3)
xlabel('Excitation Wavelength (nm)')

```

```

ylabel('Emission Wavelength (nm)')
caxis auto
kk = num2str(ConPlot(:,3));
titlestr = ['PC Loading ' , kk, ' (' , num2str(VEx(ConPlot(3)),4),
'%) '];
title(titlestr, 'FontSize',13, 'FontName', 'Helvetica')
colorbar
colormap(FEEMMap)

subplot(2,2,4)
Contour4 = reshape(ConPlot4, [length(emWave), length(exWave')]);
%Contour4 (Contour4<0.00001) = 0;
contourf(exWave, emWave, Contour4)
xlabel('Excitation Wavelength (nm)')
ylabel('Emission Wavelength (nm)')
caxis auto
kk = num2str(ConPlot(:,4));
titlestr = ['PC Loading ' , kk, ' (' , num2str(VEx(ConPlot(4)),4),
'%) '];
title(titlestr, 'FontSize',13, 'FontName', 'Helvetica')
colorbar
colormap(FEEMMap)
hold off
end

```

```

%Plot three columns of scores in a three space
%This function works for PCA_FEEM_Quick

prompt4 = 'Which PCs do you want to view in 3-space?[use square
brackets]: '; %This gives the option to plot the PC Contour
PlotPCs = input(prompt4);

scorenames = zeros(length(score),4);
scorenames(:,1) = score(:,PlotPCs(1,1));
scorenames(:,2) = score(:,PlotPCs(1,2));
scorenames(:,3) = score(:,PlotPCs(1,3));

kk = (1:length(scorenames));
kk = kk';

scorenames(:,4) = kk;
scorenames = [scorenames(:,4) scorenames(:,1) scorenames(:,2)
scorenames(:,3)];

labels = cellstr( num2str(scorenames(:,1)) ); % # labels correspond to
their order

figure
scatter3(scorenames(:,2), scorenames(:,3), scorenames(:,4), 'rx');
text(scorenames(:,2), scorenames(:,3), scorenames(:,4), labels);

titlestrx = ['PC Score ' , num2str(PlotPCs(1,1))];
xlabel(titlestrx)

titlestry = ['PC Score ' , num2str(PlotPCs(1,2))];
ylabel(titlestry)

titlestrz = ['PC Score ' , num2str(PlotPCs(1,3))];
zlabel(titlestrz)

```

```

%2D Distancing PCA

clear Plot2D

prompt8 = 'Enter PCs for 2D plot: '; %This gives the option to plot the
PC Contour
PC2D = input(prompt8);

Plot2D(:, :) = score(:, PC2D(:, :));

kk = (1:length(Plot2D));
kk = kk';

Plot2D(:, 4) = kk;
Plot2D = [Plot2D(:, 4) Plot2D(:, 1) Plot2D(:, 2) Plot2D(:, 3)];
labels = cellstr( num2str(Plot2D(:, 1)) ); % # labels correspond to
their order

text(Plot2D(:, 2), Plot2D(:, 3), Plot2D(:, 4), labels);

figure
hold on
    subplot(2, 2, 1)
    scatter(Plot2D(:, 2), Plot2D(:, 3))
    xlabel = ['PC Score', num2str(PC2D(1)), ' (', num2str(VEx(PC2D(1))), 4),
'%) '];
    ylabel = ['PC Score', num2str(PC2D(2)), ' (', num2str(VEx(PC2D(2))), 4),
'%) '];
    text(Plot2D(:, 2), Plot2D(:, 3), labels);
    xlabel(xlabel)
    ylabel(ylabel)

    subplot(2, 2, 2)
    scatter(Plot2D(:, 2), Plot2D(:, 4))
    xlabel = ['PC Score', num2str(PC2D(1)), ' (', num2str(VEx(PC2D(1))), 4),
'%) '];
    ylabel = ['PC Score', num2str(PC2D(3)), ' (', num2str(VEx(PC2D(3))), 4),
'%) '];
    text(Plot2D(:, 2), Plot2D(:, 4), labels);
    xlabel(xlabel)
    ylabel(ylabel)

    subplot(2, 2, 3)
    scatter(Plot2D(:, 3), Plot2D(:, 4))
    xlabel = ['PC Score', num2str(PC2D(2)), ' (', num2str(VEx(PC2D(2))), 4),
'%) '];
    ylabel = ['PC Score', num2str(PC2D(3)), ' (', num2str(VEx(PC2D(3))), 4),
'%) '];
    text(Plot2D(:, 3), Plot2D(:, 4), labels);
    xlabel(xlabel)
    ylabel(ylabel)

    subplot(2, 2, 4)
    scatter3(Plot2D(:, 2), Plot2D(:, 3), Plot2D(:, 4))

```

```
    xlabel = ['PC Score', num2str(PC2D(1)), ' (' , num2str(VEx(PC2D(1)), 4),  
'% ) '];  
    ylabel = ['PC Score', num2str(PC2D(2)), ' (' , num2str(VEx(PC2D(2)), 4),  
'% ) '];  
    zlabel = ['PC Score', num2str(PC2D(3)), ' (' , num2str(VEx(PC2D(3)), 4),  
'% ) '];  
    text(Plot2D(:,2), Plot2D(:,3), Plot2D(:,4), labels);  
    xlabel(xlabel)  
    ylabel(ylabel)  
    zlabel(zlabel)  
hold off
```

```

% K-Means Distancing of PCA
clear DisScore DisClus Center

clus = 'Enter the 3 principal components for analysis: '; %This gives
the option to plot the PC Contour
DisClus = input(clus);

%DisScore = Plot2D;

DisScore(:,1) = score(:,DisClus(1,1)); % Call the scores you want

kk = 1:length(DisScore);
kk = kk';

DisScore(:,1) = kk;
DisScore(:,2) = score(:,DisClus(1,1));
DisScore(:,3) = score(:,DisClus(1,2));
DisScore(:,4) = score(:,DisClus(1,3));

labels = cellstr( num2str(kk) ); % # labels correspond to their order

[numInst,numDims] = size(DisScore);

% K-means clustering- Bucket is the group. Center is the centroid.

prompt = 'Conduct k-means distancing in 3-dimensions?: ';
YesNoRemove = input(prompt, 's');
check = strcmp(YesNoRemove, 'Y');

if check == 1

    clusnum = 'Enter the number of clusters: ';
    clusnum = input(clusnum);
    [Bucket,Center] = kmeans(DisScore(:,2:4), clusnum,
'distance','sqEuclidean', 'start','sample');

% show points and clusters (color-coded)
clr = lines(clusnum);
% Keep in mind that the DisScore values are shifted by one because
% column 1 is a list of sample numbers

hold on

subplot(2,2,1)
scatter(DisScore(:,2),DisScore(:,3), [],clr(Bucket,:), 'o', 'filled')
xlabel(['PC Score', num2str(DisClus(1)), ' ',
(',',num2str(VEx(DisClus(1)),4), '%) ']);
ylabel(['PC Score', num2str(DisClus(2)), ' ',
(',',num2str(VEx(DisClus(2)),4), '%) ']);
text(DisScore(:,2), DisScore(:,3), labels);
xlabel(xlbl, 'FontSize',12, 'FontWeight', 'Bold')
ylabel(ylbl, 'FontSize',12, 'FontWeight', 'Bold')

subplot(2,2,2)

```

```

        scatter(DisScore(:,2),DisScore(:,4),[],clr(Bucket,:), 'o', 'filled')
        xlabel = ['PC Score', num2str(DisClus(1)), '
(' ,num2str(VEx(DisClus(1)),4), '%) '];
        ylabel = ['PC Score', num2str(DisClus(3)), '
(' ,num2str(VEx(DisClus(3)),4), '%) '];
        text(DisScore(:,2), DisScore(:,4), labels);
        xlabel(xlbl, 'FontSize',12, 'FontWeight', 'Bold')
        ylabel(ylbl, 'FontSize',12, 'FontWeight', 'Bold')

        subplot(2,2,3)
        scatter(DisScore(:,3),DisScore(:,4),[],clr(Bucket,:), 'o', 'filled')
        xlabel = ['PC Score', num2str(DisClus(2)), '
(' ,num2str(VEx(DisClus(2)),4), '%) '];
        ylabel = ['PC Score', num2str(DisClus(3)), '
(' ,num2str(VEx(DisClus(3)),4), '%) '];
        text(DisScore(:,3), DisScore(:,4), labels);
        xlabel(xlbl, 'FontSize',12, 'FontWeight', 'Bold')
        ylabel(ylbl, 'FontSize',12, 'FontWeight', 'Bold')

        subplot(2,2,4)
        hold on
        scatter3(DisScore(:,2), DisScore(:,3), DisScore(:,4), 24,
clr(Bucket,:), 'o', 'filled')
        scatter3(Center(:,1), Center(:,2), Center(:,3), 72, 'k',
'Marker', 'x', 'LineWidth',2)

        view(3), axis vis3d, box off, rotate3d on
        xlabel = ['PC Score', num2str(DisClus(1)), '
(' ,num2str(VEx(DisClus(1)),4), '%) '];
        ylabel = ['PC Score', num2str(DisClus(2)), '
(' ,num2str(VEx(DisClus(2)),4), '%) '];
        zlbl = ['PC Score', num2str(DisClus(3)), '
(' ,num2str(VEx(DisClus(3)),4), '%) '];
        text(DisScore(:,2), DisScore(:,3), DisScore(:,4), labels);
        xlabel(xlbl, 'FontSize',12, 'FontWeight', 'Bold')
        ylabel(ylbl, 'FontSize',12, 'FontWeight', 'Bold')
        zlabel(zlbl, 'FontSize',12, 'FontWeight', 'Bold')
        hold off
end

if check == 1

        figure
        kk = (1:length(DisScore));
        kk = kk';
        LabelKMean = cellstr( num2str(kk) ); %Makes the numbers for plot
markers

        hold on

        % Makes the plot markers white
        %scatter3(DisScore(:,2), DisScore(:,3), DisScore(:,4), 24, 'w',
'Marker', 'o')

```

```

scatter3(DisScore(:,2), DisScore(:,3), DisScore(:,4), 24,
clr(Bucket,:), 'o', 'filled')
scatter3(Center(:,1), Center(:,2), Center(:,3), 72, 'k',
'Marker', 'x', 'LineWidth', 2)
view(3), axis vis3d, box on, rotate3d on

xlbl = ['PC Score', num2str(DisClus(1)), '
(', num2str(VEx(DisClus(1)), 4), '%)'];
ylbl = ['PC Score', num2str(DisClus(2)), '
(', num2str(VEx(DisClus(2)), 4), '%)'];
zlbl = ['PC Score', num2str(DisClus(3)), '
(', num2str(VEx(DisClus(3)), 4), '%)'];
%text(DisScore(:,2), DisScore(:,3), DisScore(:,4), labels);
legend('Clusters', 'Centroids');
xlabel(xlbl, 'FontSize', 12, 'FontWeight', 'Bold')
ylabel(ylbl, 'FontSize', 12, 'FontWeight', 'Bold')
zlabel(zlbl, 'FontSize', 12, 'FontWeight', 'Bold')

hold off

end

prompt = 'Conduct k-means distancing in 2-dimensions?: ';
YesNoRemove = input(prompt, 's');
check = strcmp(YesNoRemove, 'Y');
clr = lines(8);

if check == 1
figure
clusnum = 'Plot 1- Enter the number of clusters: ';
clusnum = input(clusnum);

[Bucket1, Center1] = kmeans(DisScore(:,2:3), clusnum,
'distance', 'sqEuclidean', 'start', 'sample');

subplot(3,1,1)
hold on
clr2 = clr([3:4 1], :);
scatter(DisScore(:,2), DisScore(:,3), [], clr2(Bucket1,:), 'o', 'filled')
scatter(Center1(:,1), Center1(:,2), 'k', 'Marker', 'x', 'LineWidth', 2)
xlbl = ['PC Score', num2str(DisClus(1)), '
(', num2str(VEx(DisClus(1)), 4), '%)'];
ylbl = ['PC Score', num2str(DisClus(2)), '
(', num2str(VEx(DisClus(2)), 4), '%)'];
%text(DisScore(:,2), DisScore(:,3), labels);
xlabel(xlbl, 'FontSize', 12, 'FontWeight', 'Bold')
ylabel(ylbl, 'FontSize', 12, 'FontWeight', 'Bold')
hold off

clusnum = 'Plot 2- Enter the number of clusters: ';
clusnum = input(clusnum);

[Bucket2, Center2] = kmeans(DisScore(:,3:4), clusnum,
'distance', 'sqEuclidean', 'start', 'sample');

```

```

subplot(3,1,2)
hold on
clr2 = clr([5:6 2],:);
scatter(DisScore(:,3),DisScore(:,4),[],clr2(Bucket2,:), 'o', 'filled')
scatter(Center2(:,1),Center2(:,2), 'k', 'Marker', 'x', 'LineWidth', 2)
xlabel = ['PC Score', num2str(DisClus(2)), ' ',
(' ', num2str(VEx(DisClus(2)), 4), '%)'];
ylabel = ['PC Score', num2str(DisClus(3)), ' ',
(' ', num2str(VEx(DisClus(3)), 4), '%)'];
%text(DisScore(:,3), DisScore(:,4), labels);
xlabel(xlbl, 'FontSize', 12, 'FontWeight', 'Bold')
ylabel(ylbl, 'FontSize', 12, 'FontWeight', 'Bold')
hold off

clusnum = 'Plot 3- Enter the number of clusters: ';
clusnum = input(clusnum);

[Bucket3,Center3] = kmeans(DisScore(:,[2 4]), clusnum,
'distance', 'sqEuclidean', 'start', 'sample');

subplot(3,1,3)
hold on
clr2 = clr([7:8 3],:);
scatter(DisScore(:,2),DisScore(:,4),[],clr2(Bucket3,:), 'o', 'filled')
scatter(Center3(:,1),Center3(:,2), 'k', 'Marker', 'x', 'LineWidth', 2)
xlabel = ['PC Score', num2str(DisClus(1)), ' ',
(' ', num2str(VEx(DisClus(1)), 4), '%)'];
ylabel = ['PC Score', num2str(DisClus(3)), ' ',
(' ', num2str(VEx(DisClus(3)), 4), '%)'];
%text(DisScore(:,2), DisScore(:,4), labels);
xlabel(xlbl, 'FontSize', 12, 'FontWeight', 'Bold')
ylabel(ylbl, 'FontSize', 12, 'FontWeight', 'Bold')
hold off

end

```

```

%I want to create a function that will pair a vector of data based on
the
%names that are associated with the data

%One set will be the FEEM matrices and the second one will be the
predicted
%variable

%Code this so that 'any' paired variable will be able to be fed into
%the prediction. As long as the naming nomenclature is consistent
between
%samples.

%Use the logical operator to compare each of the list to check for
%discrepancies. Then multiply the T/F vector by the data in each of the
%compared matrices. Then send them off to the prediction.

%Downside of this approach is that the names need to be identical. This
is
%less robust but when comparing strings, you are going to have problems
if
%there is ambiguity in what you are comparing.

%Other problem is the Filtered/Unfiltered issue. One solution would be
to
%be able to toggle between comparing F and UF samples. Insert a prompt
that
%will alter the F UF that we are searching for in each of the vectors.

clearvars ia ib ParamData

prompt5 = 'Enter Paired Data Filename: '; %This feeds in the filename
into the function
PairPrompt = input(prompt5, 's');

[num,txt,PairData] = xlsread(PairPrompt); %This will create our PairData
set.

[IndexNames,ia,ib] = intersect(PairData(:,1),names); %Creates the list
of names that are common to both of the indices

b = length(ia);
a = length(X);
CutMatrixData = ones(b,a);
CutScoreData = ones(b,1);

CutMatrixData(:, :) = X(ib(:,1),:);
ParamData(:,1) = num(ia(:,1),1);

```

```

%Linear Fit of the Data
clearvars CutScoreData ParamDataOnes
prompt7 = 'Enter PC Score(s) to Pair [1:n]: '; %This feeds in the
filename into the function
k = input(prompt7);

CutScoreData(:,1:length(k)) = score(ib(:,1),k(1,:)); %Extracts the data
for desired PCs
ParamData(:,1) = num(ia(:,1),1);
CutScoreData(:,(length(k)+1)) = ones(length(CutScoreData),1); %Extra
column of ones for regress can have an intercept
[b,bint,r,rint,stats] = regress(ParamData,CutScoreData);
b = b';
LinCombo = zeros(length(CutScoreData),(length(k)+1));

for i = 1:(length(k)+1)

    LinCombo(:,i) = b(1,i) * CutScoreData(:,i);

end

% Sum the linear coefficients for the
% regression. Give the predicted value for our parameter

PredictedVal = sum(LinCombo,2); %sums each row to calculate the
predicted total

%Creates the fitted line that can be plotted against the predicted vs
%observed measurement

RMSE = sqrt(nanmean((PredictedVal - ParamData).^2));
ASE = nanmean(abs(PredictedVal - ParamData));
%Durbin-Watson Test for autocorrelation
% = dwtest(r, );

%NEED TO FIGURE OUT THE PREDLINE VARIABLE ORIGIN. CURRENTLY ARISING FROM
%PHANTOM ZONE

%Want the slope of the line between the predicted and the actual
%measurements

figure
hold on
%lwrwnd = PredictedVal - nanmin([RMSE ASE]);
%uprbnd = PredictedVal + nanmin([RMSE ASE]);
if RMSE < ASE
    lgnd = 'RMSE';
elseif RMSE > ASE
    lgnd = 'ASE';
end
end
line(ParamData,ParamData,'Color','r'); %Y=X line to gauge the fit
plot(ParamData,PredictedVal,'x k'); %scatterplot of the data
PredLine = ;

```

```

line(ParamData, (PredLine + RMSE), ...
     'Color','m','LineStyle',':');
line(ParamData, (PredLine - RMSE), ...
     'Color','m','LineStyle',':');
line(ParamData,PredLine);
xlabel('Observed Organic Carbon (mg/L)')
ylabel('Predicted Organic Carbon (mg/L)')
Rsq = stats(1);
if length(k) <= 5
    title(['Fit for PC score(s) ', num2str(k), '. R^2= ',
num2str(Rsq), ' RMSE= ', num2str(RMSE), ' ASE= ', num2str(ASE)])
elseif length(k) > 5
    title(['Fit for the first ', num2str(length(k)), ' PC scores.
R^2= ', num2str(stats(1)), ' ASE= ', num2str(ASE)])
end
lgndPvO = 'Predicted vs Observed';
lgndYX = 'Y = X';
lgndSamples = 'TOC/DOC Samples';
%lgndupr = sprintf('Upper Bound %s', lgnd);
%lgndlwr = sprintf('Lower Bound %s', lgnd);
lgndlwr = sprintf('Prediction - ASE (0.5f)', nanmin([RMSE ASE]));
lgndupr = sprintf('Prediction + ASE (0.5f)', nanmin([RMSE ASE]));
%lgndfit = sprintf('Y = 0.3f X + 0.3f', b(1), b(2));
%legend({lgndPvO, lgndlwr, lgndupr,
lgndfit},'FontSize',10,'FontWeight','bold','Location','southeast');

legend({lgndYX,lgndSamples,lgndlwr,lgndupr,lgndPvO},'FontSize',10,'FontW
eight','bold','Location','southeast');
hold off

```

## APPENDIX F: High Throughput UV Exposure Supplemental Material

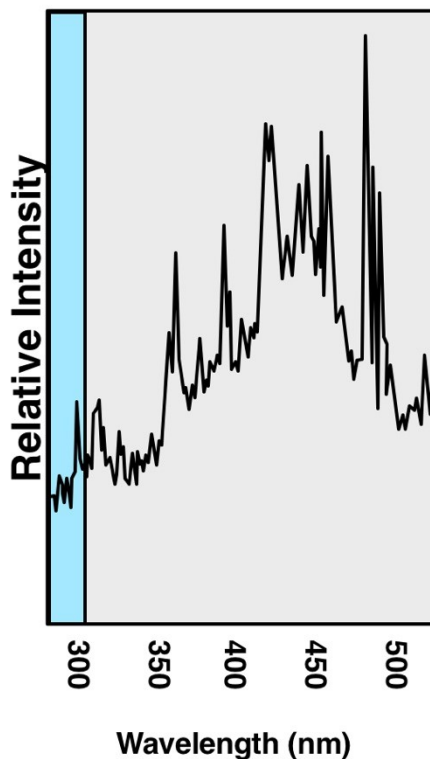


**Figure F-1** Relative output of the microplate reader xenon-flash light source with the UV region designated in blue

**Equation F-1** Moles of iron for exposed actinometry samples

$$\text{Moles of } Fe^{2+} = \frac{[A_{510}(\text{Sample}) - A_{510}(\text{Blank})]}{11,110}$$

**Equation F-2** Einsteins of UV light absorbed at a given wavelength

$$\text{einsteins of UV absorbed at wavelength } \lambda = \frac{\text{moles of } Fe^{2+} \text{ generated}}{\phi_{\text{known}}}$$

**Equation F-3** Joules per einstein at a given wavelength

$$U_{\lambda} (J \text{ einstein}^{-1}) = \frac{hcN_A}{\lambda}$$

**Equation F-4** UV power output at a given wavelength

$$P(W) = \frac{U_{\lambda}(J \text{ einstein}^{-1}) \times \text{einsteins of UV absorbed at wavelength } \lambda}{(1 - R) \times (t(s))}$$

**Equation F-5** UV fluence calculation for a given wavelength

*UV Fluence (mJ cm<sup>-2</sup>)*

$$= \left[ \frac{P(W) \times 1000(mW/W) \times t(s)}{A(cm^2)} \right] \times Ref_{factor} \times Area_{factor}$$

**Table F-2** UV fluence regression equations for 255nm to 280nm where t is in seconds of UV exposure.

| <b>Wavelength (nm)</b> | <b>Fluence Equation (mJ•cm<sup>-2</sup>)</b> | <b>R<sup>2</sup></b> |
|------------------------|--|----------------------|
| <b>255</b>             | 0.42t + 44.93                                | .929                 |
| <b>260</b>             | 0.85t + 56.78                                | .797                 |
| <b>265</b>             | 1.39t + 35.85                                | .955                 |
| <b>280</b>             | 1.56t + 17.06                                | .849                 |